ERDC/CHL TR-22-21

US Army Corps
of Engineers®
Engineer Research and
Development Center

ERDC
ENGINEER RESEARCH & DEVELOPMENT CENTER

Ship-Induced Waves at Tybee Island, Georgia

Rachel Bain, Richard Styles, and Jared M. Lopes

November 2022

Coastal and Hydraulics Laboratory

The US Army Engineer Research and Development Center (ERDC) solves the nation's toughest engineering and environmental challenges. ERDC develops innovative solutions in civil and military engineering, geospatial sciences, water resources, and environmental sciences for the Army, the Department of Defense, civilian agencies, and our nation's public good. Find out more at www.erdc.usace.army.mil.

To search for other technical reports published by ERDC, visit the ERDC online library at https://erdclibrary.on.worldcat.org/discovery.

ERDC/CHL TR-22-21
November 2022

Ship-Induced Waves at Tybee Island, Georgia

Rachel Bain and Richard Styles

Coastal and Hydraulics Laboratory
US Army Engineer Research and Development Center
3909 Halls Ferry Road
Vicksburg, MS 39180-6199

Jared M. Lopes

Savannah District
US Army Corps of Engineers
100 W Oglethorpe Ave
Savannah, GA 31401

Final report

Prepared for US Army Corps of Engineers, Savannah District
Savannah, GA 31401

Under Funding Account Code U4384772; AMSCO Code 493017

Abstract

Commercial vessels transiting the Savannah entrance channel intermittently generate large wake events at Tybee Island, Georgia, creating a potential hazard for beachgoers. However, not all commercial vessels generate large wakes, and the relationship between vessel dimensions, operating conditions, wake height, and drawdown magnitude is unclear. This study evaluates bathymetric data, high-frequency wave and vessel wake measurements, and broadcast vessel identification over a 4-month period with the goal of providing a quantitative characterization of vessel wake conditions at Tybee Island. Data from 1,386 cargo vessel passages and 202 tanker passages indicate that vessel dimensions (length and beam) are positively correlated with drawdown magnitude and secondary wake height, although large vessels do not consistently generate large wakes. Container ships, which tended to travel faster than tankers, corresponded to the largest wakes in the dataset. A further hypothesis is that tidally modulated energy dissipation may favor smaller vessel wake uprush at low tide and larger uprush at high tide, but this idea cannot be confirmed without additional measurements to quantify nonlinear wave propagation on the beach face. Based on the collected data, the study concludes with four recommendations for reducing risk to beachgoers.

Contents

Abstract ii

Figures and Tables iv

Preface viii

Executive Summary ix

1 Introduction 1

1.1 Background 1
1.2 Objective 6
1.3 Approach 7
1.3.1 Task 1: Site visit 7
1.3.2 Task 2: Bathymetric survey 7
1.3.3 Task 3: Equipment deployment and retrieval 7
1.3.4 Task 4: Analysis and reporting 7

2 Methodology 9

2.1 Bathymetric survey 9
2.2 Vessel wake patterns of large commercial ships 9
2.3 Wake data collection and processing 11
2.4 Automated Information System (AIS) data and processing 15
2.5 Other data sources 17
2.6 Wind wave analysis 20
2.7 Wake analysis 22

3 Results 24

3.1 Bathymetric survey 24
3.2 Wind wave conditions: general description 26
3.3 Vessel types and operating conditions 28
3.4 Large vessel wakes: general description 32
3.5 Comparison of energy from wind-generated and vessel-generated waves 38
3.6 Statistical analysis of ship wave characteristics 45
3.7 Nearshore wave patterns 49

4 Discussion and Summary 53

4.1 Recommendations 54
4.2 Strategies to reduce wave heights at Tybee Island 57

References 60

Appendix: Ship Wave Height at Tybee Island 63

Abbreviations 76

Report Documentation Page

Figures and Tables

Figures

Figure 1. One-third arcsecond digital elevation model from NOAA (2006) showing the bathymetry near Tybee Island. All elevations are relative to mean high water. The locations of several geographic reference points, including Savannah and Tybee Island, are indicated. 2

Figure 2. Sign on Tybee Island warning beachgoers of vessel wake hazard. 3

Figure 3. Wave types generated by commercial vessels. (A) Time series of water surface elevation during the passage of the container ship *CMA CGM Argentina* near Tybee Island. (B) Time series of the bulk cargo ship *Nevat Kalkavan*. 10

Figure 4. Overview of the study area. (a) Location of Tybee Island near Savannah, Georgia. (b) Location of existing monitoring stations at Fort Pulaski, Savannah-Hilton Head Airport (SAV), Gray's Reef, and Clyo, GA, in relation to the Tybee instruments. (c) Satellite imagery of Tybee Island and the navigation channel, with instrument locations noted. 11

Figure 5. Photos of instrument setup on Coast Guard navigation ranges. (a) Photo of North Range at mid-tide with installed solar panels. The pressure sensors are below the water. (b) Photo of Paroscientific pressure sensor (cylindrical white instrument, wrapped in black tape) mounted on navigation range. The shallow instruments were subaerially exposed at low tide. 12

Figure 6. Example of time series data from (a) the shallow South Range instrument and (b) the temporary nearshore instrument. The horizontal axis spans 35 min. Timestamps of large vessel closest approach to the South Range are indicated by the dashed vertical lines. The instruments were referenced to the NAVD88 datum under the assumption that mean water level at Tybee is equal to mean water level at Fort Pulaski. 13

Figure 7. Summary of wake data quality from the South Range and North Range pressure sensors. Black bars indicate a full 24 hr of good-quality data while gray bars indicate a partial day of usable data. Reasons for discarding data included insufficient battery power, biofouling of the sensors, and/or instrument exposure at low tide. The instruments were serviced and replaced at the end of September. 14

Figure 8. Photo of Tybee's North Beach at low tide on 2 December 2021, with the nearshore and South Range instrument locations noted. View is looking north towards the navigation channel. The bedform wavelength is approximately 3 m. The shore-perpendicular orientation of the bedform crests suggests formation by a shore-parallel current, possibly the ebbing tidal current from the south channel of the Savannah River. 15

Figure 9. Example of an AIS vessel track for the cargo ship *UBC Sydney* (MMSI 209218000), which passed the study area between 8:35 PM and 8:50 p.m. EDT on 12 August 2021 (00:35 to 00:50 UTC on 13 August 2021). The track points are colored by the vessel's AIS-broadcast speed, with darker colors indicating a faster rate of travel. The direction of travel is from west to east (outbound). 16

Figure 10. Tide and flow conditions during the Tybee Island study. Subplot (a) shows water surface elevations reported by NOAA at Fort Pulaski. Subplots (b) and (c) show flow velocity and discharge at Fort Pulaski, as reported by the

USGS. Subplot (d) shows the USGS-reported discharge for the Savannah River at Clyo, GA, which is upstream of the tidal limit. For instrument locations, see Figure 4. 18

Figure 11. Atmospheric and offshore wave conditions during the Tybee Island study. The black line shows measurements from NOAA buoy 41008, which is 70 km southeast of the Savannah entrance channel and 34 km due east of Sapelo Island. The light blue line shows data from Savannah-Hilton Head Airport. For instrument locations, see Figure 4. 19

Figure 12. April 2021 bathymetric survey data of the navigation channel and south channel of the Savannah River. 25

Figure 13. Bathymetric transects calculated from the April 2021 survey data. Subplot (a) shows a transect extending from Tybee's North Beach across the dredged navigation channel. Subplot (b) shows a transect from the south jetty to the north jetty. Transect positions appear as lines A-A' and B-B' in subplot (c). A larger version of subplot (c) with scale information appears in Figure 12. 26

Figure 14. Time series of (a) wave height and (b) wave period at the Coast Guard navigation ranges near Tybee Island. Offshore wave conditions from Figure 11 are shown in gray for comparison. 28

Figure 15. Distribution of vessel types for all vessels passing Tybee Island between 30 July 2021 00:00 UTC and 5 December 2021 00:00 UTC. *Unknown large vessels are vessels which generated visible drawdown but lack corresponding AIS data. 29

Figure 16. Minimum, average, and maximum number of cargo ship and tanker passages on each day of the week. "SEM" is the standard error of the mean. 29

Figure 17. Average number of cargo ship and tanker passages during each hour of the day. Error bars indicate the standard error of the mean. 29

Figure 18. (a) Distribution of vessel speed for various ship types at the point of closest approach to the South Range instruments. The boxes extend from the 25th to the 75th percentiles of the data, with the median indicated by the thick horizontal line. The whiskers are 1.5 times the interquartile range. (b) Distribution of vessel speeds for inbound versus outbound large ships at the point of closest approach to the South Range instruments. 31

Figure 19. Flow velocity and water level at times of large vessel passage for all cargo ships and tankers. (a) Tide data corresponding to outbound ships. Vessels which plot within the gray shaded region are traveling against the current. (b) Tide data corresponding to inbound ships. 31

Figure 20. Heat map of cargo and tanker tracks in the navigation channel near Tybee Island over the full study duration. The boundaries of the authorized channel are shown as dashed black lines. 32

Figure 21. Summary of the number of vessels with wake height and drawdown magnitude exceeding the 0.15 m analysis threshold. Subplot (a) summarizes wake characteristics from the South Range, while subplot (b) summarizes wake characteristics from the North Range. 33

Figure 22. Influence of measurement location on large vessel wake characteristics. (a) Comparison of drawdown magnitude at the South Range versus the North Range. Measured drawdown is strongly correlated at the two sites, but the magnitude is almost always larger at the South Range. (b) Comparison of peak wake height (i.e., the height of the largest oscillation in the

wake) at the South Range versus the North Range. A weak correlation exists, but neither site experiences uniformly larger wakes. 34

Figure 23. Relationships between (a) ship length and drawdown magnitude, (b) ship beam and drawdown magnitude, (c) design draft and drawdown magnitude, (d) vessel speed and drawdown magnitude, (e) ship length and wake height, (f) ship beam and wake height, (g) design draft and wake height, and (h) vessel speed and wake height. All wake data are from the North Range. Only cargo ships and tankers are plotted; note that no tankers generated a drawdown at the North Range exceeding the 0.15 m threshold for analysis. 35

Figure 24. Same as Figure 23, but using water level measurements from the South Range. 36

Figure 25. Predicted drawdown based on the equations of Schijf (1949, subplots a and b) and Almström and Larson (2020, subplots c and d). The Almström and Larson equation incorporates more physical parameters than the Schijf equation, but the improvement in correlation between measured and modeled drawdown is small. 37

Figure 26. Relative proportions of wind and vessel-generated wave energy based on data from (a) the upper North Range sensor, (b) the upper and lower North Range sensors, and (c) the upper and lower South Range sensors. Note that percentages may not sum to 100% due to rounding. *The upper instrument is used preferentially to minimize the influence of depth attenuation. Data from the lower instrument are substituted when the upper instrument is exposed or otherwise nonfunctional. †Unknown large vessels are vessels which generated a large drawdown event but lack corresponding AIS data. These are most likely cargo ships or tankers. 41

Figure 27. Time series of the daily number of large vessel passages and pilot vessel passages over the duration of the study. The large vessel count includes cargo ships, tankers, and unknown large vessels that generated measurable drawdown. 43

Figure 28. Upper limit of potential error due to missing vessels in the AIS record. Although the relative proportions of vessel energy attributed to the different vessel classes vary when compared to Figure 26, there is minimal variation in the percentage of total energy attributed to vessel-generated versus wind-generated waves. 44

Figure 29. Vessel drawdown statistical analysis for cargo and tanker carrier class vessels. (A). Probability distribution of the drawdown amplitude and the cumulative distribution (right vertical axis). (B) Probability distribution of the drawdown half-wave period and the cumulative distribution (right vertical axis). 46

Figure 30. Secondary waves statistical analysis for cargo and tanker class vessels. (A) Probability distribution of the wave height and the cumulative distribution (right vertical axis). (B) Probability distribution of the wave period and the cumulative distribution (right vertical axis). 47

Figure 31. Secondary waves and drawdown statistics. Secondary wave or drawdown percentiles as a function of vessel characteristics length (A. and B.), beam (C. and D.) and speed (E. and F.). The mean value in each percentile class includes error bounds that denote the 95% confidence interval. 48

Figure 32. Generalized illustration of different wake patterns from commercial vessels near Tybee Island. 50

Figure 33. Comparison of the drawdown measured at South Range and the drawdown measured at nearshore sensor. Solid line denotes 1:1 correlation. 52

Tables

Table 1. Summary of energy from wind waves. 39
Table 2. Summary of energy from vessel wakes. 40

Preface

This study was conducted for the US Army Corps of Engineers (USACE), Savannah District (SAS), under Funding Account Code U4384772; AMSCO Code 493017. The research was cost shared (50%) by USACE and the City of Tybee Island, which was supported by a Georgia Department of Community Affairs grant.

The work was performed by the Coastal Engineering Branch of the Navigation Division, US Army Engineer Research and Development Center, Coastal and Hydraulics Laboratory (ERDC-CHL). At the time of publication of this report, Ms. Lauren M. Dunkin was chief, Coastal Engineering Branch; Ms. Ashley E. Frey was chief, Navigation Division; Ms. Tiffany Burroughs was chief, Headquarters USACE Navigation Branch and Navigation Business Line Manager; and Mr. Charles E. Wiggins, CHL, was ERDC technical director for Navigation. Dr. Ty V. Wamsley was director of CHL, and Mr. Keith Flowers was deputy director of CHL.

The commander of ERDC was COL Christian Patterson, and the director of ERDC was Dr. David W. Pittman.

Executive Summary

Plain language summary

The navigation channel connecting the Port of Savannah, Georgia, to the Atlantic Ocean is located 1.4 km[1,2] north of Tybee Island's North Beach. Commercial cargo ships and tankers passing Tybee Island occasionally generate hazardous wake events on North Beach. During these events, the water recedes from the beach for 1 to 2 min (*drawdown*) before rapidly flooding the beach (*uprush*). However, many commercial vessels generate negligible drawdown and uprush, and it is challenging for lifeguards to warn beachgoers about the ship wake hazard when they do not know in advance whether a passing ship will generate a large wake event. The purpose of this study was to measure vessel wakes near North Beach, which will lead to a more complete understanding of which ships and operating conditions are associated with large wakes.

The US Army Corps of Engineers collected water level measurements from late July until early December 2021 using four instruments mounted on the Coast Guard navigation ranges (large concrete pillars marking the end of the navigation channel jetties). Vessel data for the same time period were obtained from the Coast Guard's Automatic Information System, which collects transmitted vessel information including the vessel identification number, the speed of travel, and location. Researchers used these datasets to look for patterns among vessel size, operating speed, and the magnitude of the generated wake. Water level measurements were also collected in the North Beach surf zone from December 2 through December 5, 2021. This allowed researchers to describe how large wakes behave as they arrive on the beach.

[1] For a full list of the spelled-out forms of the units of measure used in this document, please refer to *US Government Publishing Office Style Manual*, 31st ed. (Washington, DC: US Government Publishing Office 2016), 248-52, https://www.govinfo.gov/content/pkg/GPO-STYLEMANUAL-2016/pdf/GPO-STYLEMANUAL-2016.pdf.

[2] For a full list of the unit conversions used in this document, please refer to *US Government Publishing Office Style Manual*, 31st ed. (Washington, DC: US Government Publishing Office 2016), 345-7, https://www.govinfo.gov/content/pkg/GPO-STYLEMANUAL-2016/pdf/GPO-STYLEMANUAL-2016.pdf.

There are several key observations that were made during this study. These observations include the following:

- As vessel length and beam (width) increase, there is a greater probability that a large wake event will occur. However, the longest and widest vessels are not guaranteed to generate large wake events.
- Vessels traveling at speeds over 6.8 m/sec (13 kn) have the highest probability of generating a large wake event. However, fast-moving vessels do not always generate large wake events. In addition, there is no guarantee that vessels with speed below 6.8 m/sec will never generate a large wake event, although this was not observed in this study's data.
- Even though commercial vessel wakes are often higher than wind waves, wind waves are the more significant source of energy for moving sediment on North Beach. This is because large vessels pass the beach infrequently (average of 12 passages per day) whereas wind waves break on the beach continuously. The added influence of tidal currents for transporting sediment was not evaluated in this study.
- There are three types of vessel wake patterns that occur on the beach. These are as follows:
    - Some ships generate a gentle drawdown and a slow, swashing uprush. It is likely that this behavior has little effect on the shoreline. This was observed to occur for five vessels, which all had a drawdown height below 0.2 m.
    - Other ships generate wake events in which the uprush is sudden and accompanied by short waves. It is unclear whether this behavior results from instabilities in the drawdown or whether the shorter breaking waves are generated by the stern of the vessel. This was observed to occur for six vessels, and all vessels with AIS identification were inbound container ships or inbound vehicle carriers. However, because the number of observations is small, it is not possible to conclude that this type of wake behavior occurs only for inbound vessels.
    - Finally, some wake events have a 45 to 60 sec pause during the uprush when the water level does not change significantly. This may be caused by the wake interacting with the jetties. The behavior was observed to occur for six vessels, and all vessels with AIS identification were outbound container ships or outbound vehicle carriers. However, because the number of observations is small, it is

not possible to conclude that this type of wake behavior occurs only for outbound vessels.

The report also makes several recommendations for preventing large wake events on North Beach or for warning beachgoers that a large wake is coming. These recommendations include the following:

- Because fast-moving vessels have a higher probability of generating a large wake, reducing vessel speeds may reduce the uprush at the beach. This solution would require coordination between the US Coast Guard, the Georgia Ports Authority, and other regulatory agencies.
- Refurbishing the south jetty may reduce the height of the vessel-generated waves arriving at North Beach, but further study is required to better understand the influence of the jetties on wake behavior. Prior studies have estimated that refurbishing the south jetty would cost between $53 million and $90 million.
- Installing nearshore breakwaters may reduce the height of wake events at the beach. However, further study is required to ensure that a constructed breakwater would not disrupt natural sediment transport patterns. In addition, the breakwater position would need to comply with any regulations regarding its proximity to the navigation channel.
- An active warning system, including lighted beacons or an audio system, could be installed on North Beach to warn beachgoers that large vessel-generated waves are approaching. This system could be run using offshore wave sensors or onshore radar. However, such a system has not been previously tested, and further study would be necessary to ensure that the concept is effective.

1 Introduction

1.1 Background

Tybee Island, which is located at the mouth of the Savannah River 20 km[1,2] east of Savannah, GA, is the northernmost of Georgia's barrier islands (Figure 1). Approximately 8 km of sandy beaches span the island's eastern and northern shorelines, while the western side of Tybee Island is a back-barrier marsh fed by numerous tidal creeks. Smith et al. (2008) report a native grain size of 200 microns on the beach, although periodic beach renourishments have increased the median grain size to approximately 280 microns along the east side of the island (USACE-SAS 2019). The island's beach morphology is driven by a combination of tide and wave energy. The mean tide range is 2.1 m (NOAA 2017) with minimum neap tides of ~1 m and peak spring tides of ~3 m. Measured waves at Tybee Roads (10 km offshore at 14 m mean depth; see Figure 1) have a mean height of 0.84 m and a mean peak period of 7.9 sec (Work 2008), although numerical models suggest that waves up to 3.5 m may occur near the Tybee Island shoreline during hurricanes (Smith et al. 2008).

The 34 km Savannah entrance channel begins on the continental shelf, cuts through the ebb shoal north of Tybee Island, and continues up the Savannah River to the Port of Savannah (Gailani and Smith 2006, 2014). To accommodate increasingly larger vessels, the channel was originally deepened to 6.6 m relative to mean low water (MLW) in 1874, progressing to 7.9 m MLW in 1912, 9.1 m MLW in 1936, 11.0 m MLW in 1945, 12.2 m MLW in 1972, and 13.4 m MLW in 1994 (Smith et al. 2008). The most recent deepening to 14.9 m (49 ft) MLW was completed in 2020 (USACE 2020). The channel is currently large enough to accommodate post-Panamax vessels (Maynord 2007), and ships exceeding 360 m in length regularly pass Tybee Island en route to the port.

---

[1] For a full list of the spelled-out forms of the units of measure used in this document, please refer to *US Government Publishing Office Style Manual*, 31st ed. (Washington, DC: US Government Publishing Office 2016), 248-52, https://www.govinfo.gov/content/pkg/GPO-STYLEMANUAL-2016/pdf/GPO-STYLEMANUAL-2016.pdf.

[2] For a full list of the unit conversions used in this document, please refer to *US Government Publishing Office Style Manual*, 31st ed. (Washington, DC: US Government Publishing Office 2016), 345-7, https://www.govinfo.gov/content/pkg/GPO-STYLEMANUAL-2016/pdf/GPO-STYLEMANUAL-2016.pdf.

Figure 1. One-third arcsecond digital elevation model from NOAA (2006) showing the bathymetry near Tybee Island. All elevations are relative to mean high water. The locations of several geographic reference points, including Savannah and Tybee Island, are indicated.

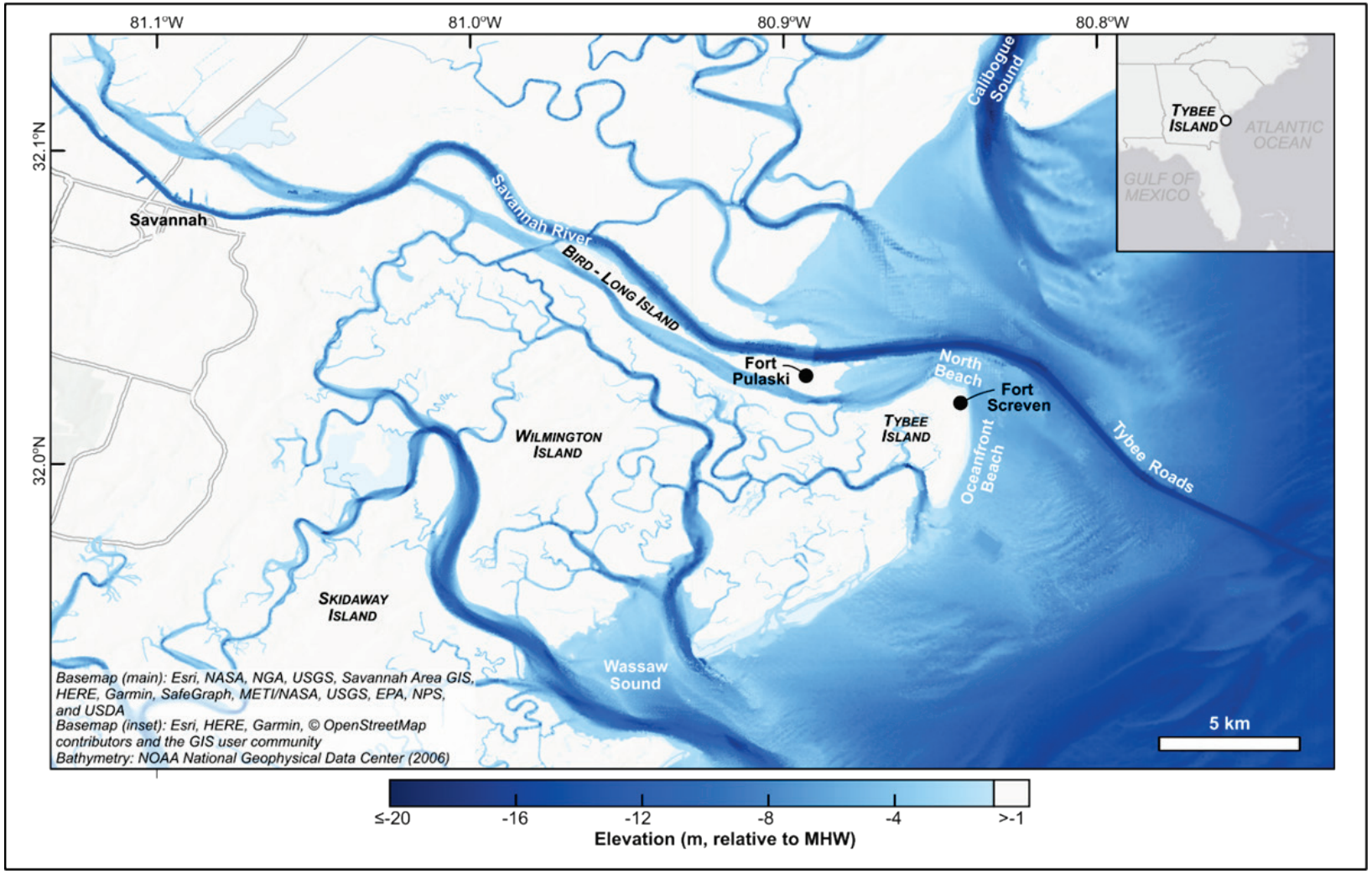

The Port of Savannah is among the largest ports in the United States, ranking thirteenth nationally by total tonnage in 2020 (43.5 million tons; USACE-IWR [2021]). The large volume of vessel traffic transiting to the port has led to concerns about hazardous wakes on Tybee Island's North Beach (see location, Figure 1). Anecdotal descriptions and several limited-scope quantitative studies indicate that many large vessels generate significant water level drawdown at Tybee Island, followed by a strong surge of water (*uprush*) onto the beach (e.g., Mosely 2018). These events are disruptive and potentially dangerous for beachgoers, and the City of Tybee has installed signage at multiple locations to warn visitors of the potential hazard (Figure 2). However, not all large ships generate significant drawdown and/or uprush, and convincing beachgoers to take precautions is difficult when a given vessel's likelihood of generating a large wake cannot be predetermined.

Figure 2. Sign on Tybee Island warning beachgoers of vessel wake hazard.

To protect the navigation channel and inhibit shoaling due to littoral transport, two parallel jetties measuring 3,660 m in length were constructed in the 1890s (Sargent 1988; Smith et al. 2008). The eastern terminus of the jetties is directly north of Tybee Island's North Beach. The northern jetty is 2.1 m above mean lower low water (MLLW) while the southern jetty has a somewhat lower elevation of 1.2 m above MLLW (Maynord 2007). The report by Mosely (2018) proposed increasing the southern jetty's elevation to mitigate vessel wake impacts at Tybee Island.

Prior studies of the Tybee Island region focus on sediment transport and shoreline erosion in the context of navigation channel deepening and/or beach nourishment. Oertel et al. (1985) summarized the history of erosion control at Tybee Island dating back to the late 1800s, noting changes in the shoreline position since the commencement of dredging. In consideration of ongoing navigation channel deepening, the Georgia Ports Authority (2002) modeled wind-generated wave conditions near Tybee Island under various dredging scenarios using the REF/DIF1 wave propagation model (Kirby and Dalrymple 1993). The results indicated that deepening the channel would enhance refraction of waves from the east and southeast, increasing wave heights near the shore at the north end of Tybee Island. However, the deeper channel was predicted to reduce wave heights near the shoreline for waves from the northeast. Interestingly, later STWAVE model results from Smith et al. (2008) predicted the opposite effect on wave height. During hurricanes and winter storms (when winds are typically out of the northeast; Oertel et al. 1985), post-dredging wave heights along the northern Tybee shoreline were found to increase by as much as 1.75 m (for hurricanes) and 1 m (for winter storms) relative to the pre-dredging wave conditions (Smith et al. 2008).

The comprehensive study by Smith et al. (2008) also modeled tidal currents and sediment transport near Tybee Island with the goal of identifying adverse impacts of ongoing navigation projects. The authors noted that the residual current direction north of Tybee Island has shifted since the late 1800s, with pre-dredging residual current directed eastward and the post-dredging residual current directed northward. This change was attributed to a 0.5 m/sec increase in current speed within the navigation channel. Velocity magnitudes along the north shore of Tybee Island were also determined to increase post-dredging. The net sediment transport direction has also reversed, with Tybee shoal switching from accretion to erosion during the 1900s.

Deepening the navigation channel over the past century interrupted the natural north-to-south littoral transport that formerly supplied sand to Tybee's beaches. In addition, the deeper channel has reduced the amount of river-transported sediment deposited on the ebb shoal. Consequently, groins for sand trapping were constructed along Oceanfront Beach on the east side of Tybee Island beginning in 1975 (Smith et al. 2008). A 4 km (13,200 ft) length of Oceanfront Beach has also been renourished on a 7 yr cycle since 1974 as part of the federally sponsored Tybee Island Shoreline Protection Project (USACE 2014). Tybee Island's North Beach, which is the focus of the present study, is outside the limits of the federal project and has not been renourished. However, modeling results from Gailani and Smith (2006, 2014) indicated that placing sediment offshore of Oceanfront Beach near Fort Screven (see location, Figure 1) would favor sediment transport onto the ebb shoal and lead to greater protection of North Beach.

Several studies have examined vessel-generated waves in the navigation channel west of Tybee Island. For example, Maynord (2007) considered vessel wake generation near Fort Pulaski under hypothetical channel depths and rates of travel. Faster-traveling ships generated larger bow and stern waves along with greater drawdown. However, deepening the channel was predicted to reduce the wake height and the drawdown magnitude. Houser (2010, 2011) also evaluated vessel wake influences on marsh erosion and sediment transport near Fort Pulaski. Those results indicate that although vessel-generated waves are responsible for 5% of cumulative wave energy and 25% of cumulative wave force near Fort Pulaski, wind-generated waves are the largest contributor to marsh scarp retreat in this region. Houser (2010) concluded that marsh retreat would not accelerate with the introduction of larger ships or more traffic. Farther upstream, Haas and Muscalus (2019) considered vessel wake effects on the shoreline of Bird-Long Island. Those model results suggest that vessel-generated waves could exceed 2 m high on the side of the island facing the navigation channel. Overall, vessels were found to contribute 68% of the total energy acting on the island shoreline, with the remainder coming from wind waves and tidal currents.

Only two studies have specifically examined vessel wakes along the Tybee Island shoreline. The first is by Maynord (2007), who collected vessel wake data offshore of the north beach from 15 September through 22 September 2005, corresponding to spring tide conditions. The study

predicted that post-Panamax ships of typical draft and velocity would generate 0.87 m drawdown in the existing navigation channel or 0.84 m drawdown if the channel were deepened. However, Maynord concluded that the drawdown would attenuate approaching the beach such that the actual drawdown at Tybee shoreline would be about one-third as large (i.e., less than 0.3 m). Given the ~1.4 km distance between the navigation channel and Tybee's North Beach, along with the tendency for short-period waves to decay with $\sqrt[3]{\text{distance}}$ (Sorensen 1966), Maynord (2007) concluded that bow and stern waves generated in the navigation channel would have negligible impacts on the beach. Maynord further concluded that neither the tidal stage nor the direction of ship travel was correlated with drawdown magnitude. The largest drawdown events corresponded to large ships traveling at high speed, but large, high-speed vessels did not always generate significant drawdown.

The second study evaluating vessel wake characteristics at Tybee Island was performed by Mosely (2018), whose results suggest that vessel wake impacts on the beach may be larger than hypothesized by Maynord (2007). Wake data for this study was collected over a 2-day period (8 October to 9 October 2018), recording only four large drawdown events. Based on these four samples, the author drew three main conclusions:

1. Given two ships of the same length, the ship that is faster and closer to shore will generate a larger wake at the beach.
2. Given two ships equidistant from shore, the longer ship will generate a larger wake even if its speed is slower.
3. Wake events act on the beach with 10 times more energy than wind waves.

However, considering the extremely limited sample size and study duration, whether Mosely's (2018) conclusions are broadly representative of all environmental conditions and ship characteristics is impossible to determine.

1.2 Objective

The project objective was to collect and analyze field measurements of vessel wake and wind waves near Tybee Island, Georgia. These data are intended to assist the Savannah District (SAS) in developing a more comprehensive understanding of the relative contribution of vessel wake and wind waves to nearshore processes on Tybee Island.

1.3 Approach

During the study, researchers collected data related to vessel-generated wave energy along Tybee Island's North Beach. This data collection effort included documenting wind, waves, water levels, and vessel traffic patterns from new or existing instrumentation. Four specific tasks were defined as components of the data collection campaign.

1.3.1 Task 1: Site visit

Researchers from the US Army Engineer Research and Development Center (ERDC) and SAS visited the site to observe the navigation channel and coastline. This site visit, completed in April 2021, allowed the team to develop a strategy for instrument deployment.

1.3.2 Task 2: Bathymetric survey

For further site characterization, a bathymetric survey of the region between North Beach and the navigation channel was planned contingent upon good weather and navigation conditions. The multibeam survey was completed between 21 April and 28 April 2021. The survey methods are detailed in Section 2.1.

1.3.3 Task 3: Equipment deployment and retrieval

Deployable equipment was transported to the study site by ERDC staff, where it was assembled and deployed using ERDC vessels. This equipment included gauges mounted on two Coast Guard navigation ranges near the end of the navigation channel jetties to measure vessel wake, wind waves, and tides. A camera system was also mounted on one of the navigation ranges to cross validate vessel information with the Coast Guard's Automated Information System (AIS) vessel records. These instruments were deployed on 26–28 July 2021, serviced and redeployed in late September, and retrieved by ERDC researchers on 4–5 December 2021. Details on the data collection methodology appear in Section 2.3.

1.3.4 Task 4: Analysis and reporting

The data to be analyzed included AIS data spanning the duration of the study, wind wave measurements, tidal conditions, and vessel wake characteristics. In particular, the following products were considered integral components of the study:

- Quantification of the total number of wakes and vessel passages, which should be correlated with AIS-derived vessel characteristics whenever possible.
- Quantification of the relative proportion of commercial vessels to other vessel types.
- Quantification of the cumulative vessel wake energy and comparison with wind wave energy.
- Statistical analysis of the relationship between wake characteristics and hydrodynamic conditions, including tidal stage and position within the navigation channel.
- Statistical analysis of the relationship between wake characteristics and vessel characteristics, including beam, draft, length, vessel type, vessel speed, and direction of travel.

2 Methodology

2.1 Bathymetric survey

To characterize the local bathymetry, the region between the navigation channel and Tybee's North Beach was surveyed between 21–28 April 2021. An R2Sonic Model 2024 multibeam echosounder mounted on the US Army Corps of Engineers (USACE) Research Vessel *T. Waller* collected high-resolution bathymetric data, with spatial positioning facilitated by a Trimble R10 GPS base station located on the beach. A SonTek Castaway CTD[1] instrument was used as a sound velocity profiler for post processing the bathymetric data. During post processing, the tidal signal was removed such that all bathymetric elevation measurements were relative to the NAVD88 datum, and XYZ point clouds were then created using HYPACK/HYSWEEP/MBMAX64 processing software. The spatial resolution of the final bathymetry is as small as 1.5 m in the most densely surveyed areas, although areas of coarser spatial resolution are also present.

2.2 Vessel wake patterns of large commercial ships

Divergent waves resulting from the rapid vertical motion of the water surface at the bow and stern of a vessel are a common hydraulic feature produced by all watercraft. Divergent waves appear as the familiar short period waves that propagate at an oblique angle from the vessel. Typical examples are the wakes that form behind recreational watercraft. For purposes of discussing large commercial vessels, divergent waves are generally referred to as secondary waves (Sorensen 1997).

In addition to divergent waves, large commercial vessels such as freighters, tankers, and container ships generate a second and generally larger and longer class of waves collectively known as *primary* waves. Primary waves can include a bow wave (different from that described above) that forms ahead of the ship due to its forward motion, stern waves that follow the ship with a phase speed equal to the ship speed, and the drawdown, which results from vessels operating in confined channels (Maynord 2003). The largest wave generated by commercial vessels transiting the Savannah ship channel is the drawdown (Maynord 2007).

[1] conductivity, temperature, depth

These waves can be detected in water surface elevation measurements if the sensor is located in the near field of the vessel (Figure 3).

The ship waves responsible for the uprush that occurs at the shoreline are likely a combination of the drawdown, stern wave, and secondary waves that follow the ship. Collectively, these waves can lead to a surge in water surface elevation on the trailing end of the drawdown, h_d, which is illustrated in Figure 3B.

Figure 3. Wave types generated by commercial vessels. (A) Time series of water surface elevation during the passage of the container ship *CMA CGM Argentina* near Tybee Island. (B) Time series of the bulk cargo ship *Nevat Kalkavan*.

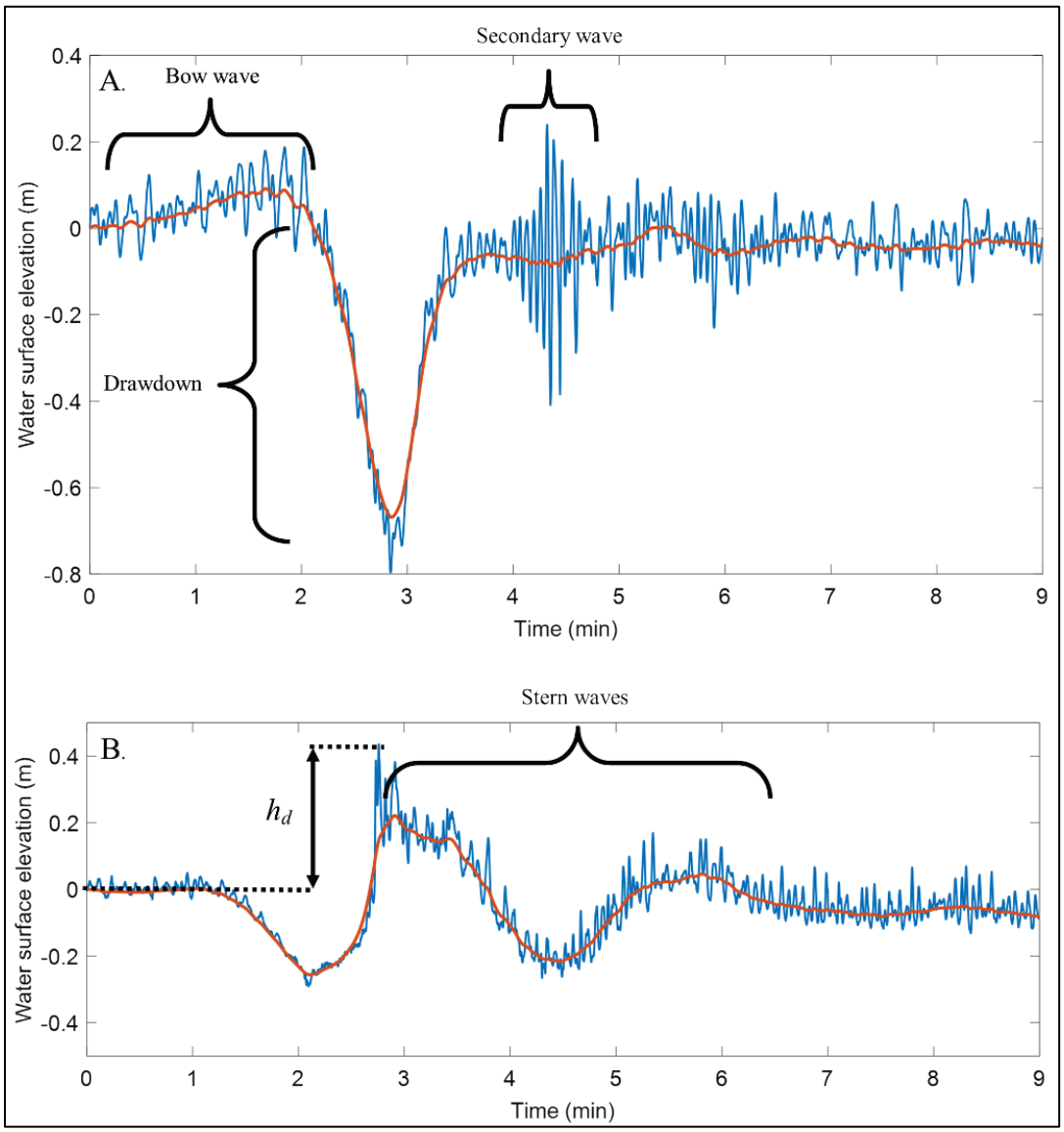

2.3 Wake data collection and processing

Several instruments were mounted on navigation ranges east of the north and south jetties (hereafter referred to as the "South Range" and the "North Range" locations; see Figure 4) in late July 2021. Two Paroscientific Digiquartz® pressure sensors were mounted at various elevations on each navigation range to collect wave and wake data at 8 Hz sampling. Barometric pressure was recorded by a fifth pressure sensor atop the South Range. The instruments were solar powered during the day (Figure 5a) and battery powered at night, with the measurements uploaded to an online server once per 24 hr period. The shallow instruments at both ranges were subaerially exposed at low tide (Figure 5b) but were less affected by pressure attenuation than the deep instruments. The instruments were serviced and replaced (if needed) at the end of September, and all equipment and mounting hardware were retrieved in early December 2021.

Figure 4. Overview of the study area. (a) Location of Tybee Island near Savannah, Georgia. (b) Location of existing monitoring stations at Fort Pulaski, Savannah-Hilton Head Airport (SAV), Gray's Reef, and Clyo, GA, in relation to the Tybee instruments. (c) Satellite imagery of Tybee Island and the navigation channel, with instrument locations noted.

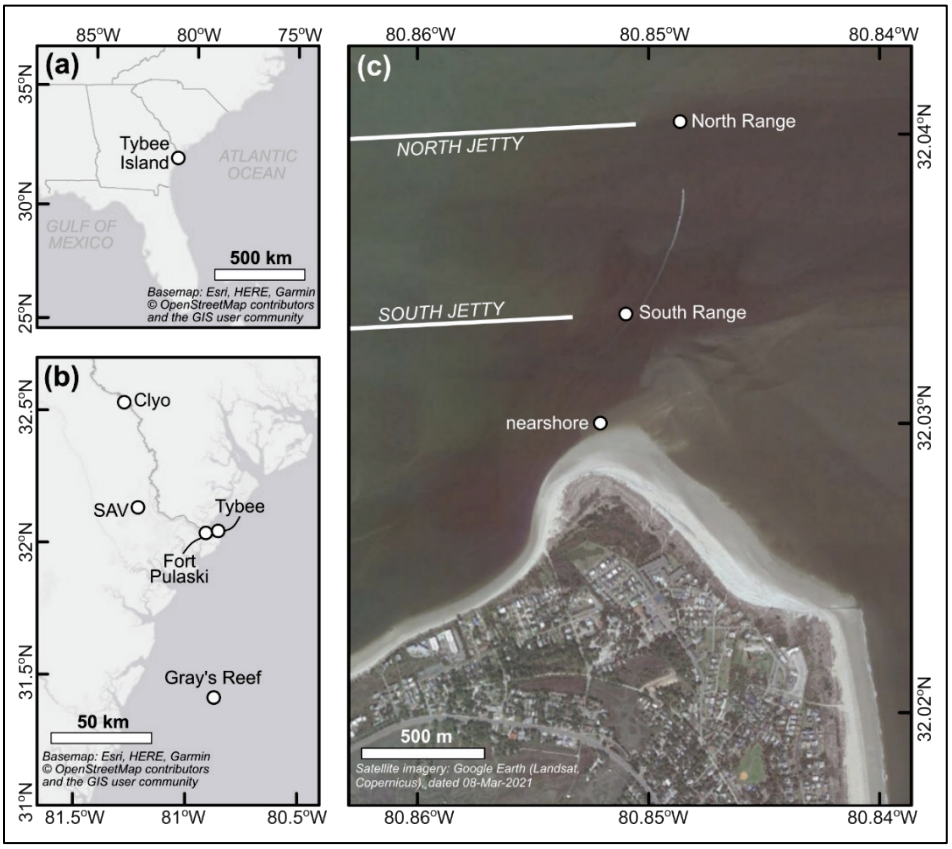

Figure 5. Photos of instrument setup on Coast Guard navigation ranges. (a) Photo of North Range at mid-tide with installed solar panels. The pressure sensors are below the water. (b) Photo of Paroscientific pressure sensor (cylindrical white instrument, wrapped in black tape) mounted on navigation range. The shallow instruments were subaerially exposed at low tide.

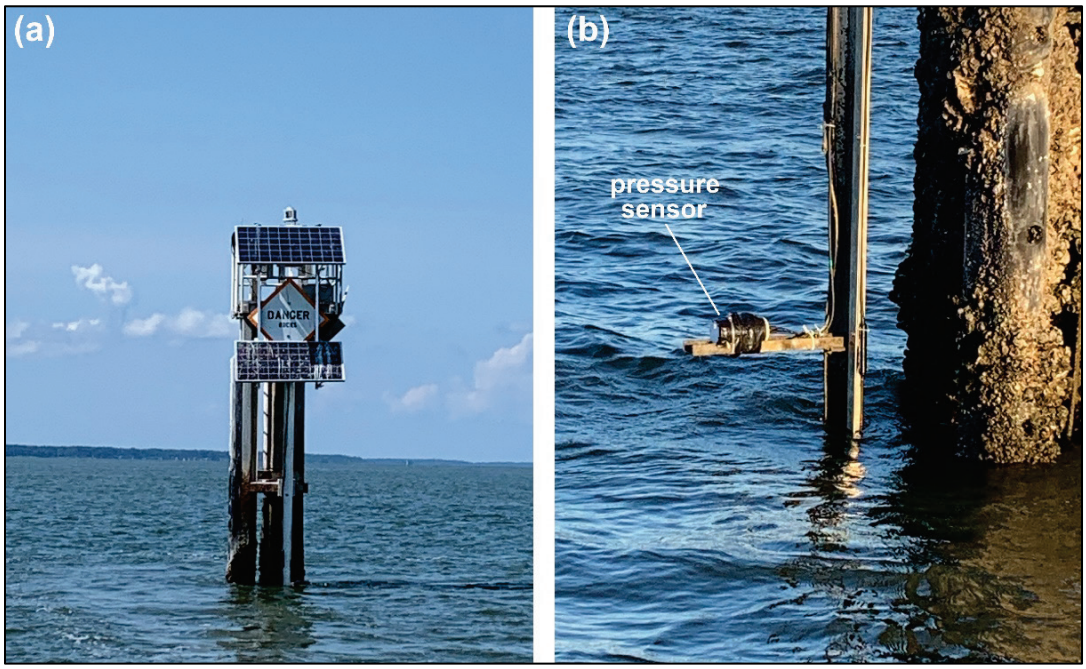

The data from the North Range and South Range pressure sensors were downloaded daily and were visually inspected for recording errors, which most frequently resulted from insufficient battery power or sensor biofouling. Any time periods with corrupted data were removed from the dataset. If an instrument was subaerially exposed at low tide, the windows of out-of-water data were also removed from further analysis. Measured atmospheric pressure was then subtracted from measured water pressure before converting to depth. An example of data collected at the South Range is shown in Figure 6a.

Due to the loss of one instrument, interruptions in battery power, and biofouling, the full wake dataset is discontinuous. The upper instruments were unaffected by biofouling but could not collect wake data at low tide whereas the lower instruments experienced biofouling within a month of installation. A summary of the data quality over the duration of the study is shown in Figure 7. Despite the data gaps caused by individual instruments, it was possible to combine data from multiple instruments to generate a time series sufficient to represent conditions over the 4-month time period. In general, the shallow sensors performed more consistently

than the deep sensors, with the shallow sensor at the North Range offering the most continuous high-tide vessel wake record.

Figure 6. Example of time series data from (a) the shallow South Range instrument and (b) the temporary nearshore instrument. The horizontal axis spans 35 min. Timestamps of large vessel closest approach to the South Range are indicated by the dashed vertical lines. The instruments were referenced to the NAVD88 datum under the assumption that mean water level at Tybee is equal to mean water level at Fort Pulaski.

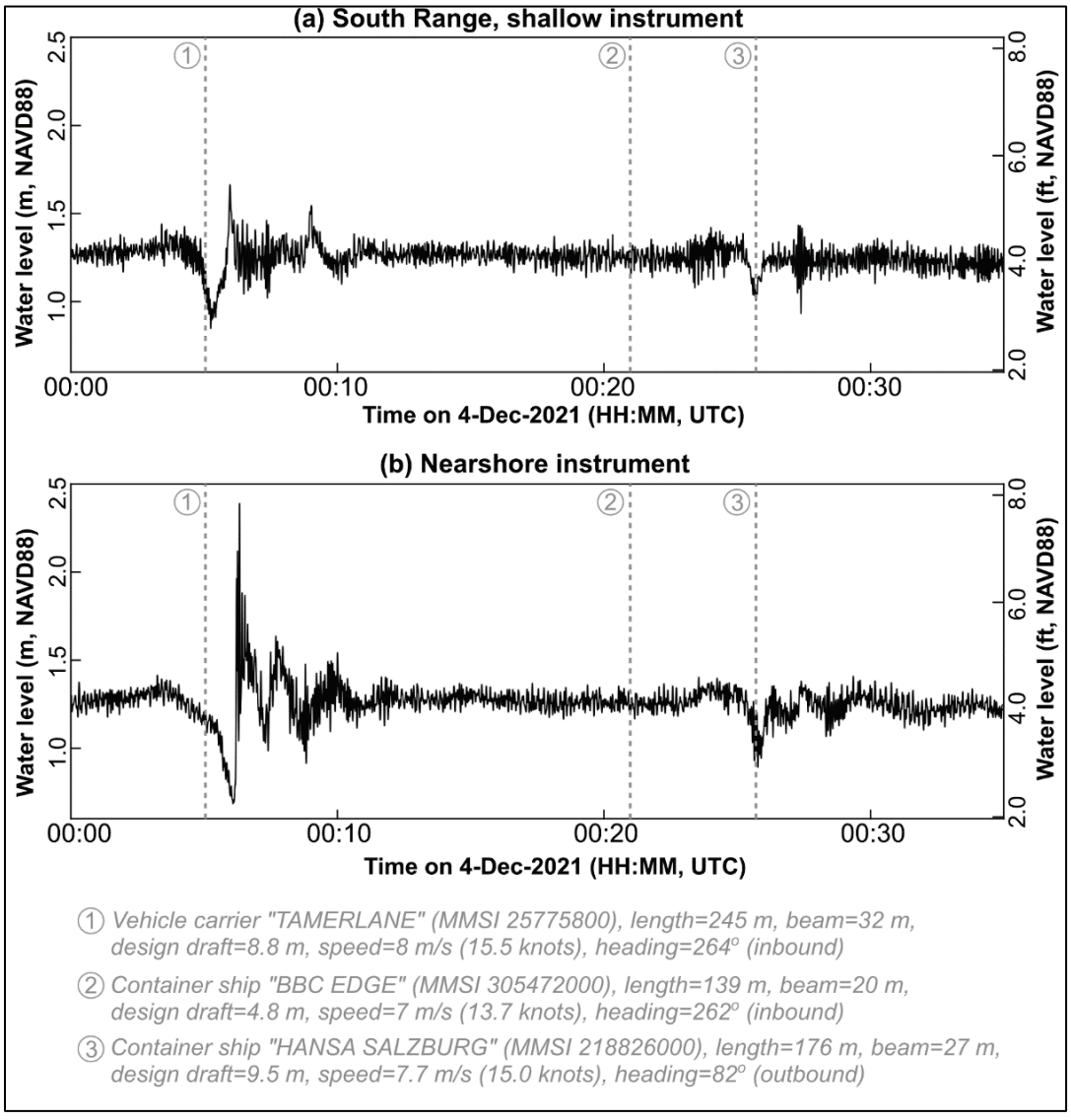

Figure 7. Summary of wake data quality from the South Range and North Range pressure sensors. Black bars indicate a full 24 hr of good-quality data while gray bars indicate a partial day of usable data. Reasons for discarding data included insufficient battery power, biofouling of the sensors, and/or instrument exposure at low tide. The instruments were serviced and replaced at the end of September.

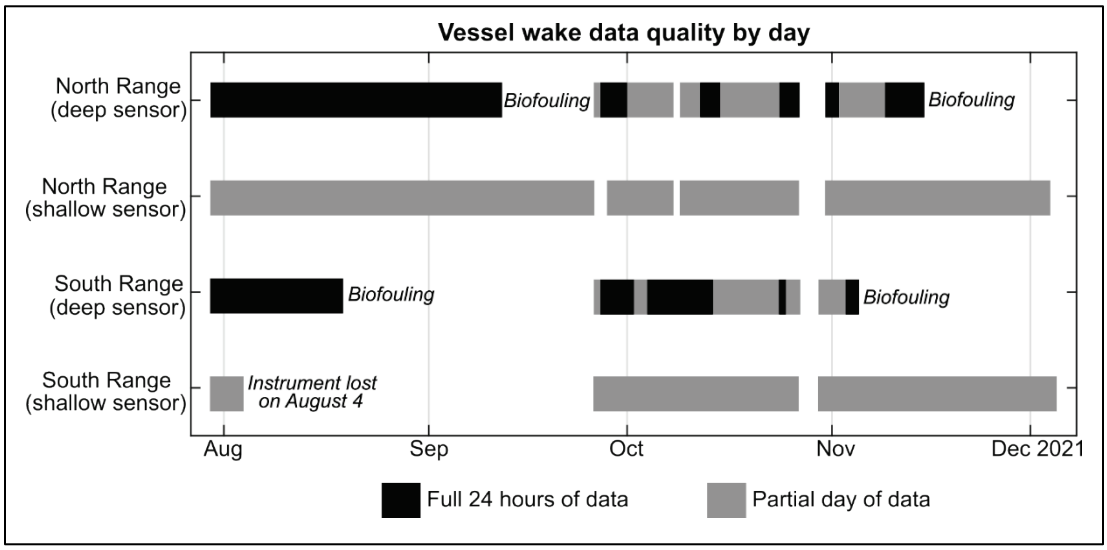

A Nortek Signature 1000 acoustic Doppler current profiler (ADCP) was installed on the channel bed near the South Range in late July 2021. Upon retrieval, the velocity data were determined to be unusable. However, the ADCP's internal pressure sensor recorded a continuous time series of the vertical tide, which was useful for vertical referencing of the remaining pressure sensors. Velocity data were obtained from the nearby US Geological Survey gage at Fort Pulaski. These data were used to help infer the current magnitude and direction at the study site (see Section 2.5).

To obtain nearshore data, a Ruskin RBRsolo pressure sensor was deployed on North Beach beginning on 2 December 2021 (Figure 8). The instrument was programmed for continuous 8 Hz logging and recorded data for a total of six semidiurnal tidal cycles, with some exposure near low water. Nearshore wakes were recorded for 27 AIS-identified large vessels (see Section 2.4), of which 19 generated measurable drawdown. Five additional large drawdown events are also visible in the data but lack corresponding AIS information. An example of the nearshore data is shown in Figure 6b. These measurements allow for a useful examination of nearshore wake behavior that could not be achieved using only the North Range and South Range sensors.

Figure 8. Photo of Tybee's North Beach at low tide on 2 December 2021, with the nearshore and South Range instrument locations noted. View is looking north towards the navigation channel. The bedform wavelength is approximately 3 m. The shore-perpendicular orientation of the bedform crests suggests formation by a shore-parallel current, possibly the ebbing tidal current from the south channel of the Savannah River.

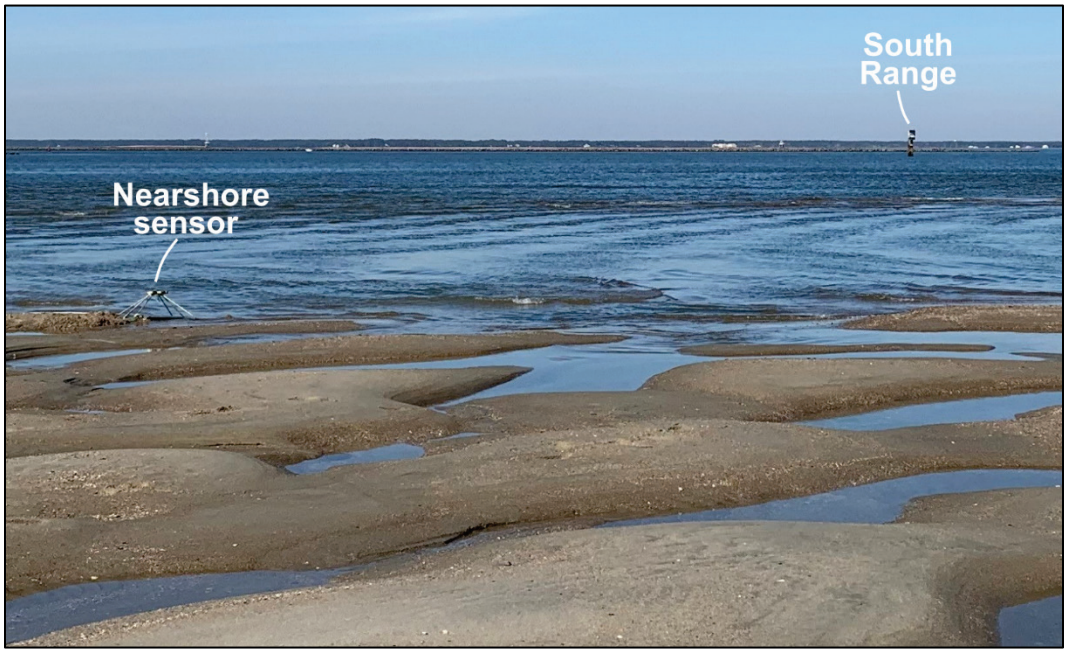

2.4 Automated Information System (AIS) data and processing

Commercial vessels operating on US waterways are required to broadcast their position, identification, and operating characteristics to the Coast Guard's AIS. To evaluate possible relationships between vessel and wake characteristics, the full AIS dataset for July through December 2021 was requested from the Coast Guard for a geographic region bounding the Savannah entrance channel. This dataset includes vessel Maritime Mobile Service Identity (MMSI) (unique vessel identification number), latitude, longitude, heading, and speed of travel. Vessels also broadcast a static draft value, which does not vary through time (Scully and Young 2021) but can be used as an estimate of the typical draft for a given ship. The time between consecutive transmissions was variable, but the majority of vessels broadcast their position several times per minute while inside the region of interest, allowing for the determination of individual vessel tracks at relatively high resolution. An example AIS track is shown in Figure 9.

Figure 9. Example of an AIS vessel track for the cargo ship *UBC Sydney* (MMSI 209218000), which passed the study area between 8:35 PM and 8:50 p.m. EDT on 12 August 2021 (00:35 to 00:50 UTC on 13 August 2021). The track points are colored by the vessel's AIS-broadcast speed, with darker colors indicating a faster rate of travel. The direction of travel is from west to east (outbound).

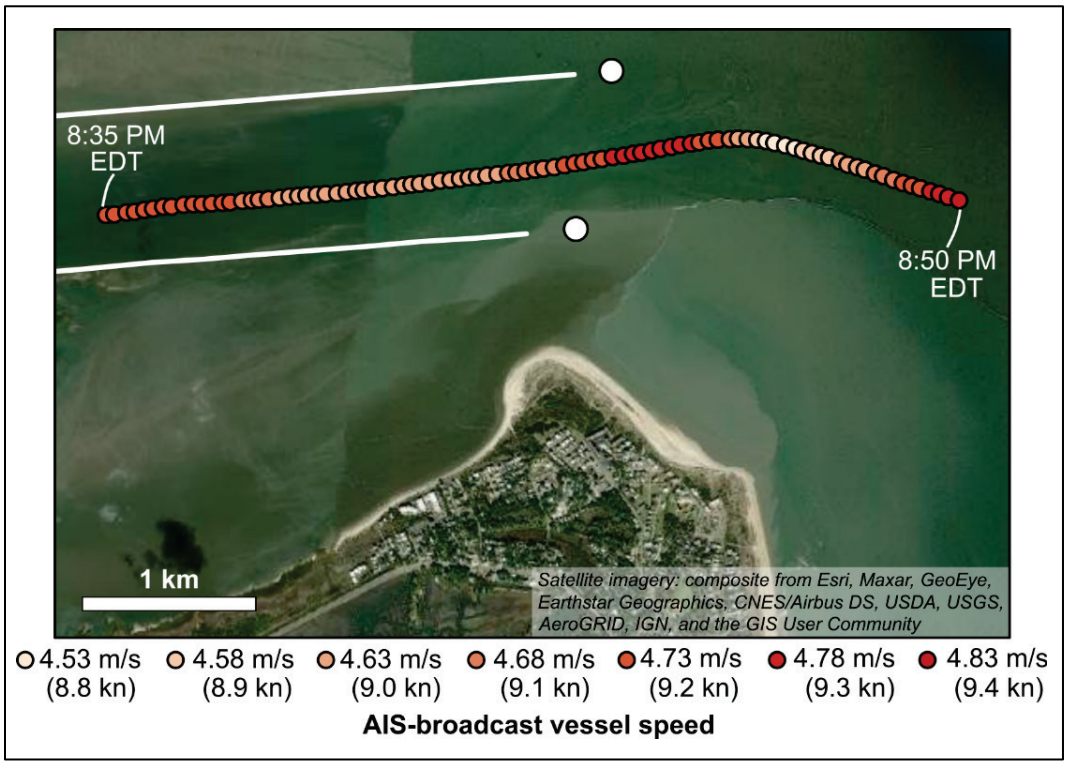

Using the AIS data, the vessel speed and heading at the moment of closest approach to the North Range and South Range instruments were extracted for comparison with the vessel wake measurements. The AIS dataset was then merged with a database of known vessel dimensions for each MMSI, which provided supplemental vessel length and beam information. This data merger also enabled separation of the dataset into the following classes: cargo ships, tankers, pilot vessels, tugs, tows, dredging vessels, military vessels, fishing vessels, sailing vessels, passenger vessels, and pleasure craft. Although some recreational vessels are present in the dataset, this class is underrepresented because privately owned, noncommercial vessels are not required to broadcast AIS data (Robards et al. 2016). A total of 19 drawdown events with no corresponding AIS data were also identified based on visual examination of the North Range and South Range pressure measurements; the timestamps of these events were added to the AIS dataset as an *unknown large vessel* class.

2.5 Other data sources

Several additional, publicly available sources of data were used to characterize the environmental conditions during the study. The National Oceanographic and Atmospheric Administration (NOAA) maintains a tide gage at Fort Pulaski[1] (Figure 4b), with the water surface elevation recorded at a 6 min sampling interval. These water level data are referenced to an absolute vertical datum, as shown in Figure 10a. Given the relatively short distance between Fort Pulaski and Tybee Island (5 km measured along-channel; see Figure 1), the mean water level at the two sites is assumed to be approximately equal. This assumption permits the estimation of the absolute water surface elevation at the east end of the jetties in the absence of a formal elevation survey.

The US Geological Survey (USGS) and USACE cooperatively maintain a stream gage and meteorological station at Fort Pulaski[2]. Measurements of gage height, precipitation, water temperature, and specific conductance (salinity) are reported at a 15 min sampling interval. The dataset also includes estimates of flow velocity and discharge (Figure 10b and Figure 10c), which are based on a rating curve. Although the rating-based velocity estimates are less precise than what would be obtained via real-time current measurements, these data enable a general determination of the flow direction relative to the direction of ship travel. An additional USGS stream gage along the Savannah River near Clyo, GA[3] (see location, Figure 4b), provides stage and discharge measurements upstream of the tidal limit (Figure 10d).

The most proximal offshore wave measurements to Tybee Island are recorded at the Gray's Reef NOAA buoy[4], which is located 70 km southeast of the Savannah entrance channel and 34 km due east of Sapelo Island (see location, Figure 4b). The dataset includes hourly measurements of offshore wind direction, wind speed, significant wave height, peak wave period, and wave direction. Examples of these data are shown in Figure 11a through Figure 11f.

[1] NOAA station 8670870; see https://tidesandcurrents.noaa.gov/stationhome.html?id=8670870

[2] USGS station 02198980; see https://waterdata.usgs.gov/nwis/uv?02198980

[3] USGS station 02198500; see https://waterdata.usgs.gov/nwis/uv?02198500

[4] NOAA buoy 41008; see https://www.ndbc.noaa.gov/station_page.php?station=41008

Figure 10. Tide and flow conditions during the Tybee Island study. Subplot (a) shows water surface elevations reported by NOAA at Fort Pulaski. Subplots (b) and (c) show flow velocity and discharge at Fort Pulaski, as reported by the USGS. Subplot (d) shows the USGS-reported discharge for the Savannah River at Clyo, GA, which is upstream of the tidal limit. For instrument locations, see Figure 4.

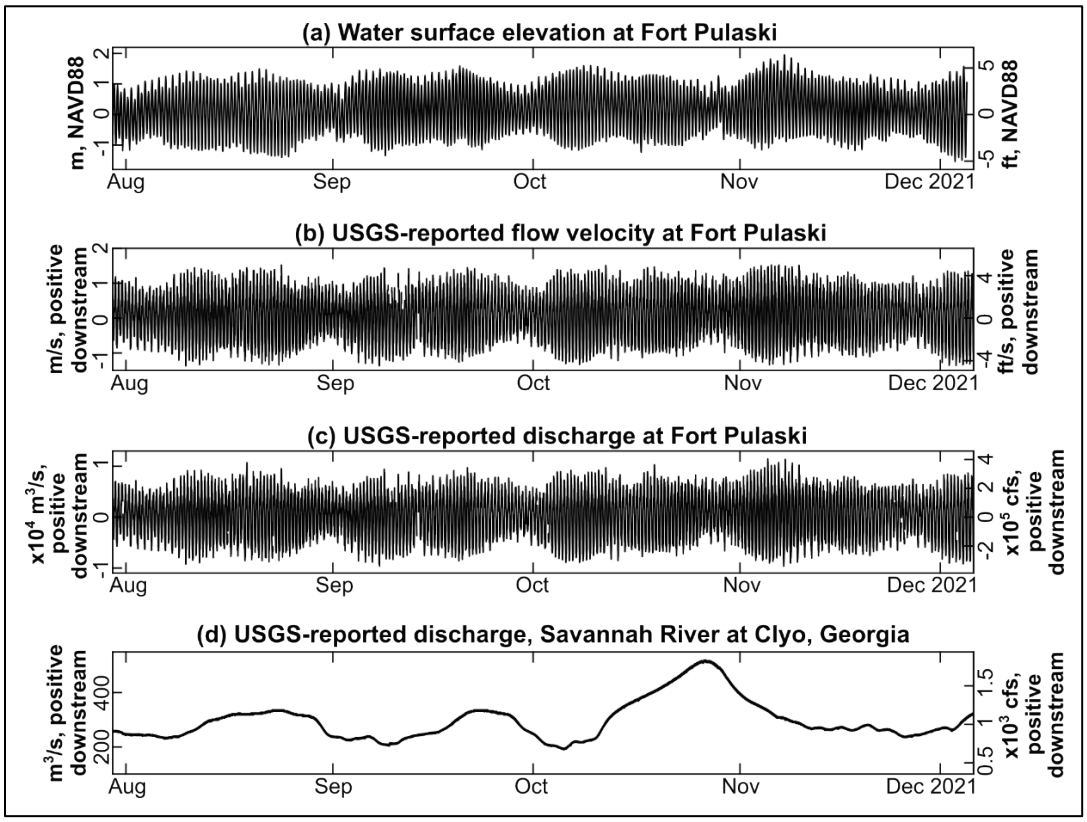

Finally, meteorological data from Savannah-Hilton Head Airport[1] (see location, Figure 4b) were downloaded to supplement the other datasets as needed. These data are reported approximately hourly and include measurements of barometric pressure, wind speed, and wind direction (light blue lines, Figure 11a through Figure 11c). Although these data were not treated as a primary data source, they were used to fill occasional gaps in the other datasets due to various occurrences (e.g., low-battery conditions that prevented the South Range atmospheric pressure sensor from collecting samples). Prior to using the Savannah-Hilton Head data, the airport measurements were overlaid onto the higher-resolution data sources, and the datasets were compared to verify their relative agreement. Visual examination indicated good correlation between the various sources of atmospheric data, and substituting airport-based atmospheric

[1] See https://www.wunderground.com/history/daily/us/ga/savannah/KSAV.

measurements when there were gaps in the South Range atmospheric data was considered appropriate.

Figure 11. Atmospheric and offshore wave conditions during the Tybee Island study. The black line shows measurements from NOAA buoy 41008, which is 70 km southeast of the Savannah entrance channel and 34 km due east of Sapelo Island. The light blue line shows data from Savannah-Hilton Head Airport. For instrument locations, see Figure 4.

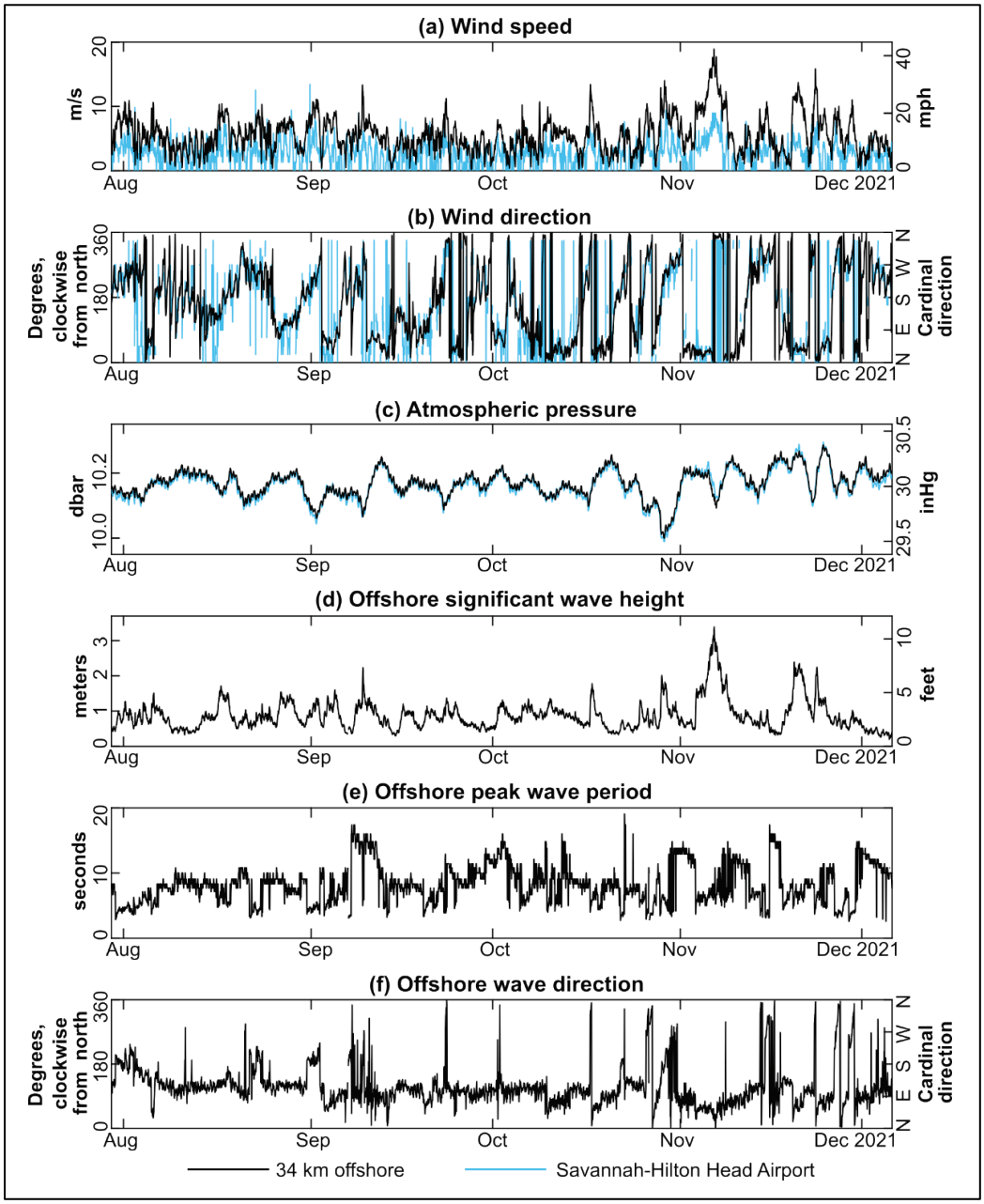

2.6 Wind wave analysis

Wind waves were analyzed for 1 hr windows of data collected at the North Range and the South Range. The raw water pressure data in each hourly window were first detrended with a quadratic polynomial to remove the low-frequency tidal signal. Pressure was then converted to depth of water column and corrected for depth attenuation using the OCEANALYZ toolbox in MATLAB (Karimpour and Chen 2017). If AIS data indicated that any vessels had passed during the 1 hr analysis window, a 5 min block of data beginning at the vessel's closest approach to the instrument was deleted from the time series. This data removal reduced the influence of vessel-generated wakes on the wind wave statistics. Finally, the significant wave height (H_{m0}) and the peak wave period (T_p) for the hour of interest were calculated via spectral analysis of the windowed time-series data.

To determine which waves were sufficiently energetic to induce sediment movement at the beach, the wave height at the Coast Guard ranges was transformed across the beach profile based on conservation of energy (e.g., Komar 1998). The breaking position x_b for the ith hour of data was identified as the cross-shore location satisfying

$$\frac{H(x_b, t_i)}{d(x_b, t_i)} = 0.78 \tag{1}$$

where H is the transformed value of H_{m0} and d is the water depth. For brevity, the conditions at breaking are subsequently notated $H_{b,i} = H(x_b, t_i)$ and $d_{b,i} = d(x_b, t_i)$. The near-bed maximum wave orbital velocity at x_b was then calculated from linear wave theory as

$$u_{b,i} = \frac{\pi H_{b,i}}{T_{p,i}\ \sinh(k_{b,i} \cdot d_{b,i})} \tag{2}$$

with the wavenumber $k_{b,i} = k(x_b, t_i)$ determined from numerical solution of the dispersion equation:

$$\left(\frac{2\pi}{T_{p,i}}\right) = g k_{b,i}\ \tanh\left(k_{b,i} \cdot d_{b,i}\right). \tag{3}$$

Here, $g = 9.81$ m/s^2 is the gravitational acceleration.

Smith et al. (2008) report a native median sediment diameter of 200 microns for the Tybee area, which is used for the present analysis because the region of interest is outside the limits of the federal renourishment area. Noting that a grain size of 200 microns corresponds to a roughness height of $z_0 = 1.3 \times 10^{-5}$ m, the bed shear stress at position x_b was calculated using

$$\tau_{b,i} = \rho_w u_{*wbi}^2 \tag{4}$$

where u_{*wbi} is the maximum shear velocity for the wave and $\rho_w = 1{,}027$ kg/m3 is the water density. The maximum shear velocity for the wave was calculated using the Styles and Glenn (2000) bottom boundary layer model for pure waves. Model inputs include z_0, $u_{b,i}$, $T_{p,i}$, and $d_{b,i}$ (see Styles et al. [2017], for model details).

Using the form of the Shields diagram presented by Julien (1995), the critical shear stress to mobilize 200-micron sand is approximately 0.2 Pa. Consequently, the wave energy was omitted from the final calculations if $\tau_{b,i} < 0.2$ Pa under the assumption that these waves do not contribute significantly to beach erosion and morphology. In addition, because the vessel wake analysis routine (Section 2.7) automatically discarded any wakes that did not exceed a height of 0.15 m at the Coast Guard ranges, all wind waves with $H_{m0} < 0.15$ m at the Coast Guard ranges were also discarded from the total wave energy. An hourly energy flux time series was therefore defined according to the formula

$$\bar{P}(t_i) = \begin{cases} \dfrac{\pi}{8T_{p,i}k_{b,i}} \rho_w g H_{b,i}^2 \left(1 + \dfrac{2k_{b,i}d_{b,i}}{\tanh(2k_{b,i}d_{b,i})}\right), & \tau_{b,i} \geq 0.2 \text{ Pa and } H_{m0} \geq 0.15 \text{ m} \\ 0, & \text{otherwise} \end{cases} \tag{5}$$

(USACE 1984)[1]. Finally, the cumulative wind wave energy per unit width of shoreline over a total duration of N hours was estimated as

[1] Scully, B., R. Styles, and S. J. Smith. Unpublished letter report. *Wave Climate and Vessel Wake Data Collection and Analysis: For the Charleston District of the USACE South Atlantic Division.* ERDC/CHL LR-20-7. Vicksburg, MS: US Army Engineer Research and Development Center.

$$E_{tot} = (1 \text{ hour}) \cdot \sum_{i=1}^{N} \bar{P}(t_i) \, . \tag{6}$$

2.7 Wake analysis

Vessel wake analysis proceeded similarly to the wind wave analysis described in Section 2.6, with several modifications to account for the ephemeral character of vessel-generated energy. For each known vessel passage time in the AIS data, a 1 hr window centered on the timestamp of vessel closest approach was detided with a quadratic polynomial and corrected for depth attenuation using the OCEANALYZ toolbox (Karimpour and Chen 2017). A subset of this corrected data was then extracted for further processing using the automated wake identification algorithm described by Scully[1]. For large vessels (cargo ships and tankers), the wake analysis window is 10 min in duration, centered on the AIS-determined closest approach to the instrument. This window-sizing process allows for the possibility that the vessel-generated drawdown may arrive at the instrument before the vessel passes whereas the higher-frequency secondary wake is expected to arrive at the instrument after the vessel passes. For all other vessels, the wake analysis window used was 5 min in duration and began at the AIS-determined closest approach to the instrument under the assumption that the wake arrival could not precede the vessel passage. Using these 5 or 10 min analysis windows reduced the chances of multiple vessel passages appearing within the same window (which the automated routine could not consistently distinguish) while still retaining sufficient data to fully encompass the wake of interest.

The automated wake identification routine first low-pass filtered the data to identify drawdown events, with the drawdown magnitude defined as the vertical distance between the minimum water surface elevation in the low-pass filtered data and the still water level. Drawdown events with a magnitude below 0.15 m were discarded under the assumption that drawdown below this threshold could not be accurately measured. To characterize the high-frequency wakes, the data were high-pass filtered, and the actual wake start and end times were determined based on

[1] Scully, B., R. Styles, and S. J. Smith. Unpublished letter report. *Wave Climate and Vessel Wake Data Collection and Analysis: For the Charleston District of the USACE South Atlantic Division*. ERDC/CHL LR-20-7. Vicksburg, MS: US Army Engineer Research and Development Center.

automated outlier detection. The height $H_v^{\max}$ of the largest oscillation in the wake was measured as twice the vertical distance between the most extreme water surface elevation during the wake and the still-water level. The peak wake period $T_{p,v}$ was then determined based on the maximum-amplitude coefficient of the wavelet-transformed time series. The total number M of half-oscillations (i.e., crests or troughs) exceeding 0.15 m in height was also recorded, with this 15 cm threshold selected based on the assumption that smaller oscillations would be indistinguishable from the background wind wave signal.

For each wake event, $H_v^{\max}$ was transformed across the beach profile based on conservation of energy, and Equations 1 through 4 were again applied to determine the bed shear stress at the breaking position. The energy flux corresponding to $H_v^{\max}$ was then calculated as

$$\overline{P_v^{\max}} = \begin{cases} \dfrac{\pi}{8T_{p,v}k_{b,v}}\rho_w g\left(H_{b,v}^{\max}\right)^2\left(1+\dfrac{2k_{b,v}d_{b,v}}{\tanh(2k_{b,v}d_{b,v})}\right), & \tau_{b,v} \geq 0.2 \text{ Pa and } H_v^{\max} \geq 0.15 \text{ m} \\ 0, & \text{otherwise,} \end{cases} \tag{7}$$

Equation 7 is identical to Equation 5 with the exception that all variables now correspond to breaking conditions for the largest oscillation in the wake. The total energy in a single wake was estimated as

$$(E_{tot})_v = \frac{M}{2} \cdot T_{p,v} \cdot \overline{P_v^{\max}}\,. \tag{8}$$

Note that Equation 8 will always overestimate the wake total energy because it assumes that the energy flux corresponding to the largest oscillation persists over the entire duration of the wake whereas in reality, the smaller oscillations will contain less energy. Finally, the wake energy generated by all vessels within some duration of interest may be obtained by summing the individual vessels' $(E_{tot})_v$ values.

3 Results

3.1 Bathymetric survey

Bathymetric data from the April 2021 survey are shown in Figure 12, with two cross-channel transects appearing in Figure 13. Typical depths in the navigation channel were between 16 and 16.5 m relative to the NAVD88 datum, which is consistent with the authorized depth of 14.9 m (49 ft) at mean low water (USACE 2020). The maximum measured depth in the navigation channel was 21 m NAVD88 at isolated scour locations. At the North and South Coast Guard ranges, where the instruments were mounted, the surveyed depth was between 5 and 6 m NAVD88. Near Tybee's North Beach, the south channel of the Savannah River is seen hugging the beach in Figure 12, with a maximum depth of 8 m NAVD88 immediately north of the beach.

Prior studies have found ship drawdown to be related to the channel cross-sectional area (e.g., Almström and Larson [2020]). To apply these relationships to the present study, the cross-sectional area of the navigation channel between the South Jetty and the North Jetty (Transect B-B' in Figure 13b) was calculated to be 7,902 m² for a water level of 0 m NAVD88. The magnitude of this value is consistent with the cross-sectional areas of 6,064 m² to 8,009 m² reported by Maynord (2007). Approximating the jetties as vertical walls, the navigation channel cross section as a function of tidal stage is given by

$$A_c(z) = (747\ \text{m}) \cdot z + 7{,}902\ \text{m}^2\ , \tag{9}$$

where z is water level in meters relative to the NAVD88 datum. The wetted perimeter between the jetties is given by

$$P_c(z) = 2z + 755\ \text{m}\ . \tag{10}$$

Figure 12. April 2021 bathymetric survey data of the navigation channel and south channel of the Savannah River.

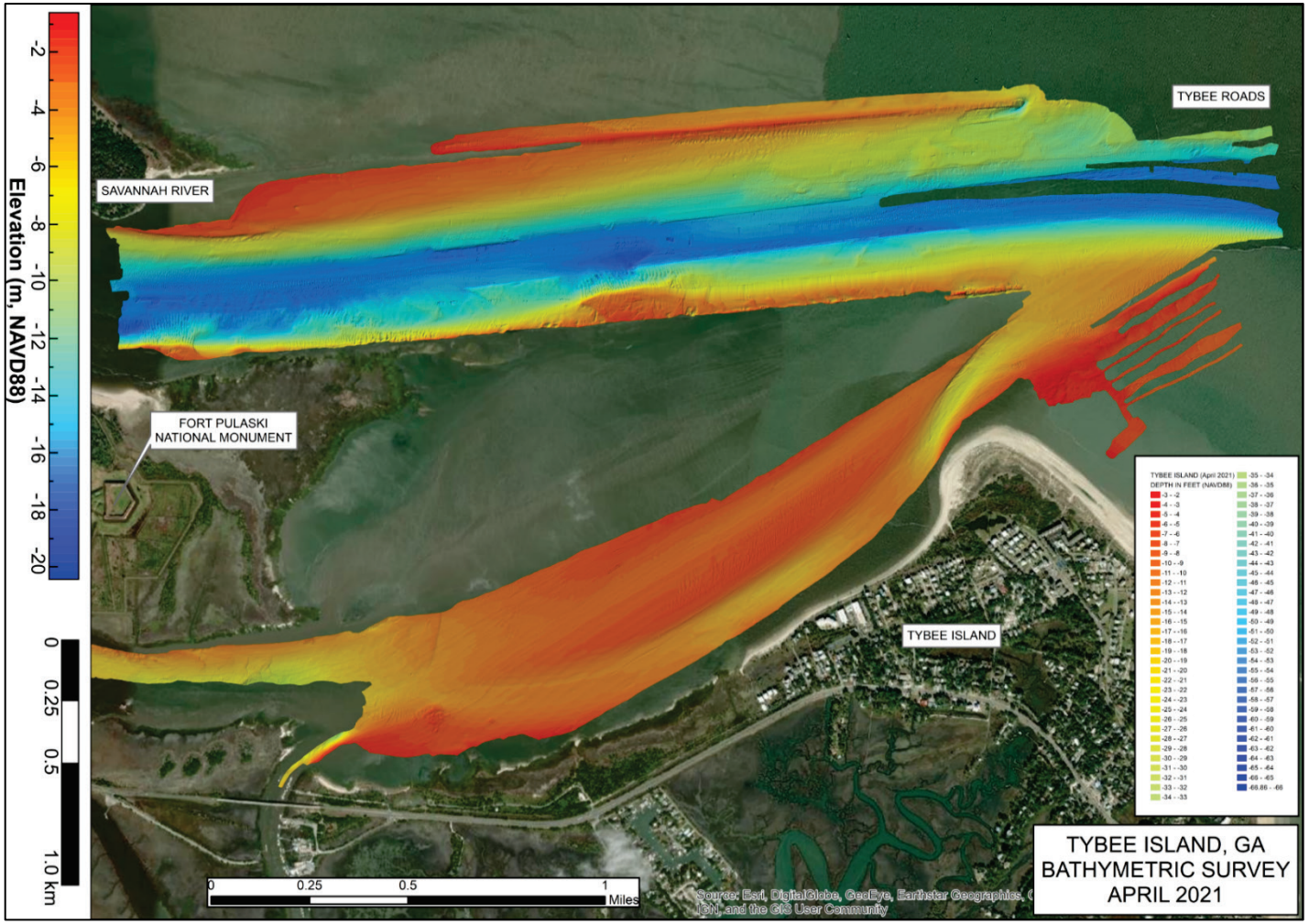

Figure 13. Bathymetric transects calculated from the April 2021 survey data. Subplot (a) shows a transect extending from Tybee's North Beach across the dredged navigation channel. Subplot (b) shows a transect from the south jetty to the north jetty. Transect positions appear as lines A-A' and B-B' in subplot (c). A larger version of subplot (c) with scale information appears in Figure 12.

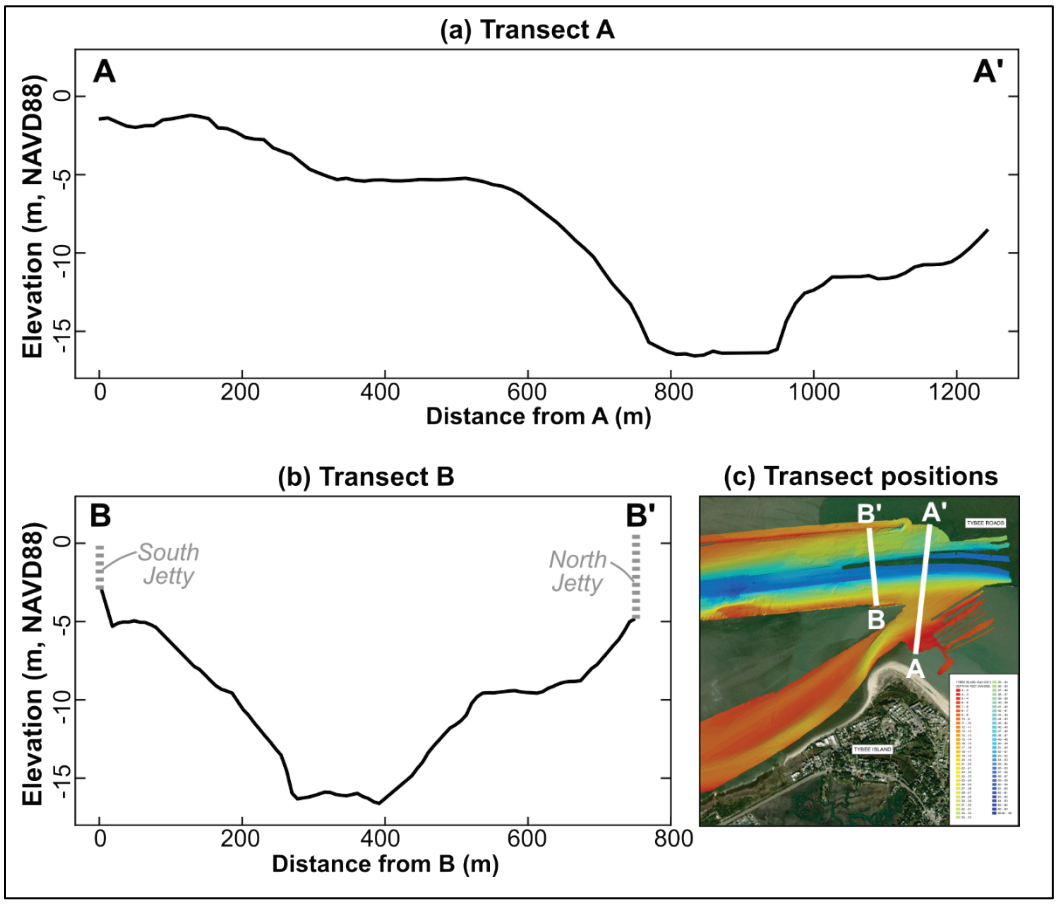

3.2 Wind wave conditions: general description

Wind wave conditions at the Coast Guard ranges are shown in Figure 14. As described in Section 2.6, the wind wave statistics were calculated after removing 5 min windows of data corresponding to each AIS-identified vessel closest approach, so Figure 14 should be interpreted as primarily representative of wind wave conditions with no vessel energy. During this study, the average and maximum significant wave heights at the shallow North Range sensor were $H_{m0} = 0.22$ m and $H_{m0} = 0.89$ m, respectively (thick dark blue line in Figure 14a). The Pearson correlation coefficient between nearshore and offshore wave heights was $R = 0.79$. However, offshore wave heights were substantially larger than the nearshore measurements, with the Gray's Reef NOAA buoy reporting a maximum value of $H_{m0} = 3.39$ m. Because the shallow North Range instrument was subaerially exposed at low tide, the measured values may not represent the

full breadth of wave conditions which occurred during the study. However, the measured wave height magnitudes are consistent with the SWAN[1] wave modeling results of Haas and Muscalus (2019), who display a maximum significant wave height of ~0.7 m near the Coast Guard ranges during a strong wind event.

The duration of available data may be increased by substituting wave measurements from the deep instruments when the shallow instruments are subaerially exposed or otherwise nonfunctional. These results are shown in Figure 14 as a thin light blue line for the North Range and a thin light green line for the South Range. For the combined shallow and deep datasets, the average significant wave height at the North Range is reduced to 0.21 m, while the maximum remains 0.89 m. At the South Range, the average significant wave height is again 0.21 m, and the maximum is 0.76 m. The reduction in maximum wave height at the South Range is likely due to the greater dependence on data from the deep instrument, which was more affected by pressure attenuation with depth despite the implementation of a dynamic pressure correction during post-processing (see Section 2.6).

Peak period at the shallow North Range sensor was between $T_p = 2.0$ and 9.9 sec (Figure 14b), with an average T_p of 5.0 sec. When data from the deep North Range sensor are substituted for missing data from the shallow sensor, the average T_p is reduced to 4.9 sec. The average T_p for the combined shallow and deep South Range sensors was slightly larger at 6.1 sec. No correlation was observed between nearshore and offshore measurements of T_p ($R = 0.08$), although the reported offshore wave period was larger than nearshore period for 83% of hourly measurements taken at the shallow North Range sensor. This increase may indicate a relative amplification of short-period wind waves north of Tybee Island. Alternatively, although all wakes from AIS-equipped vessels were removed from the time series before calculating the wind wave statistics (see Section 2.6), removing all small vessel wakes was impossible because non-commercial vessels are not required to broadcast their position to AIS. Therefore, the smaller average values of T_p in the nearshore may be caused by the inclusion of higher-frequency wakes generated by small vessels.

[1] Simulating waves nearshore

Figure 14. Time series of (a) wave height and (b) wave period at the Coast Guard navigation ranges near Tybee Island. Offshore wave conditions from Figure 11 are shown in gray for comparison.

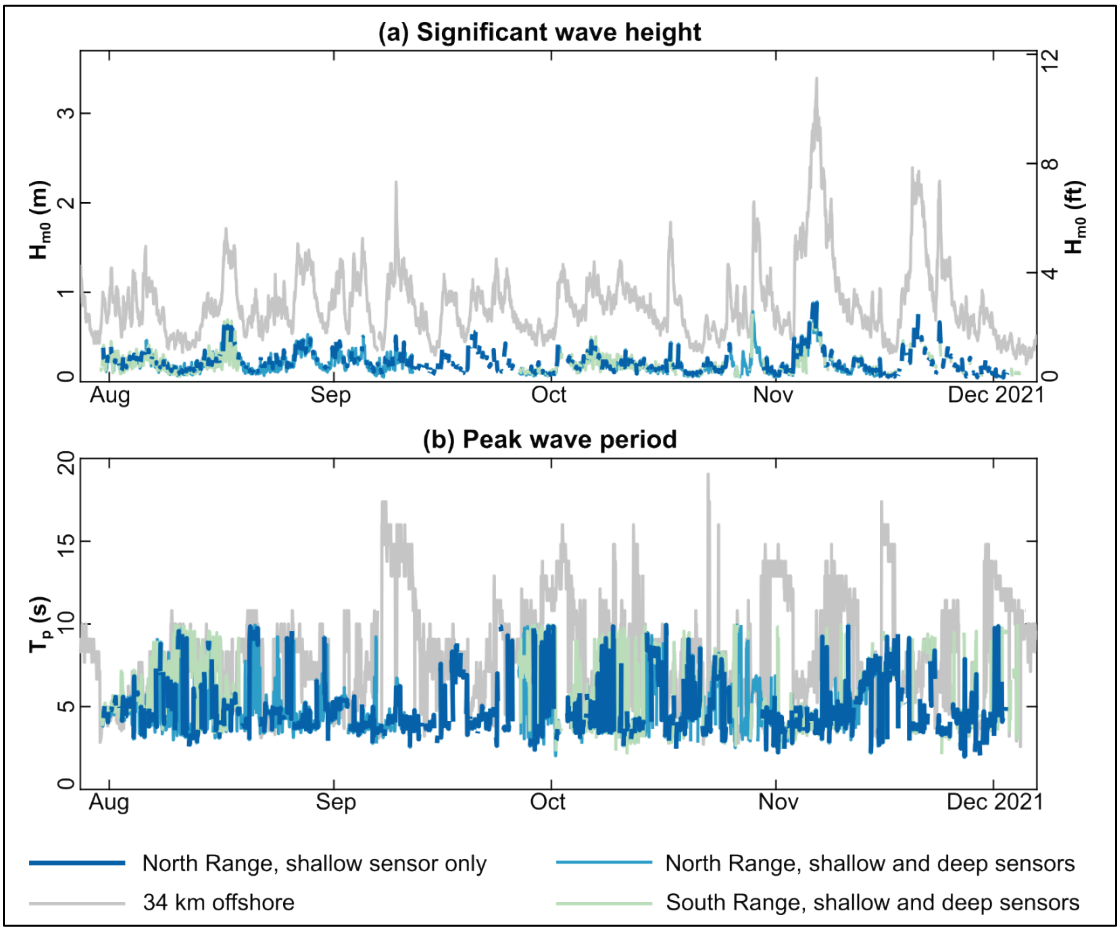

3.3 Vessel types and operating conditions

The distribution of vessel types by class is shown in Figure 15. In this figure, a *vessel passage* is defined as a single inbound or outbound trip separated from the previous trip by at least 10 min, so a single ship traveling roundtrip to the Port of Savannah will generate two vessel passages. The dataset is dominated by cargo ships; AIS recorded 1,386 cargo ship passages between 30 July 2021 00:00 UTC and 5 December 2021 00:00 UTC. A total of 202 tanker passages were recorded by AIS during the same period of record. Analysis of the North Range and South Range pressure data identified an additional 19 drawdown events which lack a corresponding AIS record. These events were possibly generated by cargo ships or tankers, but no AIS data exist either due to malfunction of the AIS receiver or because the ships were not broadcasting their position. Among the smaller vessels, pilot boats passed Tybee Island most

frequently, with 1,268 passages recorded by AIS. Relatively few vessels were recorded for the other vessel classes, but many of these classes are likely undercounted because privately owned, noncommercial vessels are not required to broadcast an AIS signal.

Figure 15. Distribution of vessel types for all vessels passing Tybee Island between 30 July 2021 00:00 UTC and 5 December 2021 00:00 UTC. *Unknown large vessels are vessels which generated visible drawdown but lack corresponding AIS data.

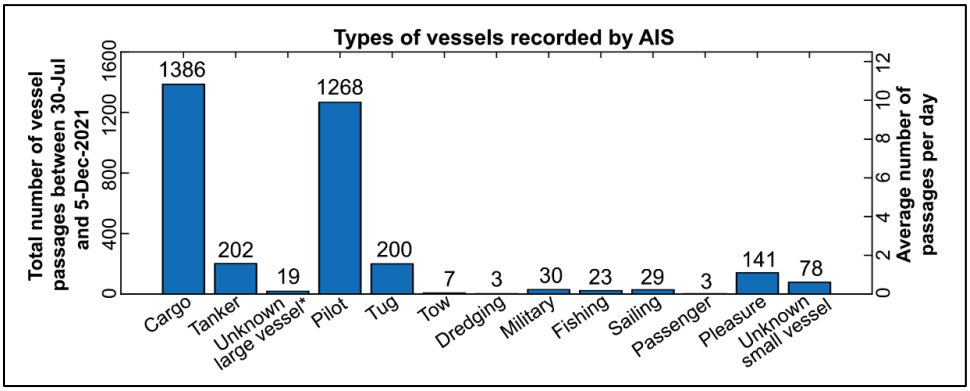

Figure 16. Minimum, average, and maximum number of cargo ship and tanker passages on each day of the week. "SEM" is the standard error of the mean.

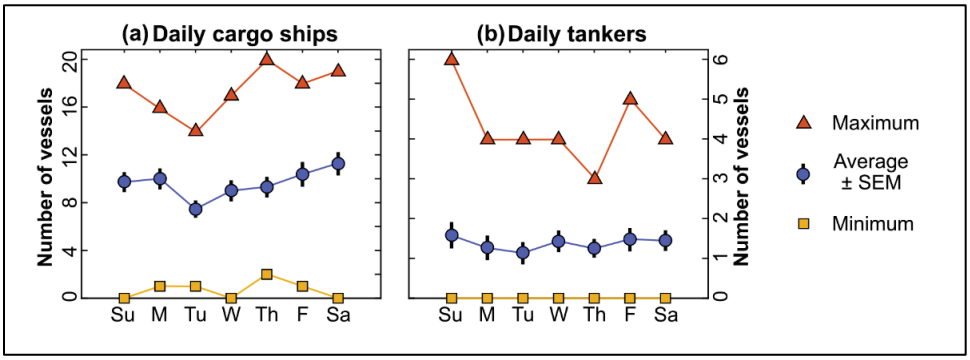

Figure 17. Average number of cargo ship and tanker passages during each hour of the day. Error bars indicate the standard error of the mean.

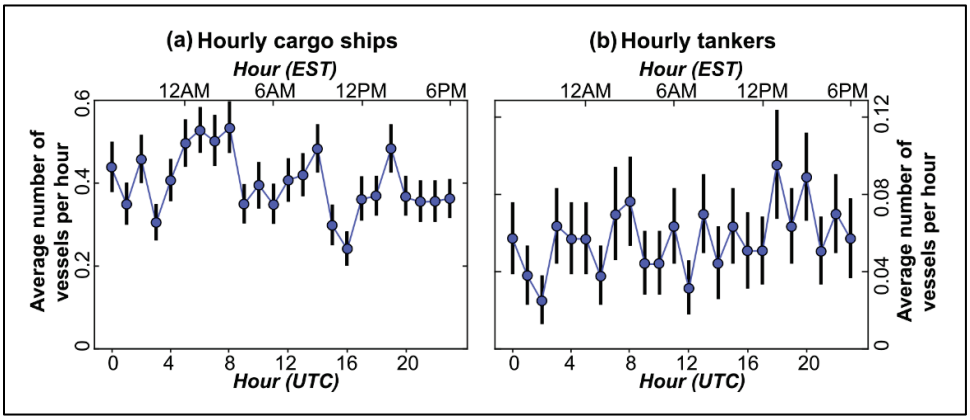

For beachgoer safety, considering whether large vessels pass most frequently on particular days of the week or at particular times of day is informative. This analysis is shown in Figure 16 and Figure 17. The maximum number of cargo ships to pass on a single day was 20 on Thursday, 26 August 2021 (Figure 16a), while the maximum number of tankers on a single day was 6 on Sunday, 14 November 2021 (Figure 16b). Tuesdays tended to have the fewest large vessel passages, with an average of eight cargo ships and one tanker. Large vessels were recorded passing Tybee Island during all 24 hr of the day, with no obvious preference for passages during daylight versus nondaylight hours (Figure 17).

Typical vessel speeds near Tybee Island depend on the vessel type and the direction of travel. The fastest-moving vessels were pilot vessels, which had a median speed of 17.2 m/sec (33.5 kn) and a maximum recorded speed of 20.4 m/sec (39.6 kn) at their closest approach to the South Range instruments (Figure 18a). The large vessels travel more slowly; cargo ships had a median speed of 6.9 m/sec (13.5 kn) and a maximum of 9.4 m/sec (18.3 kn) near the South Range, while tankers had a median speed of 6.1 m/sec (11.8 kn) and a maximum of 8.3 m/sec (16.1 kn). Further dividing the dataset into inbound and outbound passages indicates that there is a tendency for reduced speed when moving up-channel, although not all vessels adhere to this pattern (Figure 18b). The greatest direction-based reduction in typical speed occurs for inbound tankers, which had a median speed of 5.8 m/sec (11.3 kn) and a maximum of 7.6 m/sec (14.7 kn).

Large vessels pass Tybee Island under all tidal conditions. Figure 19 displays the USGS-reported flow velocity and NOAA-reported water level at Fort Pulaski at the time of the vessels' closest approach to the South Range instruments. Given the expansion of the channel as it nears open water, there is likely to be some difference in velocity magnitude between the two locations. However, the Fort Pulaski velocities are assumed to provide a reasonable approximation of the current direction within the entrance channel jetties. These data indicate that cargo ships and tankers traverse the entrance channel both with and against the current (indicated by the gray shaded region in Figure 19a and Figure 19b). The ships also display no preference for high- or low-tide travel, with recorded vessel passages occurring at all stages of the tidal cycle.

The AIS-recorded vessel tracks indicate a strong preference for large vessels to remain in the center of the authorized navigation channel.

Figure 20 displays a heat map of all cargo ship and tanker tracks passing Tybee Island, with the brighter colors indicating the most common ship positions. In this figure, the dashed black lines indicate the boundaries of the authorized channel, which is maintained to a depth of 14.9 m (49 ft) at low tide. A large majority of ships tracked near the channel centerline during the duration of the study.

Figure 18. (a) Distribution of vessel speed for various ship types at the point of closest approach to the South Range instruments. The boxes extend from the 25th to the 75th percentiles of the data, with the median indicated by the thick horizontal line. The whiskers are 1.5 times the interquartile range. (b) Distribution of vessel speeds for inbound versus outbound large ships at the point of closest approach to the South Range instruments.

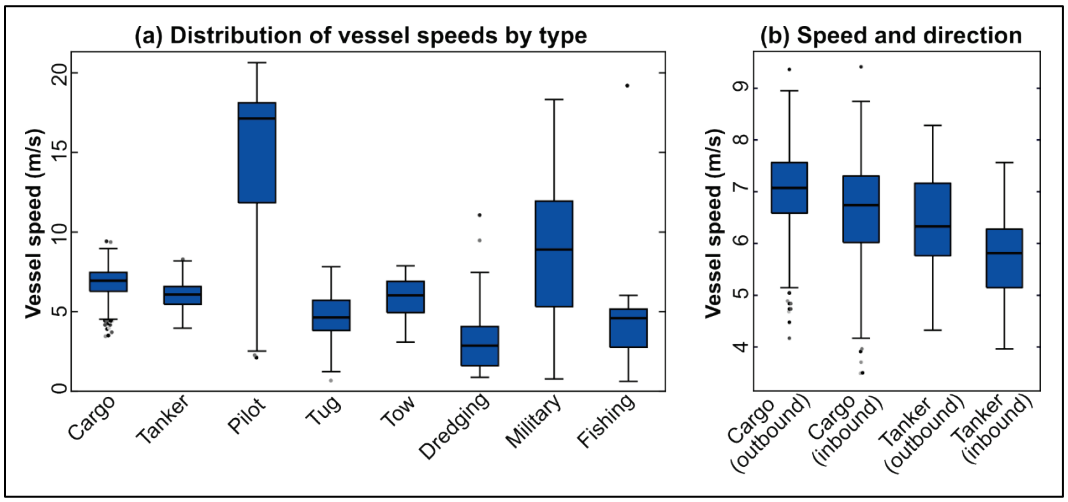

Figure 19. Flow velocity and water level at times of large vessel passage for all cargo ships and tankers. (a) Tide data corresponding to outbound ships. Vessels which plot within the gray shaded region are traveling against the current. (b) Tide data corresponding to inbound ships.

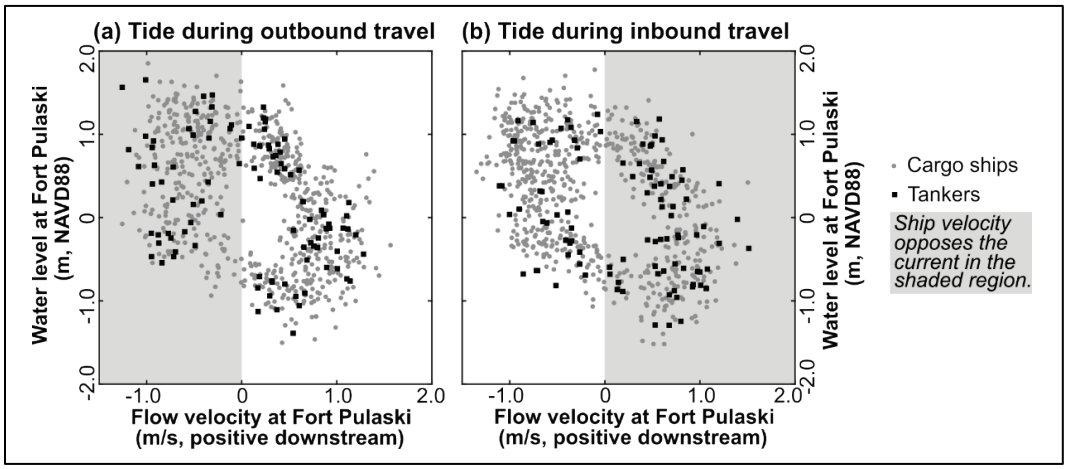

Figure 20. Heat map of cargo and tanker tracks in the navigation channel near Tybee Island over the full study duration. The boundaries of the authorized channel are shown as dashed black lines.

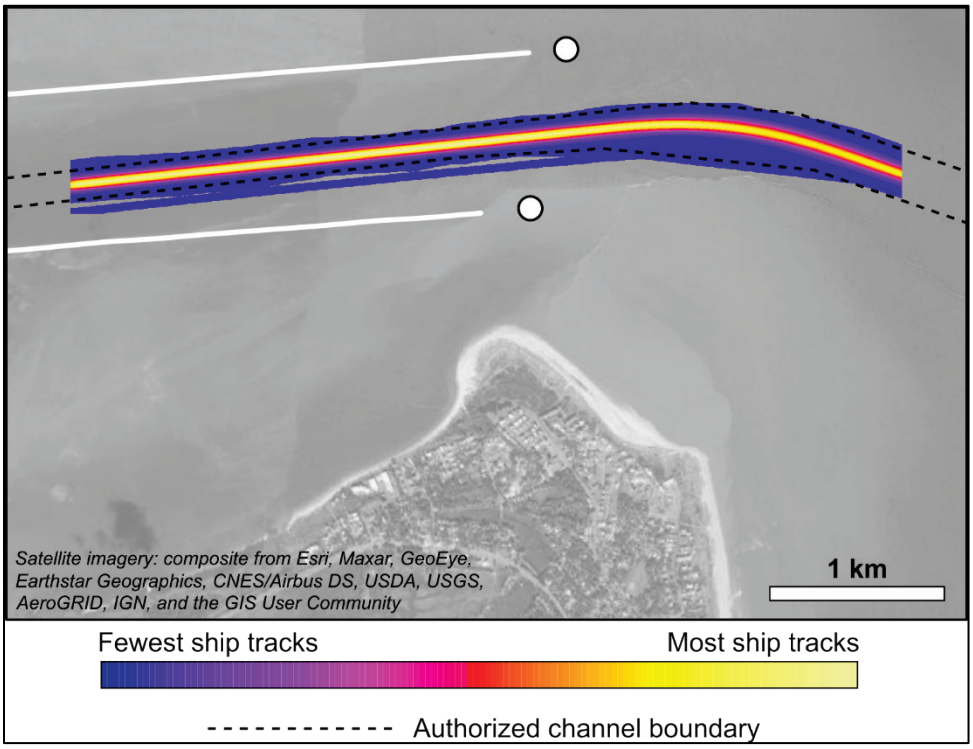

3.4 Large vessel wakes: general description

The results of the vessel wake analysis are summarized by vessel type in Figure 21. At the South Range, 65% of recorded cargo ships and 48% of recorded tankers generated wakes exceeding the 0.15 m wake height threshold[1]. At the North Range, 59% of recorded cargo ships and 50% of recorded tankers exceeded the 0.15 m wake threshold. Vessels exceeding the 0.15 m drawdown threshold included 60% of cargo ships and 3% of tankers at the South Range, along with 45% of cargo ships at the North Range. No tankers exceeded the drawdown threshold at the North Range. Very few pilot vessels or other small craft exceeded the wake height threshold at either instrument location (23% of pilot vessels and 17% of all other small vessels at the South Range; 16% of pilot vessels and 15% of all other small vessels at the North Range).

[1] Recall from Section 2.7 that the 0.15 m analysis threshold was selected because these were the smallest oscillations that could be distinguished over other surface elevation disturbances.

Figure 21. Summary of the number of vessels with wake height and drawdown magnitude exceeding the 0.15 m analysis threshold. Subplot (a) summarizes wake characteristics from the South Range, while subplot (b) summarizes wake characteristics from the North Range.

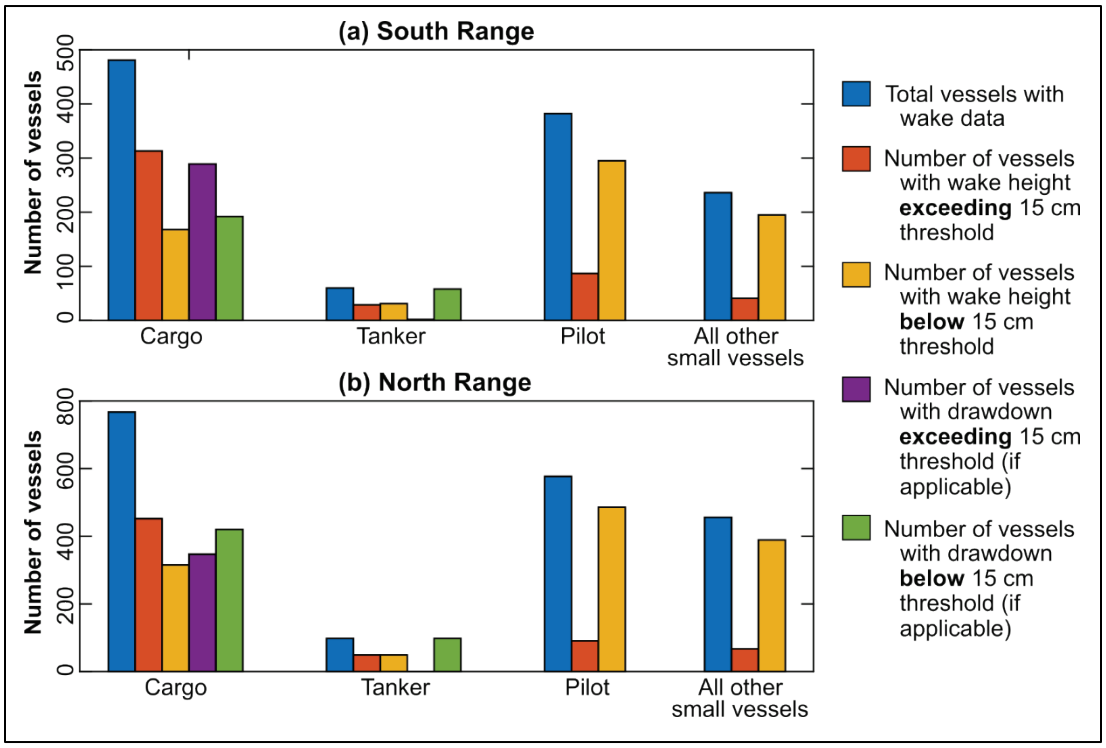

The tendency for larger drawdown at the South Range compared to the North Range is confirmed in Figure 22a. Although drawdown magnitude at the two instrument locations is strongly correlated (Pearson correlation coefficient $R = 0.82$), the measured drawdown is almost always larger at the South Range. Considering that drawdown magnitude is known to be inversely correlated with distance from the vessel (Almström and Larson 2020), the larger drawdown at the South Range may be related to the tendency for vessels to track closer to this position (*e.g.*, Figure 20). The North Range is also farther from the confined cross section between the north and south jetties, which may further reduce the locally generated drawdown magnitude.

Vessel wake heights at the two locations are less strongly correlated ($R = 0.57$), and there is no obvious tendency for larger wakes to occur preferentially at either location (Figure 22b). These results are unexpected considering that prior studies have observed wakes heights decreasing exponentially with distance from the ship (e.g., Johnson 1957; Nece et al. 1985; Macfarlane 2012; David et al. 2017). Since most large vessels

approach the South Range more closely than the North Range (e.g., Figure 20), more ships were expected to plot above the 1:1 line in Figure 22b. The absence of the anticipated behavior likely indicates that the existing methodology to quantify differences in wake height between the two sensor locations is insufficiently precise. The range of ship-to-sensor distances is also relatively small due to the narrow channel width; for example, a ship traversing the exact center of the navigation channel would have a closest approach of 350 m to the South Range and 400 m to the North Range. Resolving distance-dependent wake attenuation would likely be more achievable with greater horizontal offset. Alternatively, it is possible that faster ship velocities at the moment of closest approach to the North Range (e.g., Figure 9) locally increased the wake height relative to what was generated near the South Range.

Figure 22. Influence of measurement location on large vessel wake characteristics. (a) Comparison of drawdown magnitude at the South Range versus the North Range. Measured drawdown is strongly correlated at the two sites, but the magnitude is almost always larger at the South Range. (b) Comparison of peak wake height (i.e., the height of the largest oscillation in the wake) at the South Range versus the North Range. A weak correlation exists, but neither site experiences uniformly larger wakes.

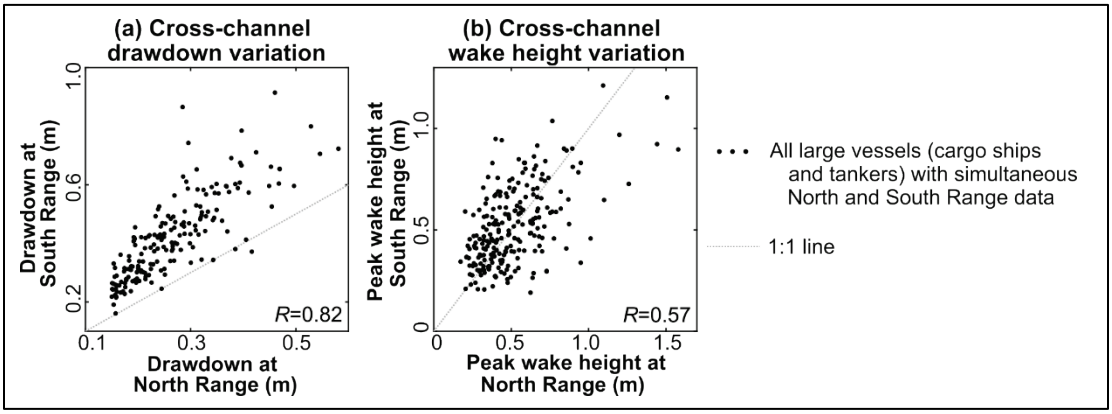

Drawdown is correlated with certain vessel characteristics, but the measurements have considerable scatter. Given two ships of varying length, the longer ship has a greater probability of producing a larger drawdown (Figure 23a). However, this behavior is not guaranteed; for example, ships ranging between 180 and 360 m long generated drawdown at or below the 0.15 m analysis threshold. Similarly, given two ships of varying beam, the wider ship is more likely to generate a larger drawdown (Figure 23b), but this correlation is not guaranteed. Little correlation is observed between design draft (Figure 23c) or vessel speed (Figure 23d) and drawdown magnitude. Concerning the former, the absence of a relationship may result from the unavailability of real-time draft data, since a ship's actual draft

while passing the instruments may differ from its design draft. Note that Figure 23 displays data only from the North Range; the results from the South Range (Figure 24) are qualitatively similar.

Figure 23. Relationships between (a) ship length and drawdown magnitude, (b) ship beam and drawdown magnitude, (c) design draft and drawdown magnitude, (d) vessel speed and drawdown magnitude, (e) ship length and wake height, (f) ship beam and wake height, (g) design draft and wake height, and (h) vessel speed and wake height. All wake data are from the North Range. Only cargo ships and tankers are plotted; note that no tankers generated a drawdown at the North Range exceeding the 0.15 m threshold for analysis.

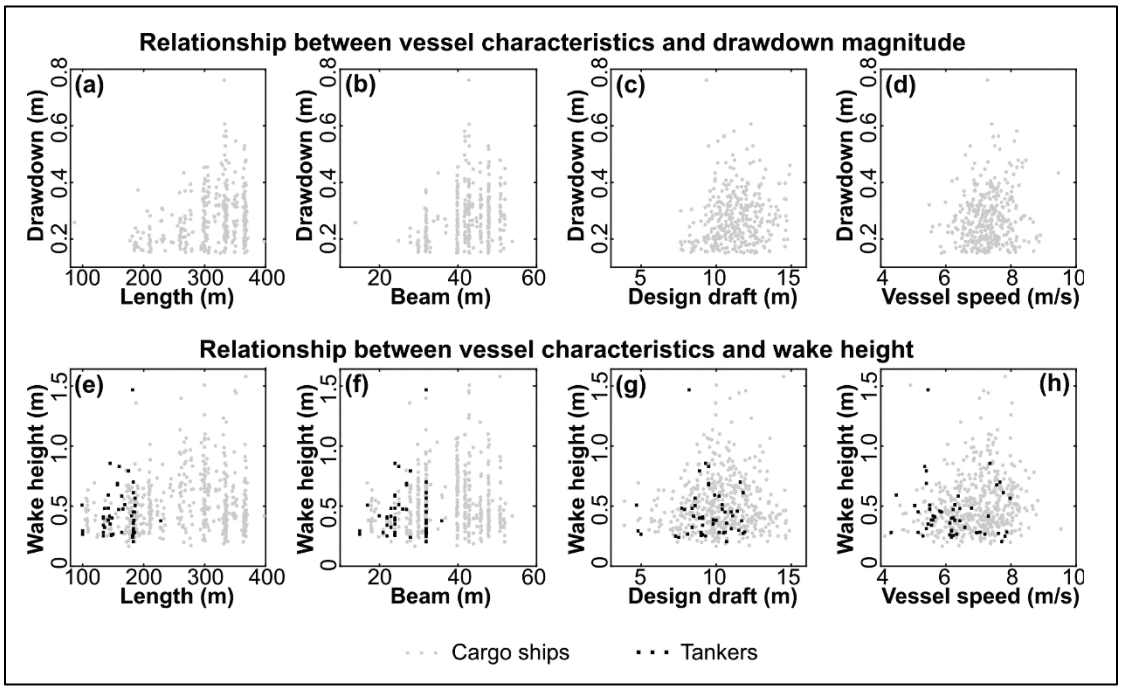

The relationships between vessel length and wake height (Figure 23e) and between vessel beam and wake height (Figure 23f) are similar to those observed for drawdown but with more scatter. Increasing the length or beam of a vessel increases the probability of a larger wake, but vessels of all sizes were also observed to generate wakes at or below the 0.15 m height threshold for analysis. The correlation between design draft and wake height is weak (Figure 23g), although an interesting note is that wake heights remain relatively small for design drafts below approximately 7 m, above which there is a marked increase in the probability of a larger wake occurring. Little correlation is observed between vessel speed and wake height (Figure 23h).

Figure 24. Same as Figure 23, but using water level measurements from the South Range.

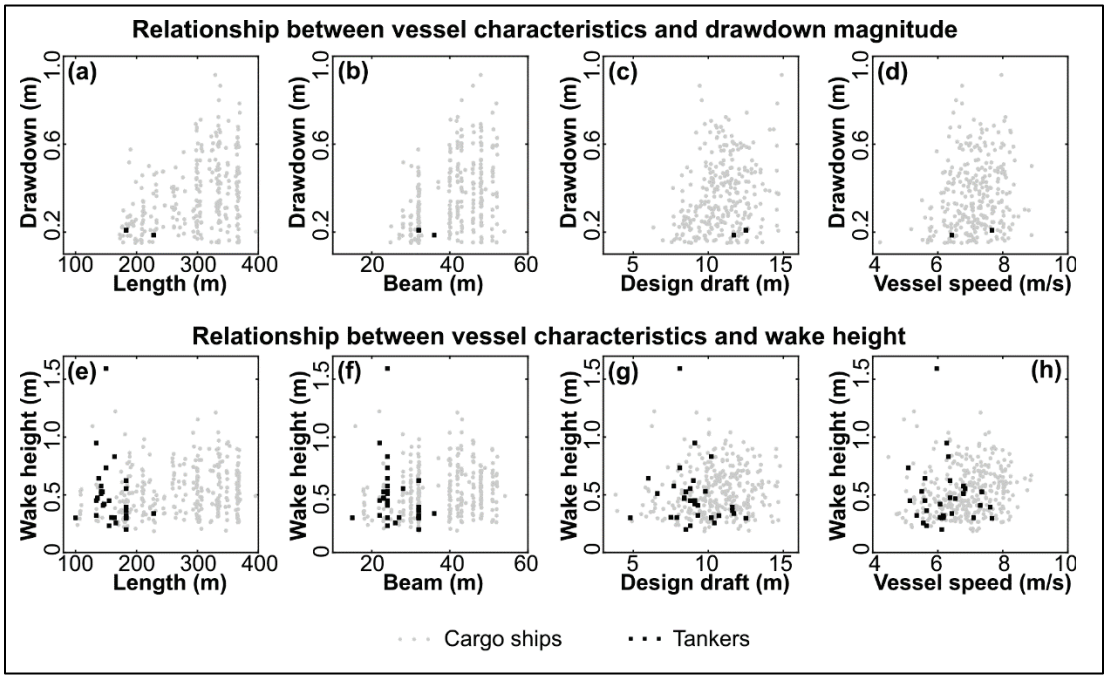

Various studies have attempted to derive predicted equations for drawdown magnitude based on ship dimensions, channel geometry, and velocity. One such equation was proposed by Schijf (1949):

$$H_D = \frac{v^2}{2g}\left[\left(\frac{A_c}{A_c - B \cdot D}\right) - 1\right], \tag{11}$$

where H_D is the drawdown magnitude, v is the ship velocity, g is gravitational acceleration, A_c is the channel cross-sectional area, B is the ship beam, and D is the ship draft. Almström and Larson (2020) later evaluated a compilation of published drawdown equations and determined that the best-performing formula was

$$H_D = 0.22\left(\frac{v^2}{2g}\right)\left(\frac{v}{\sqrt{gR_c}}\right)^{0.42}\left(\frac{B}{X}\right)^{0.85}\left(\frac{B}{W_c}\right)^{0.32}\left(\frac{D}{R_c}\right)^{1.46}\left(\frac{L}{D}\right)^{0.80}, \tag{12}$$

where L is the ship length, R_c is the channel hydraulic radius, W_c is the channel top width, and X is the distance between the ship and the measurement location. To evaluate Equations 11 and 12 for measurements collected near Tybee Island, the channel cross-sectional area $A_c(z)$ was calculated using Equation 9. The wetted perimeter $P_c(z)$ was calculated

using Equation 10, and the hydraulic radius was calculated as $R_c(z) = A_c/P_c$. The channel top width W_c was taken as a constant 747 m (*i.e.*, the distance between the jetties; see Figure 13b). The remaining variables were obtained from the AIS data, with X and v representing conditions during the vessel's closest approach to either the North Range or the South Range.

Figure 25. Predicted drawdown based on the equations of Schijf (1949, subplots a and b) and Almström and Larson (2020, subplots c and d). The Almström and Larson equation incorporates more physical parameters than the Schijf equation, but the improvement in correlation between measured and modeled drawdown is small.

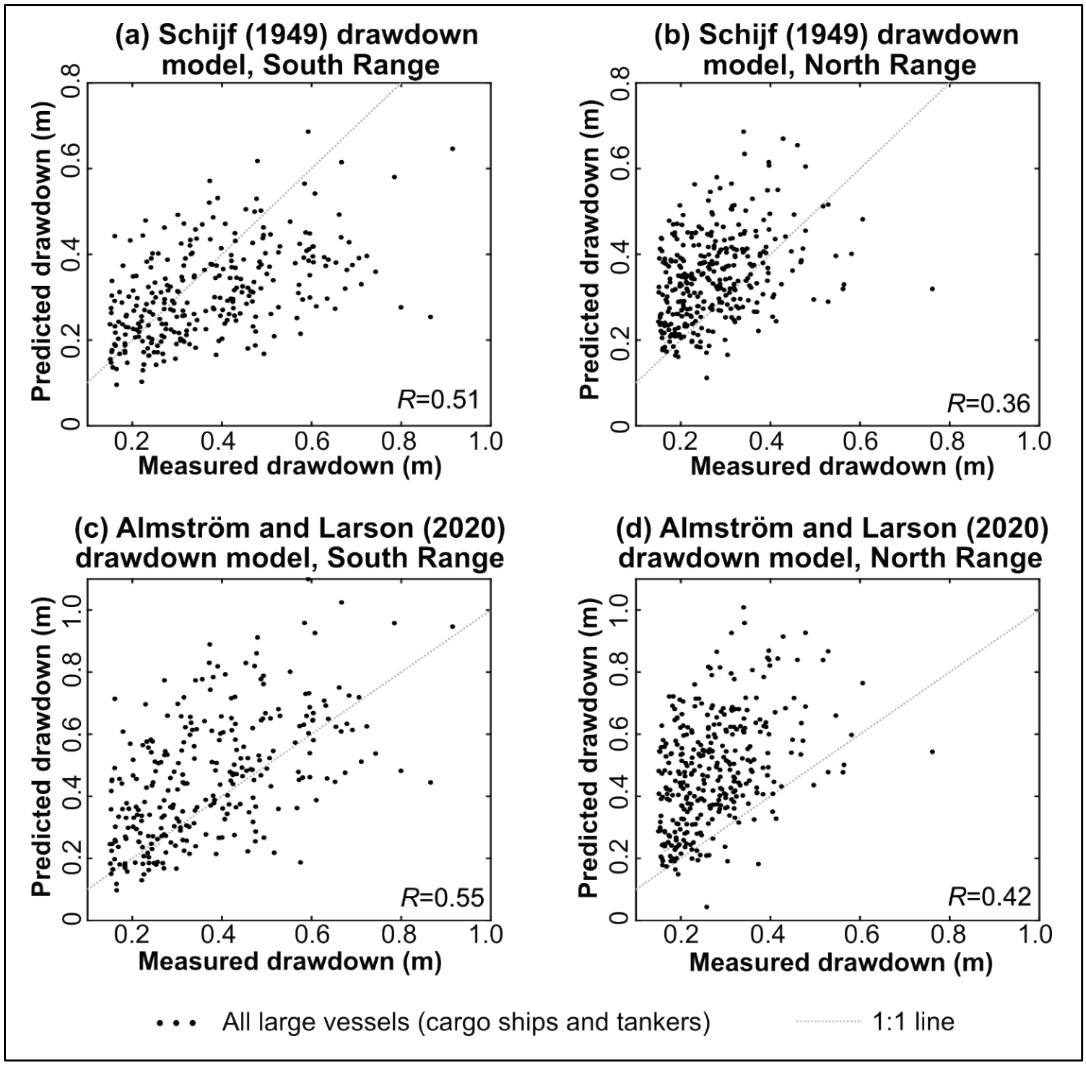

The results of the theoretical drawdown models are shown in Figure 25. At the South Range, the predictions of Schijf's (1949) equation are weakly correlated with measured drawdown; the correlation coefficient is $R = 0.51$. Equation 11 performs poorly at the North Range, with a correlation $R = 0.36$ between measured and modeled drawdown. The poor

performance may result from substituting design draft for real-time draft measurements, which were unavailable at the time this report was published. Using Almström and Larson's (2020) equation leads to a small improvement in the predictions, with $R = 0.55$ at the South Range and $R = 0.42$ at the North Range. Considering that Equation 12 incorporates a greater number of physically relevant parameters than Equation 11, such as vessel length L and distance to the instrument X, the Almström and Larson (2020) model not offering a more substantial increase in predictive ability is surprising. This unexpected prediction behavior may again result from the necessary substitution of design draft for real-time draft. The positively biased predictions at the North Range may also be related to the relatively greater distance from the confined region between the jetties. Because the top width of the channel W_c appears in the denominator of Equation 12, the drawdown predictions would fall closer to the 1:1 line if W_c were increased to account for the flow expansion at the end of the jetties. However, the literature does not clearly explain how the drawdown equations should be adapted for the scenario in which a confined channel transitions into a wide bay.

3.5 Comparison of energy from wind-generated and vessel-generated waves

As a next step in the analysis, the total energy generated by wind waves over the duration of the study was compared to the total energy generated by all vessels. This comparison provides insight into the relative erosional potential of the two wave sources. Summing the available samples of wind-wave generated $\bar{P}$ (Equation 6) based on data from the shallow North Range sensor generates a cumulative energy of $E_{tot} = 1.13 \times 10^6$ kJ/m over 1,164 hr (see Line C of Table 1), which is approximately one-third of the total study duration due to the instrument's exposure at low tide. Assuming that wave statistics over the full study duration conform to the same probability distribution as the sampled wave statistics, the average measured energy flux may be treated as representative of typical wave conditions when the instrument was not recording data. Based on this assumption, the cumulative energy from wind waves during the full study duration linearly scales to $E_{tot} = 2.99 \times 10^6$ kilojoules of energy per meter length of shoreline (kJ/m; Table 1, Line E).

Table 1. Summary of energy from wind waves.

Value	North Range (upper sensor only)	North Range (upper and lower)*	South Range (upper and lower)*
A. Total # hours in study period†	3,072	3,072	3,072
B. # hours with wave measurements	1,164	2,181	1,301
C. Total energy for measured hours (kJ/m)	1.13×10^6	1.89×10^6	1.21×10^6
D. Mean energy per measured hour‡ (kJ/m/hr)	974.0	867.2	929.1
E. Energy for entire study period¶ (kJ/m)	2.99×10^6	2.66×10^6	2.85×10^6

*The upper instrument is used preferentially to minimize the impacts of pressure attenuation with depth. When the upper instrument is subaerially exposed or otherwise nonfunctional, data from the lower instruments are substituted.

†The study period is defined as 30 July 2021 00:00 UTC to 5 December 2021 00:00 UTC.

‡Calculated as Row C ÷ Row B.

¶Calculated as Row D × (Row A − Row B) + Row C.

To increase the number of hourly samples, $\bar{P}$ and E_{tot} can alternatively be calculated by substituting measurements from the deep sensor when the shallow sensor was subaerially exposed or otherwise nonfunctional. Performing the calculations with more data serves as a check on the above assumption that unmeasured wave conditions may be approximated by the average statistics of the sampled waves. At the North Range, including deep sensor data raises the number of hourly wave measurements to 2,181 (71% of the total study duration) but has the drawback of introducing data that may be more affected by depth attenuation. The measured value of E_{tot} over 2,181 hr is 1.89×10^6 kJ/m, which scales to $E_{tot} = 2.66 \times 10^6$ kJ/m for the full study duration (Table 1). The reduction in cumulative energy relative to the shallow North Range sensor is likely a consequence of uncertainty in the dynamic pressure correction for the deep instrument. Repeating this procedure for the South Range instruments produces an estimated total energy of 2.85×10^6 kJ/m over the full study duration (Table 1). The similar magnitude of the three total energy estimates in Table 1 increases confidence that the assumptions underlying these calculations are justified and that the magnitude of the total energy from wind waves has been accurately represented.

Analogous calculations for the vessel-generated waves are summarized by vessel type in Table 2. Considering data from just the shallow North Range instrument, the cumulative energy from cargo ships (Equation 8) was determined to be 6.92×10^4 kJ/m when extrapolated to the full study duration based on the average energy of measured cargo ships (Table 2, Row E1). The next-highest energy contribution came from pilot vessels at 1.28×10^4 kJ/m, followed by tankers at 7.66×10^3 kJ/m, other small vessels at 3.37×10^3 kJ/m, and then the unknown large vessels (i.e., cargo ships or tankers with no AIS record) at 8.66×10^2 kJ/m. If data from the deep North Range instrument are included to increase the number of samples, the estimated energy contributions from all vessel classes

decreases slightly. Repeating this analysis using data from the upper and lower South Range instruments generates estimated total energy contributions of 7.62×10^4 kJ/m from cargo ships, 9.36×10^3 kJ/m from tankers, 6.63×10^3 kJ/m from pilot vessels, 1.60×10^3 kJ/m from all other small vessels, and 2.93×10^2 kJ/m from unknown large vessels.

Table 2. Summary of energy from vessel wakes.

Value	North Range (upper sensor only)	North Range (upper and lower)*	South Range (upper and lower)*
A1. Total # cargo ships in study period†	1,386	1,386	1,386
B1. # cargo ships with usable wake measurements	497	769	481
C1. Total energy for measured cargo ships (kJ/m)	2.48×10^4	3.63×10^4	2.64×10^4
D1. Mean energy per measured cargo ship‡ (kJ/m/vessel)	49.9	47.1	55.0
E1. Energy for all cargo ships in study period¶ (kJ/m)	6.92×10^4	6.53×10^4	7.62×10^4
A2. Total # tankers in study period†	202	202	202
B2. # tankers with usable wake measurements	55	98	60
C2. Total energy for measured tankers (kJ/m)	2.08×10^3	2.96×10^3	2.78×10^3
D2. Mean energy per measured tanker‡ (kJ/m/vessel)	37.9	30.2	46.4
E2. Energy for all tankers in study period¶ (kJ/m)	7.66×10^3	6.09×10^3	9.36×10^3
A3. Total # unknown large vessels in study period†	19	19	19
B3. # unknown large vessels with usable wake measurements§	7	15	13
C3. Total energy for measured unknown large vessels (kJ/m)	3.19×10^2	4.69×10^2	2.01×10^2
D3. Mean energy per measured unknown large vessel‡ (kJ/m/vessel)	45.6	31.3	15.4
E3. Energy for all unknown large vessels in study period¶ (kJ/m)	8.66×10^2	5.95×10^2	2.93×10^2
A4. Total # pilot vessels in study period†	1,268	1,268	1,268
B4. # pilot vessels with usable wake measurements	425	767	460
C4. Total energy for measured pilot vessels (kJ/m)	4.28×10^3	7.62×10^3	2.41×10^3
D4. Mean energy per measured pilot vessel‡ (kJ/m/vessel)	10.1	9.9	5.2
E4. Energy for all pilot vessels in study period¶ (kJ/m)	1.28×10^4	1.26×10^4	6.63×10^3
A5. Total # other small vessels in study period†	514	514	514
B5. # other small vessels with usable wake measurements	168	285	169
C5. Total energy for other measured small vessels (kJ/m)	1.10×10^3	1.27×10^3	5.25×10^2
D5. Mean energy per other measured small vessel‡ (kJ/m/vessel)	6.6	4.5	3.1
E5. Energy for all other small vessels in study period¶ (kJ/m)	3.37×10^3	2.30×10^3	1.60×10^3

*The upper instrument is used preferentially to minimize the impacts of pressure attenuation with depth. When the upper instrument is subaerially exposed or otherwise nonfunctional, data from the lower instruments are substituted.

†The study period is defined as 30-Jul-2021 00:00 UTC to 5-Dec-2021 00:00 UTC.

‡Calculated as Row C ÷ Row B for each block of measurements.

¶Calculated as Row D × (Row A − Row B) + Row C for each block of measurements.

§Because the unknown large vessels were identified from visible drawdown events in the North or South Range data, all unknown large vessels technically have wake data. However, individual vessels' energy measurements were discarded if another vessel also passed the sensors during the same 5-minute window because the automated wake identification routine could not consistently distinguish between the two vessel signatures.

The calculations used to produce the values listed in Table 1 and Table 2 are visually summarized in Figure 26. Regardless of which instrument or combination of instruments is considered (i.e., shallow North Range sensor alone, combination of shallow and deep North Range instruments, or combination of shallow and deep South Range instruments), wind-generated waves are found to generate approximately 97% of total wave energy acting on the beach, while vessel-generated waves contribute the remaining 3%. The relative proportions of vessel-generated energy are also reasonably consistent for the different combinations of instruments (Figure 26, second row). Cargo ships contribute between 74% and 81% of the vessel-generated energy, while tankers contribute between 7% and 10%, and the unknown large vessels contribute less than 1%. Pilot vessels were found to contribute between 7% and 14% of the vessel-generated energy, with the remaining 2% to 4% generated by other small vessels.

Figure 26. Relative proportions of wind and vessel-generated wave energy based on data from (a) the upper North Range sensor, (b) the upper and lower North Range sensors, and (c) the upper and lower South Range sensors. Note that percentages may not sum to 100% due to rounding. *The upper instrument is used preferentially to minimize the influence of depth attenuation. Data from the lower instrument are substituted when the upper instrument is exposed or otherwise nonfunctional. †Unknown large vessels are vessels which generated a large drawdown event but lack corresponding AIS data. These are most likely cargo ships or tankers.

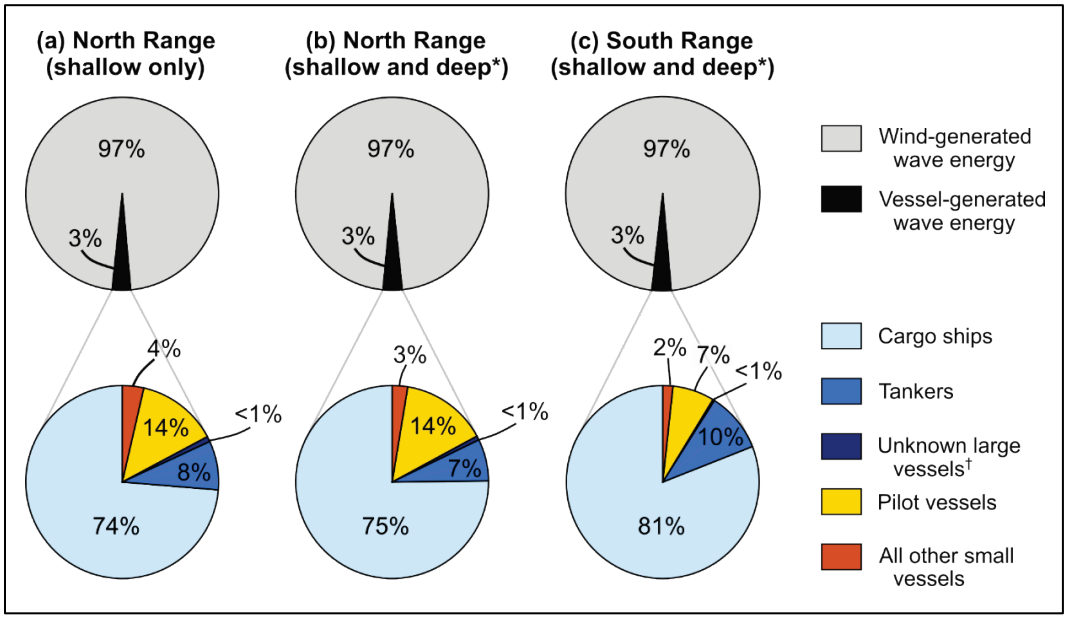

Similar energy budget analyses have been performed during several previous studies of the Savannah entrance channel. The relative proportions of wind-generated and vessel-generated wave energy in Figure 26 are comparable to results from Houser (2010), who determined that vessel-generated wakes were responsible for 5% of total energy near Fort Pulaski. In contrast, Haas and Muscalus (2019) estimated that 68% of total energy is generated by vessel wakes at Bird-Long Island, which is upstream of Fort Pulaski (see location, Figure 1). Considering the greater fetch near Tybee Island, a larger proportion of wind wave energy is physically reasonable for measurements collected at the North Range and South Range, so the two sets of results are not necessarily contradictory. The results of the present study also do not appear to agree with the findings of Mosely (2018), who concluded that wake events act on the beach with 10 times more energy than wind waves. However, there are considerable differences between the methodological approaches of Mosely's (2018) study versus the present study. Mosely (2018) focused on the energy generated by long-period uprush, whereas the results in Figure 26 are based on energy from shorter-period bow or secondary waves (Figure 3). In addition, Mosely (2018) did not consider that wind wave energy acts continuously on the beach whereas vessel-generated waves are ephemeral events with limited temporal duration.

One possible consideration related to the accuracy of Figure 26 is the quality of the AIS record, which was used to define the windows of data that were included in the vessel wake analysis. Large vessels with no AIS record were also identified based on visible drawdown and added to the dataset as *unknown large vessels* (Figure 15 or Table 2). However, as previously seen in Figure 21, 40% of measured cargo ships and 97% of measured tankers generated no measurable drawdown at the South Range, while 55% of measured cargo ships and 100% of measured tankers generated no measurable drawdown at the North Range. This behavior suggests that there may be additional large vessels that have been omitted from the calculated total energy.

Figure 27. Time series of the daily number of large vessel passages and pilot vessel passages over the duration of the study. The large vessel count includes cargo ships, tankers, and unknown large vessels that generated measurable drawdown.

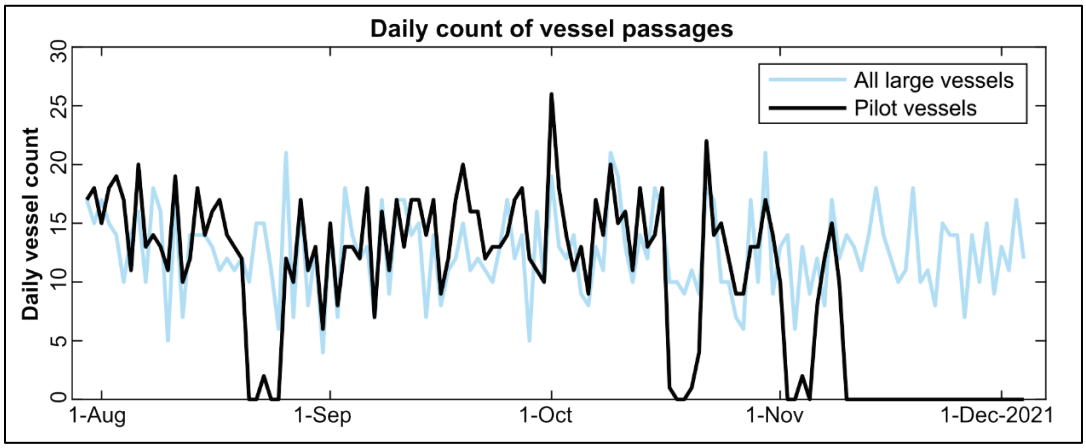

Moreover, because small vessels do not generate drawdown, any small vessels which lacked an AIS record were also omitted from the summation of total vessel energy. Of particular concern is the observation that the number of pilot vessel passages (1,268) is smaller than the number of large vessel passages (1,386 cargo ships, 202 tankers, and 19 unknown large vessels for a total of 1,607). Examining a time series of vessel counts by day (Figure 27) reveals that no pilot vessels were recorded by AIS after the first week of November, although at least seven large vessels transited the entrance channel each day of November and early December. Consequently, pilot vessels likely generated a greater amount of wake energy than what appears in Figure 26.

To determine the upper limit of potential error introduced by missing vessels in the AIS record, the energy calculations were repeated by increasing the number of vessels according to the following assumptions:

1. Using the relative proportions of vessels that did and did not generate measurable drawdown at the North Range (Figure 21), an additional 23 cargo ships and 5 tankers are assumed to have passed with no AIS record during the 2,181 hr in which the North Range instruments were recording (Table 1). Over the full 3,072 hr study duration, this additional vessel traffic linearly scales to a total of 66 vessels in the unknown large vessel class (Row A3 of Table 2).
2. Two pilot vessel passages (outbound and inbound) are assumed for each large vessel passage. Specifically, Row A4 of Table 2 increases from 1,268 to 3,308 total pilot vessel passages.

3. In the absence of another method for determining the actual number of other small vessel passages, Row A5 of Table 2 increases from 514 to 1,341 vessels, mimicking the percent increase in the number of pilot vessels.

As in the previous calculations, each unmeasured vessel is assumed to generate a wake energy equal to the mean energy from the measured vessels in that class. The updated vessel energy percentages are shown in Figure 28. Due to the assumed increase in the number of unknown large vessels, pilot vessels, and other small vessels, the relative proportions of vessel energy generated by each vessel class differ when compared to the lower row of Figure 26. In particular, the percentage of vessel energy attributed to pilot vessels is now between 16% and 29%. However, despite significantly increasing the total number of vessels passing Tybee Island, wind waves are still estimated to generate 96% of total energy acting on the beach (Figure 28). In combination with the knowledge that the individual vessels' energy is already overestimated by Equation 8, a reasonable conclusion is that the incomplete AIS record has limited influence on the energy balance calculations and the overall conclusions of this study.

Figure 28. Upper limit of potential error due to missing vessels in the AIS record. Although the relative proportions of vessel energy attributed to the different vessel classes vary when compared to Figure 26, there is minimal variation in the percentage of total energy attributed to vessel-generated versus wind-generated waves.

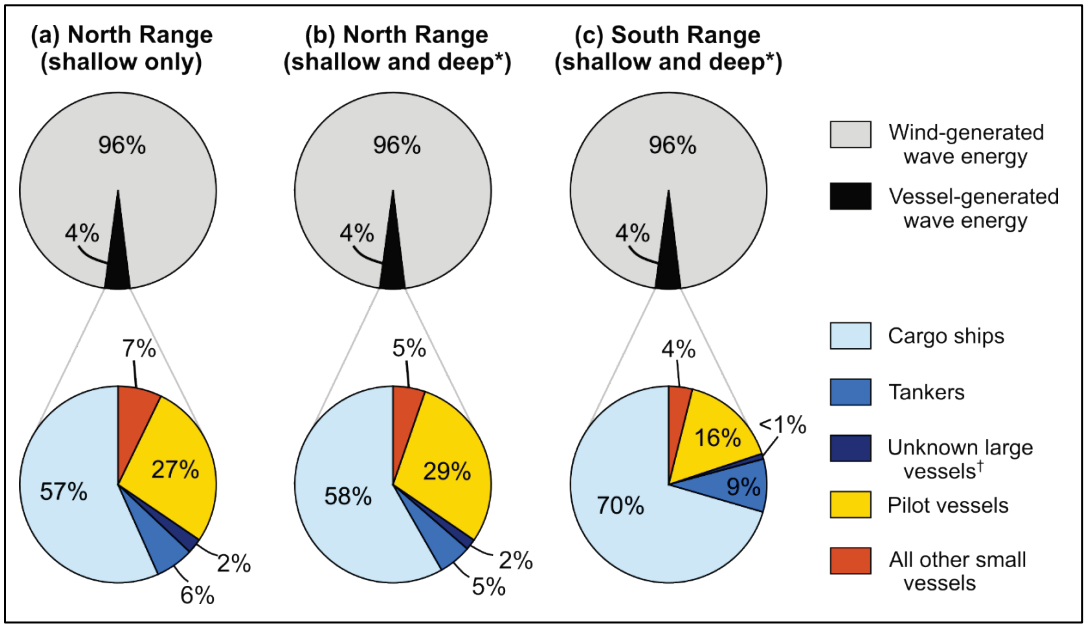

3.6 Statistical analysis of ship wave characteristics

The South Range monitoring station is positioned to capture all wakes originating from commercial vessels operating in the navigation channel that eventually arrive at Tybee Island. The distribution of the drawdown amplitude for all data collected at the South Range were extracted from the pressure records as described above. The half-wave period was determined by measuring the time interval between the point where the water level begins to drop as the drawdown approaches and the minimum water level (drawdown trough). Expressed as a percentage, the distribution of the drawdown indicates that half the occurrences are less than 0.31 m and 90% are less than 0.55 m (Figure 29). The median half-period, which gives an indication of the duration of the drawdown, is 54 sec. Ninety percent of the half-period is less than 72 sec. The secondary waves have a mean wave height of 0.4 m and 90% are less than 0.6 m. The mean wave period is 4.1 sec (Figure 30).

Because the magnitude of the uprush is a function of the height of the incoming vessel-generated waves, the data have been evaluated in terms of the statistical percentiles to identify the vessel characteristics most correlated to the measured wave heights. Considering that the highest waves are the primary source of uprush, the data have been grouped into the 95^{th}, 75^{th}, and 50^{th} percentiles. Vessel length and beam show a consistent trend with the drawdown and secondary waves (Figure 31). This trend supports the generally-accepted idea that the highest waves are generated by the longest and widest vessels. The lack of an overall positive trend between wave height and vessel speed is consistent with the results for the full dataset (Figure 23d and Figure 23h). This is likely due to the small speed range of commercial vessels. However, there is a marked decrease in the average drawdown and secondary waves when the speed is below 6.8 m/sec (13 kn). As previously noted, the AIS reports only the design draft, so the draft while in transit is unknown and has not been correlated with wave height.

Figure 29. Vessel drawdown statistical analysis for cargo and tanker carrier class vessels. (A). Probability distribution of the drawdown amplitude and the cumulative distribution (right vertical axis). (B) Probability distribution of the drawdown half-wave period and the cumulative distribution (right vertical axis).

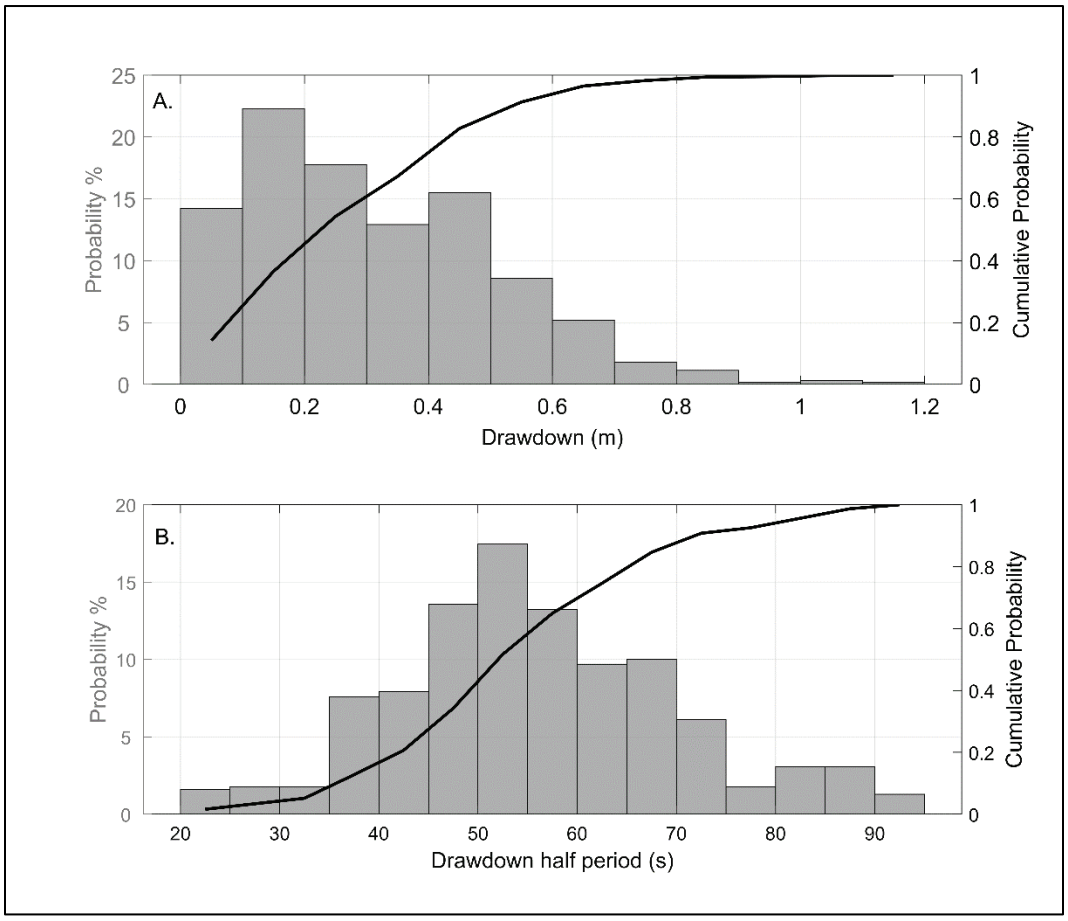

Figure 30. Secondary waves statistical analysis for cargo and tanker class vessels. (A) Probability distribution of the wave height and the cumulative distribution (right vertical axis). (B) Probability distribution of the wave period and the cumulative distribution (right vertical axis).

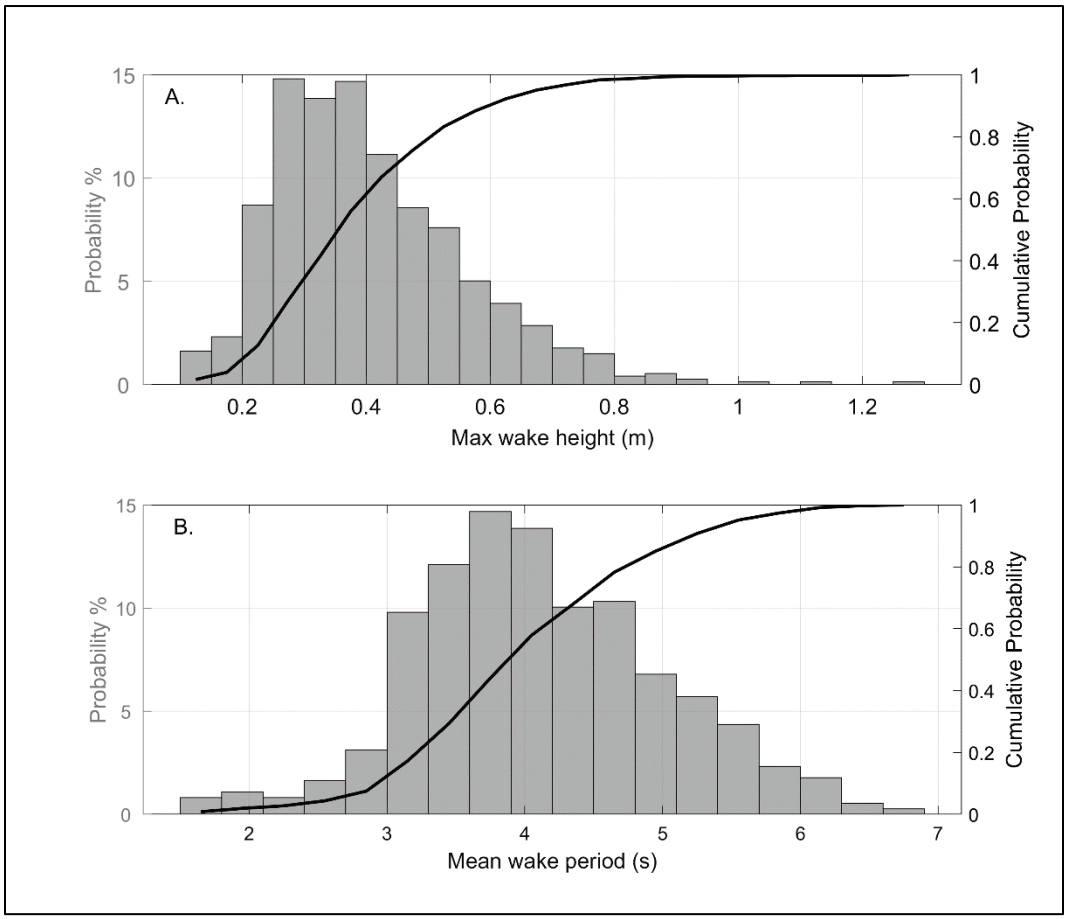

Figure 31. Secondary waves and drawdown statistics. Secondary wave or drawdown percentiles as a function of vessel characteristics length (A. and B.), beam (C. and D.) and speed (E. and F.). The mean value in each percentile class includes error bounds that denote the 95% confidence interval.

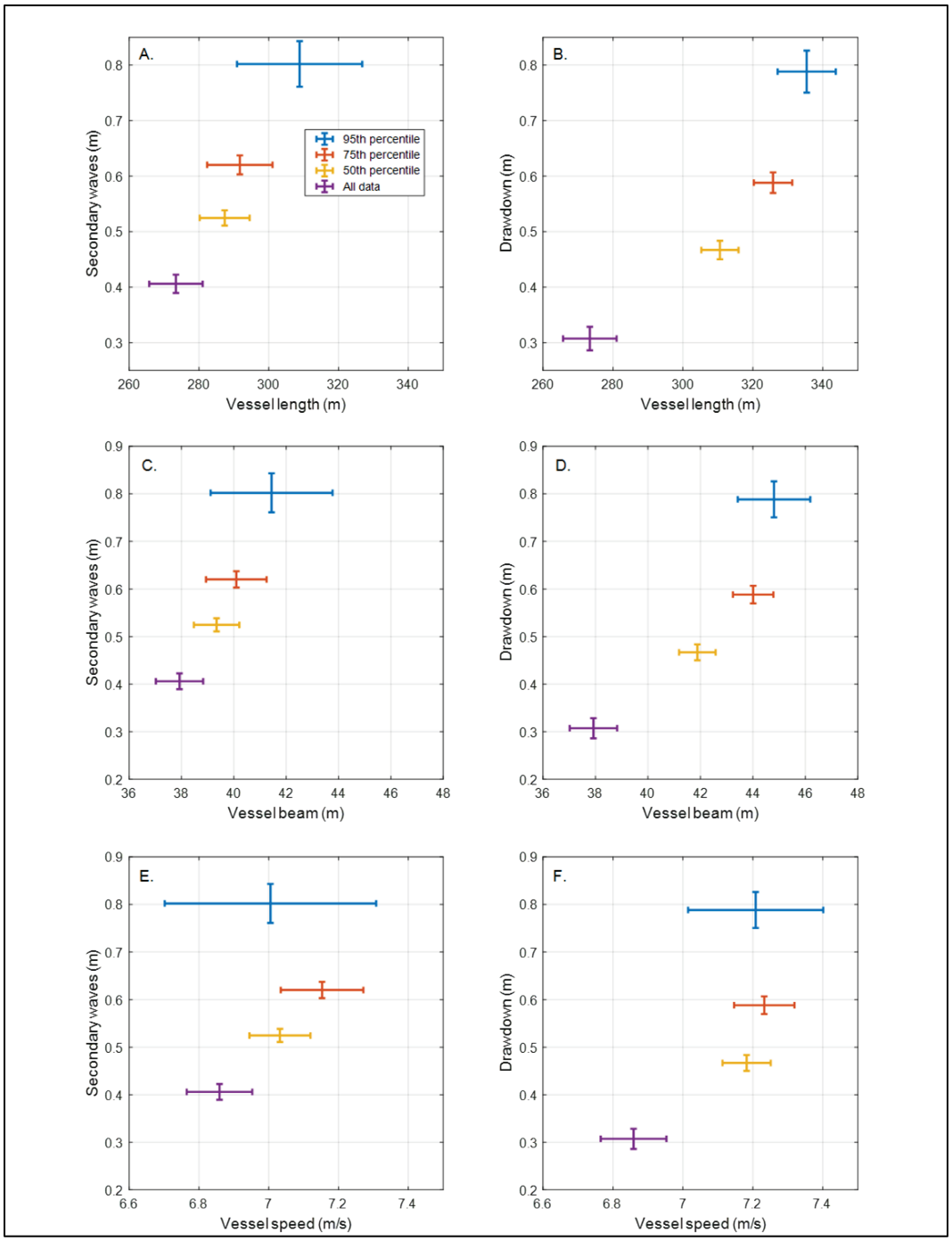

3.7 Nearshore wave patterns

The nearshore sensor captured water surface disturbances generated by vessels during the last 4 days of the experiment (2 December to 5 December 2021). These data have been examined to better understand potential vessel impacts at the shoreline and to determine any relationship between this location and the data collected at the South Range. A total of 24 vessel passages with a distinct drawdown signal were identified in the time series record. Of these passages, all but five had a corresponding AIS signal. The time series of water depth for the 24 events are shown in the appendix. Each event is somewhat unique in terms of the vessel-generated waveform, but within this variability three distinct patterns emerge. Each of these patterns and a possible physical mechanism is described below.

The first pattern observed in the nearshore wave patterns involves wake events in which the drawdown first recedes from the beach and then advances in a slow and gentle swashing motion (see illustration in Figure 32a). Examples of this type of wave motion are depicted in the appendix (e.g., Figure A-1, Figure A-3, Figure A-5, Figure A-8, and Figure A-15). In all observed examples, the drawdown amplitude is less than 0.2 m, and there is no amplification of higher frequency waves at the trailing edge of the drawdown. Vessel-generated waves under these conditions likely have little effect at the shoreline other than the slow retreat and advance due to the drawdown effect.

The second pattern visible in certain nearshore measurements is a larger-amplitude drawdown followed by a sharp increase in water depth accompanied by higher-frequency (3 to 8 sec period) waves. A generalized sketch of this behavior appears in Figure 32b. The physical conditions which generate this behavior are not well understood, but one possible explanation is that a large-amplitude drawdown may develop instabilities. If the wave becomes unstable, then the initial gentle retreat will be followed by a rapid uprush with small higher-frequency waves that appear near the end of the drawdown event. Other long waves such as solitary waves or tidal bores (Dalrymple 2021) produce abrupt increases in water depth that are usually accompanied by higher-frequency fluctuations that can quickly become unstable and break. By analogy, it is conceivable that a similar mechanism could cause the conditions at Tybee Island. Examples of this type of wave are depicted in the appendix (e.g., Figure A-4, Figure A-10, Figure A-12, Figure A-14, Figure A-16, and Figure A-23). All six events have a drawdown amplitude greater than 0.25 m, and all AIS-

identified ships that generated this type of drawdown behavior are either inbound container ships or inbound vehicle carriers.

Figure 32. Generalized illustration of different wake patterns from commercial vessels near Tybee Island.

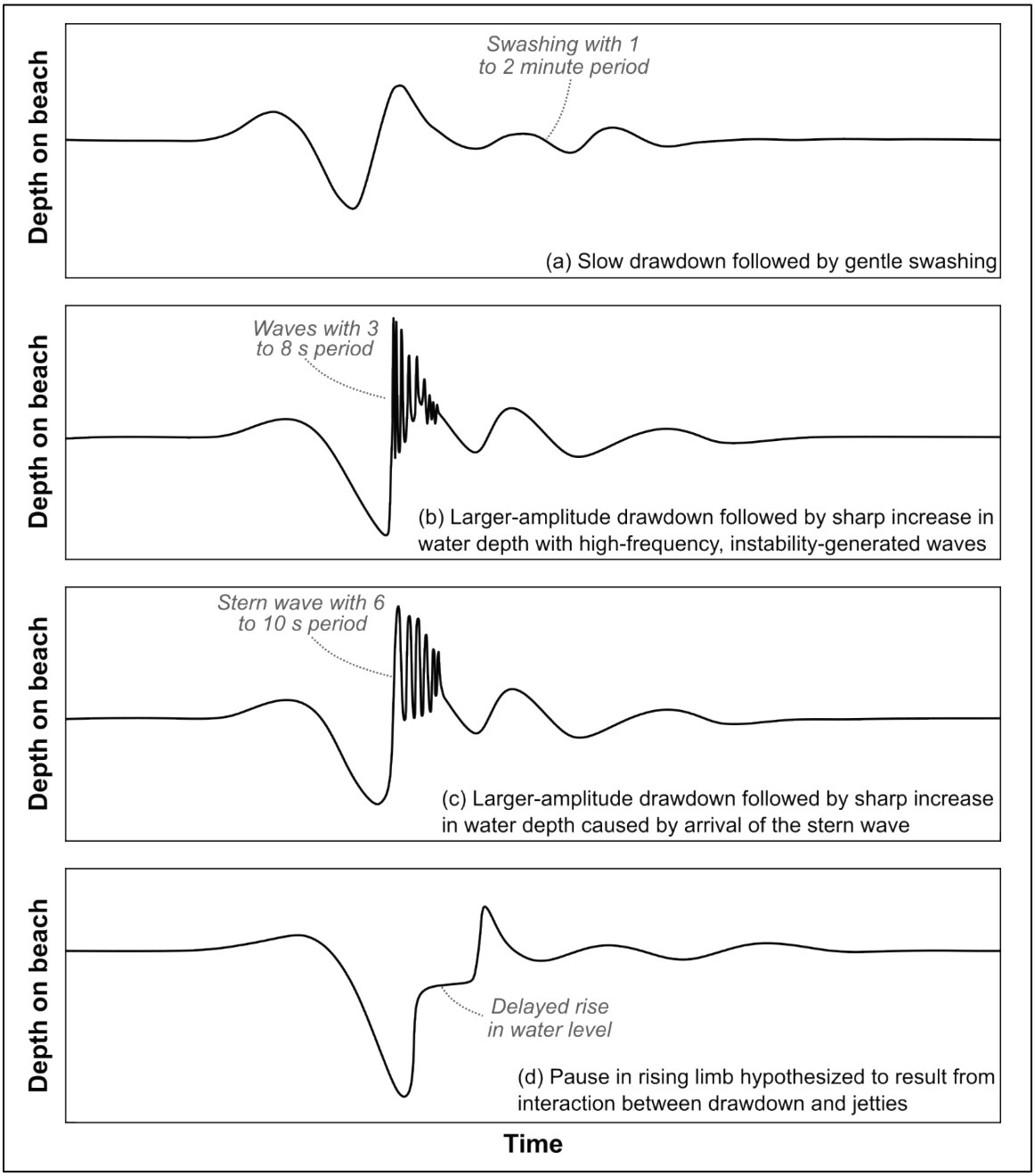

Another possible explanation for the second nearshore wake pattern is an interaction between the drawdown, the stern wave (which is also a primary wave), and possibly the secondary waves (Figure 32c). In a study of commercial ship wake in the Sabine-Neches Waterway, Maynord (2003) noted that the combination of the drawdown and stern wave was the primary cause of highest waves, but he did not specifically address the role of secondary waves, which were small or absent. The surge depicted in Figure A-10, Figure A-14, and Figure A-23 is comprised of 8 to 10 sec waves that are at a higher frequency than the stern waves (> 1 min) and may represent a contribution from the secondary waves. Thus, the secondary waves could contribute to the surge in addition to the drawdown and stern wave. However, a larger dataset that included primary waves (drawdown, stern wave) and secondary waves would help to determine if this behavior is a general manifestation of vessel wake characteristics at Tybee Island.

The third nearshore wake pattern shows a brief period of fairly constant mean water level on the rising limb of the drawdown, followed by a peak (illustrated in Figure 32d, with real-world examples shown in Figure A-6, Figure A-9, Figure A-17, Figure A-19, Figure A-20, and Figure A-24). In all six examples, the drawdown amplitude is above 0.3 m, and all ships identified with AIS are outbound container ships or outbound vehicle carriers. Considering that this behavior is observed only for outbound vessels, it is possible that the jetties may cause the brief pause in water level on the rising limb of the drawdown. This explanation would indicate that the jetties may damp or interfere with the wave as it propagates towards the shoreline. Similar patterns were seen in a previous study investigating ship forces at Tybee Island (Maynord 2007). Even so, the present dataset is limited in size and offers insufficient information to establish if this wave pattern is limited only to outbound ships. If a larger dataset were to reveal that this pattern also occurs for inbound ships, then it would be less justifiable to attribute this behavior to the presence of the jetties.

Because the sensors were exposed during low tide, the number of overlapping vessel passages that were captured by both the South Range sensor and the near-shore sensor is 7. Regression analysis shows that the drawdown at the shoreline is positively correlated with the drawdown at the South Range (Figure 33). While the number of data points is small compared to the number of total offshore observations, the high

correlation coefficient indicates very little change in the amplitude, and thus, little energy loss as the drawdown wave propagates to shore. Note that these results differ from the conclusions of Maynord (2007), who measured vessel-generated waves several hundred meters west of the sensor placement for the present study. Maynord predicted that the drawdown would attenuate by approximately two-thirds of its height between the navigation channel and the beach whereas Figure 32 indicates almost no attenuation in drawdown height. It is possible that the drawdown attenuation observed by Maynord resulted from interactions between the drawdown and the south jetty, which is likely to have greater influence at more westward portions of the beach. Nevertheless, Maynord's conclusion that the drawdown (rather than the short-period bow and stern waves) is the largest-magnitude wave acting on the beach is consistent with the observations in Figure A-1 through Figure A-24.

Figure 33. Comparison of the drawdown measured at South Range and the drawdown measured at nearshore sensor. Solid line denotes 1:1 correlation.

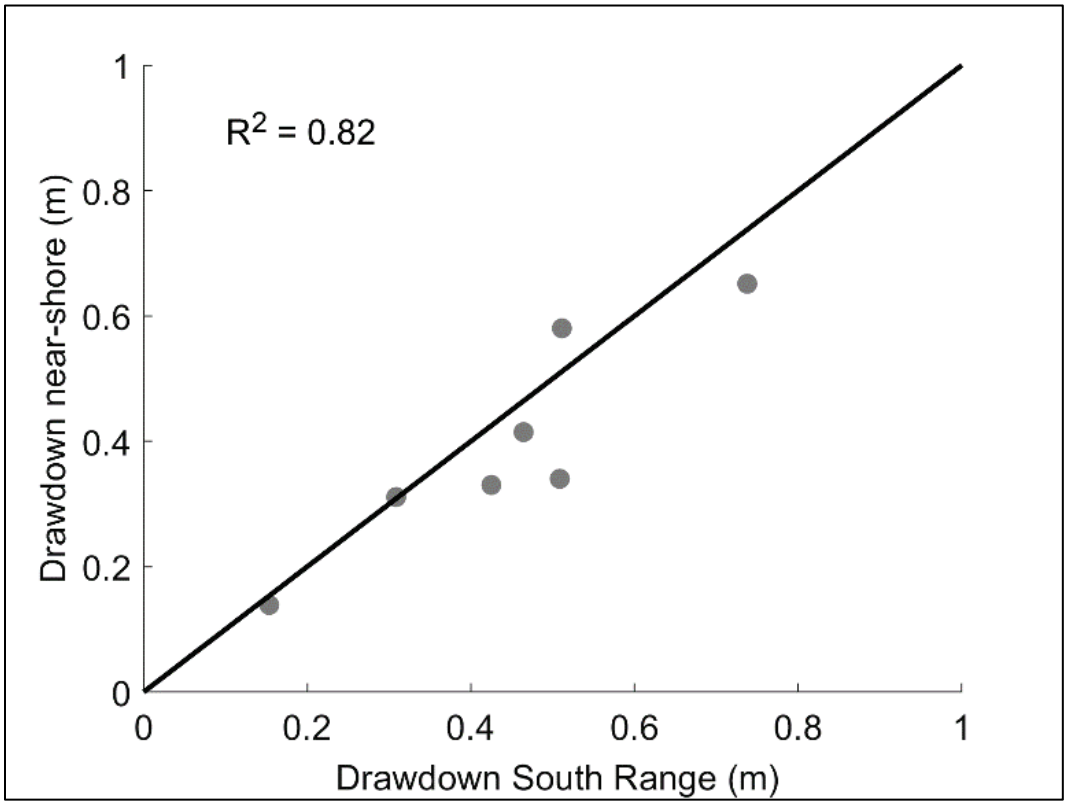

4 Discussion and Summary

During this study, the wave characteristics of commercial vessels transiting the entrance channel to Savannah, GA, have been investigated. Waves generated by commercial vessels sometimes are well known to produce a large uprush on the northern shore of Tybee Island that can be hazardous to unsuspecting beachgoers that are unaware of this phenomenon. The City of Tybee Island has installed warning signs along the beach alerting beachgoers of the possibility of a large surge. However, the scale of the uprush varies greatly among seemingly similar types of vessels, so the combination of vessel operations and environmental conditions that lead to these large surges on the northern shore of Tybee Island is unclear.

Nearly 4 months of vessel transits and simultaneous water level measurements have been analyzed to look for links between vessel operations and the higher surge. The study has identified a few factors that likely contribute to the phenomenon.

1. **Commercial vessels**—the drawdown generated by commercial vessels transiting the navigation channel is the primary cause of large water level changes at the beach. When categorized by percentiles (95^{th}, 75^{th}, and 50^{th}), the waves show a positive correlation with ship dimensions (length and beam). Thus, the largest ships have a higher probability of generating a large drawdown. In addition, the largest fluctuations in water level (secondary waves) occurred on the trailing end of the drawdown, and the highest of these waves were generated by inbound container ships (see the appendix). Compared to tankers, container ships generally have faster speeds (Figure 18) and are therefore more likely to generate the largest secondary waves (Maynord 2007).
2. **Beach slope and tide level**—The northernmost point of Tybee Island has a very low relief beach face, which increases the likelihood of a greater horizontal uprush length in the study area. In contrast, west of the study area (where the south channel of the Savannah River hugs the shoreline; Figure 12), the beach slope is notably steeper. In this area, qualitative observations of wake behavior suggest a significantly shorter vessel wake uprush distance. Additionally, given that the beach slope is not constant, the maximum uprush on North Beach may vary as a function of the tidal stage. At low tide, especially spring low tide, a

larger portion of the surge may lose energy before reaching the shoreline owing to the shallow areas that extend offshore. Around mid and high tide, the waves may retain more of their energy as they approach the shore and, thus, produce a larger uprush at landfall.

3. **Erosion due to deep draft navigation activity**—Beach erosion related to navigation channel deepening has also been identified as a concern in previous studies of the Tybee Island region (e.g., Oertel et al. 1985; Smith et al. 2008). These studies indicate that this beach erosion primarily results from disruption of natural littoral and riverine sediment delivery to the Tybee Shoal. However, whether vessel wakes may contribute to beach erosion in the study area should be considered. Wave energy calculations indicate that wind waves generate 97% of total wave energy acting on North Beach, with vessel-generated waves contributing the remaining 3% (Table 1, Table 2, and Figure 26). Even after artificially increasing the number of vessels passing the beach to account for gaps in the AIS record, vessel wakes still contributed only 4% of total wave energy (Figure 28). Of note is that these calculations incorporate only short-period energy from the vessels' secondary waves (Figure 3), and future studies should consider installing additional instrumentation (e.g., an array of ADCP; see example from Raubenheimer et al. [2004]) on the beach to characterize the erosion potential of vessel uprush. Future energy calculations for North Beach should also incorporate energy from tidal currents, especially considering that the shore-perpendicular bedform crest orientation (Figure 8) supports the conclusion that shore-parallel currents significantly influence local sediment transport.

4.1 Recommendations

While this analysis was unable to identify the precise vessel operations and environmental conditions that lead to the largest surge, trends that could be used to guide future research have been identified, which would better constrain the physical mechanisms responsible for the phenomenon. Recommendations for future studies include the following:

1. Adding more long-term measurements of wave propagation characteristics across the beach face. When combined with previously-collected data (Maynord 2007), the data from the present study elucidate the non-linear nature of the waves and the wide variety of wave forms generated by commercial vessels. These complexities make it difficult to isolate the precise hydrodynamic mechanisms that

generate the largest wake events at the beach, beyond noting that the largest uprush is caused by cargo ships. Beach slope, long-wave instabilities, bottom friction, the superposition of drawdown, and secondary waves likely all contribute to the near-shore wave patterns. Previous studies have included near-shore measurements at a single point several hundred meters west of our study site, where the surge effect is less of an issue (Maynord 2007). Deploying an array of water level sensors from below MLLW up to the high water mark would provide direct measurements of the incoming waveform and permit an analysis of the full non-linear transformation as waves propagate up the beach. These sensors would also provide a robust dataset to conduct a statistical analysis of the vessel waves and the conditions that generate the largest impact.

2. In support of the first recommendation, a complete survey should be conducted of the beach face encompassing the northern tip of the island and points further west, where the beach is steeper. In combination with water level measurements, the extent of the uprush could be quantified, providing the required information to establish the role of tides in controlling the magnitude of the uprush. The necessary water level measurements could be achieved using one or more cross-shore arrays of pressure sensors. Considering that an average of 12 large vessels transit the navigation channel each day (e.g., Figure 27), an uprush dataset containing several hundred vessel passages could be acquired in less than 1 month.
3. Previous studies have not captured the nearshore velocity field generated by the ship waves. Velocity measurements would help to determine the speed and direction of the waves, which are vital parameters for understanding the propagation characteristics of the incoming primary waves. Wave speed and direction measurements would elucidate the point of origin of the largest vessel waves. For example, a nearshore velocity field dataset would provide information about where in the channel a vessel is located when it produces the largest effect at the shore (e.g., within the jetties, immediately north of the beach). These measurements would also help to further quantify the asymmetry between waves associated with inbound versus outbound vessels.
4. Video monitoring at the shoreline would also help to determine the ship type responsible for the largest waves and would also identify all ships that pass the study site if there are gaps in the AIS record. The video may also be able to record the beach for further visualization of

the drawdown and uprush lengths for different classes of vessels and operating conditions. A live video feed with public access could additionally serve to educate beachgoers and tourists about wake behavior on North Beach, building on efforts to promote beachgoer safety.

5. The role of secondary waves in generating large uprush is still unclear. A question remains whether the waves seen on the trailing edge of the drawdown are manifest only due to instabilities in the drawdown or are also coupled to the secondary waves. In other words, are these large waves present even when the offshore amplitude of the secondary waves is small? This knowledge would help confirm the type of ship operations responsible for the largest uprush as the secondary waves tend to be higher for faster vessels.
6. Depending on the desired accuracy for predicted drawdown, measurement of the vessel draft during transit may be beneficial to future research. Models of ship waves in confined channels rely on accurate draft measurements. The AIS system provides design draft, as opposed to the draft of the ship while in transit. The Waterborne Commerce Statistics Center acquires draft information for commercial vessels, but distribution is delayed by 1 to 2 yr. Once this information becomes available for August through December 2021, the actual draft of each ship could be determined, and the data could be reevaluated with the corrected values. However, note that theoretical drawdown predictions (e.g., Equations 11 and 12) may show only marginal improvement when actual draft values are substituted. For example, Equation 11 predicts that a ship with 55 m beam, 13 m draft, and 7 m/sec velocity that transits the navigation channel at low spring tide (1.5 m below the NAVD88 datum) will generate a drawdown of 0.29 m. Holding all other parameters constant but increasing the draft to 14 m increases the predicted drawdown to 0.32 m (i.e., an increase of only 3 cm). Consequently, a reanalysis of the data with updated draft data may offer little added benefit to the present results.
7. Numerical modeling is recommended to better understand the waves generated by different vessel types. Numerical models provide quantitative information that can be used to better constrain the magnitude of the drawdown and other long waves as well as the higher frequency secondary waves. They can also predict the wave propagation and shoaling characteristics, which would help elucidate the role of the jetties, bathymetry, and tides in generating the ship

waves responsible for the highest uprush. They can also be used to explore the sensitivity of wave height to ship speed.

4.2 Strategies to reduce wave heights at Tybee Island

The long-term goal is to reduce the potential risk to beachgoers by reducing the impact of the vessel-generated waves reaching the north shore of Tybee Island. There are two approaches to reduce the wave impact: (1) modify navigation conditions to reduce wave heights near the source or (2) reduce the height of the waves near the shoreline. The following suggestions do not address the potentially substantial engineering requirements needed to implement these strategies. The feasibility of implementing wave reduction measures would need to be addressed at the project scoping level. In addition, implementing many of these strategies would require coordination among various regulatory agencies, as discussed below.

1. **Ship speed**—Reducing the maximum ship speed would reduce the surge at the beach. The largest waves were associated with vessels speeds greater than 6.8 m/sec (13 kn). The sensitivity to vessel speed suggests small reductions in maximum speed could reduce the height of the waves reaching Tybee Island. Speed reduction for vessels transiting the navigation channel would need to be coordinated by the US Coast Guard, the Georgia Ports Authority, and other local regulatory agencies.
2. **Refurbish and extend the south jetty**—The south jetty has experienced considerable deterioration since its construction in the late 1800s. There are visible signs of decay along the entire length of the jetty, but the decay is worse near the offshore terminus. Rebuilding and extending the jetty could reduce the vessel waves arriving at Tybee Island. However, even though an asymmetry in wave height distribution between inbound and outbound vessels is evident, the present study has not unequivocally determined the role of the south jetty in modulating the propagation characteristics of the vessel generated waves. Further investigation through numerical modeling would help to determine if jetty rehabilitation would be an effective way to reduce the waves arriving at Tybee Island. Mosely (2018) previously estimated a total cost between $53 million and $90 million to refurbish the south jetty, with the large range attributed to uncertainties in the condition of the existing structure.

3. **Install nearshore breakwaters**—Breakwaters dissipate wave energy and could be installed within the vessel wake impact zone. An effective breakwater system would not only need to reduce the waves arriving at the northern shore but also ensure effective sediment management. The Savannah River entrance is a very complex morphodynamic system, with two navigation channels, a dual jetty system, strong tidal currents, and an adjacent tidal inlet. Extensive testing of a breakwater system should focus on both wave reduction and the potential for increased erosion/deposition along the northern shore of Tybee Island and the adjacent navigation channel. Given the limited distance between North Beach and the navigation channel, a scoping study would be necessary prior to breakwater construction to determine regulatory restrictions on its position.
4. **Channel modifications** – Channel deepening and widening produces a smaller blockage ratio (vessel cross-sectional area measured at mid-ship divided by channel cross-sectional area). The drawdown decreases as the blockage ratio decreases (i.e., as the channel becomes deeper and or/wider [Maynord 2004]). This may reduce the size of the surge, but it is likely that the channel would need to be expanded significantly before the surge would no longer present a hazard. Furthermore, if the primary cause of the surge are the short waves, then reducing the drawdown by increasing the cross-sectional area of the channel would have less of an effect. Given the uncertainty in how much larger the channel would need to be in order to reduce the effect, combined with the uncertainty in the type of vessel waves (long waves versus short waves) that generate the surge, further analysis to better constrain these unknows is necessary. Specific recommendations would include simulations of vessel drawdown and wake generation with different channel cross-section scenarios.
5. **Channel realignment** – Beyond the jetties, the navigation channel turns towards the southeast as it passes the northern shore of Tybee Island. Conceptually, this may act to focus wave energy on the large shoal that fronts the northern shoreline. Realigning the channel towards the north as it exits the jetties may re-focus the vessel wake energy away from the shoaling area, thereby reducing the drawdown and secondary waves along the north shore of Tybee Island. A scoping level study would be required to investigate this alternative to determine if the vessel wake energy would be reduced south of the jetties and produce a lesser effect at the shoreline. To help economize the effort, the channel modification recommendation could also be

incorporated into a realignment study, as they both require a modeling component.

6. **Active warning system**—At present, warning signs are posted in the impact zone to alert beachgoers of the potential hazard posed by vessel wake. Warning beacons or an audio system could be developed to augment the existing warning signs. One possibility would be an array of offshore sensors that measure vessel wake height prior to reaching the beach. Alternatively, a land-based remote sensing system that uses high-frequency radar, or other technology, could scan the nearshore for large vessel wakes. The system could be programmed to trigger a warning when the waves are approaching. However, an active warning system would require further research and development to determine the feasibility and effectiveness of such a system in this environment. In addition, better characterizing the probability of large uprush events occurring under different conditions would reduce the number of false alarms during which lifeguards clear the beach but no large wake occurs.

References

Almström, B., and M. Larson. 2020. "Measurements and Analysis of Primary Ship Waves in the Stockholm Archipelago, Sweden." *Journal of Marine Science and Engineering* 8: 1–23. https://doi.org/10.3390/ jmse8100743.

Dalrymple, R. W. 2021. "Sedimentation on High-Energy Sand Flats in the Bay of Fundy: The Record of Tidal-Bore Activity and Deposition from High-Concentration Suspensions of Sand. *Sedimentology* 68(5): 2195–2226. https://doi.org/10.1111/sed.12851.

David, C. G., V. Roeber, N. Goeseberg, and T. Schlurmann. 2017. "Generation and Propagation of Ship-Borne Waves: Solutions from a Boussinesq-Type Model." *Coastal Engineering* 127: 170–187. https://doi.org/10.1016/j.coastaleng.2017.07.001.

Gailani, G. Z., and S. J. Smith. 2006. "Numerical Modeling Studies Supporting Nearshore Placement of Dredged Material from the Savannah River Entrance Channel." In *Proceedings of the 38th Annual Texas A&M Dredging Conference*, 197–212, San Diego, CA.

Gailani, J. Z., and S. J. Smith. 2014. "Nearshore Placement of Dredged Material to Support Shoreline Stabilisation." *Maritime Engineering: Proceedings of the Institution of Civil Engineers* 167(MA2): 97–108. https://doi.org/10.1680/maen.12.00016.

Georgia Ports Authority. 2002. *Savannah Harbor Beach Erosion Study: Savannah Harbor Expansion Project*. Technical report, prepared by Applied Technology and Management, Inc., Charleston, SC.

Haas, K. A., and A. C. Muscalus. 2019. *Bird-Long Island Management Study Phase 1B: Hydrodynamic Characterizations for Bird/Long Island*. Technical Report FHWAGA-19-1634. Forest Park, GA: Georgia Department of Transportation.

Houser, C. 2010. "Relative Importance of Vessel-Generated and Wind Waves to Salt Marsh Erosion in a Restricted Fetch Environment." *Journal of Coastal Research* 26(2): 230–240. https://doi.org/10.2112/08-1084.1.

Houser, C. 2011. "Sediment Resuspension by Vessel-Generated Waves along the Savannah River, Georgia." *Journal of Waterway, Port, Coastal, and Ocean Engineering* 137(5): 246–257. https://doi.org/10.1061/ (ASCE)WW.1943-5460.0000088.

Johnson, J. W. 1957. "Ship Waves in Navigation Channels." In *Coastal Engineering Proceedings*, vol. 6, 666–690. https://doi.org/10.9753/icce.v6.40.

Julien, P. Y. 1995. *Erosion and Sedimentation*. 1st edition. Cambridge, UK: Cambridge University Press.

Karimpour, A., and Q. Chen. 2017. "Wind Wave Analysis in Depth Limited Water Using OCEANALYZ, a MATLAB toolbox." *Computers & Geosciences* 106:181–189. https://doi.org/10.1016/j.cageo. 2017.06.010.

Kirby, J. T., and R. A. Dalrymple. 1993 *REF/DIF1 Version 2.5 Documentation and Users' Manual*. Technical Report. Newark, DE: Center for Applied Coastal Research, University of Delaware.

Komar, P. D. 1998. *Beach Processes and Sedimentation*. 2nd edition. Upper Saddle River, NJ: Prentice Hall.

Macfarlane, G. J. 2012. *Marine Vessel Wave Wake: Focus on Vessel Operations within Sheltered Waterways*. PhD thesis, Australian Maritime College, Newnham, Tasmania.

Maynord, S. T. 2003. *Ship Effects before and after Deepening of Sabine-Neches Waterway, Port Arthur, Texas*. ERDC/CHL TR-03-15. Vicksburg, MS: US Army Engineer Research and Development Center.

Maynord, S.T. 2004. "Ship Effects at the Bankline of Navigation Channels." *Marine Engineering* 157(2): 93–100. https://doi.org/10.1680/maen. 2004.157.2.93.

Maynord, S. T. 2007. *Ship Forces on the Shoreline of the Savannah Harbor Project*. ERDC/CHL TR-07-7. Vicksburg, MS: US Army Engineer Research and Development Center.

Mosely, C. L. 2018. *Report to USACE Savannah District concerning Ship Wakes at Tybee Island*. Technical report prepared by The Eurybia Group, Atlanta, GA.

Nece, R. E., M. R. McCaslin, and D. R. Christensen. 1985. *Ferry Wake Study*. Final Report WA-RD-70.1. Seattle, WA: Washington State Transportation Center.

NOAA (National Oceanic and Atmospheric Administration). 2006. *Savannah, Georgia 1/3 Arc-Second MHW Coastal Digital Elevation Model*. NOAA National Geophysical Data Center/NOAA National Centers for Environmental Information. https://www.ncei.noaa.gov/ metadata/geoportal/rest/metadata/item/gov.noaa.ngdc.mgg.dem:303/html.

NOAA. 2017. *Datums for Fort Pulaski, GA*. National Oceanographic and Atmospheric Administration. https://tidesandcurrents.noaa.gov/ datums.html?id=8670870.

Oertel, G. F., J. E. Fowler, and J. Pope. 1985. *History of Erosion and Erosion Control Efforts at Tybee Island, Georgia*. Miscellaneous Paper CERC-85-1. Vicksburg, MS: US Army Corps of Engineers, Waterways Experiment Station.

Raubenheimer, B., S. Elgar, and R. T. Guza. 2004. "Observations of Swash Zone Velocities: A Note on Friction Coefficients." *Journal of Geophysical Research-Oceans* 109:C01027. https://doi.org/10.1029/ 2003JC001877.

Robards, M. D., G. K. Silber, J. D. Adams, J. Arroyo, D. Lorenzini, K. Schwehr, and J. Amos. 2016. "Conservation Science and Policy Applications of the Marine Vessel Automatic Identification System (AIS)–A Review." *Bulletin of Marine Science* 92(1): 75–103. https://doi.org/10.5343/bms.2015.1034.

Sargent, F. E. 1988. *Case Histories of Corps Breakwater and Jetty Structures, Report 2: South Atlantic Division*. TR-REMR-CO-3. Vicksburg, MS: US Army Corps of Engineers.

Schijf, J. B. 1949. "Protection of Embankments and Bed in Inland and Maritime Waters, and in Overflow or Weirs." In *XVII International Navigation Congress, Lisbon, Section I*, 61–78, Brussels, Belgium. PIANC.

Scully, B., and D. Young. 2021. "Evaluating the Underkeel Clearance of Historic Vessel Transits in the Southwest Pass of the Mississippi River." *Journal of Waterway, Port, Coastal, and Ocean Engineering* 147(5): 1–13. https://doi.org/10.1061/(ASCE)WW.1943-5460.0000655.

Smith, J. M., D. K. Stauble, B. P. Williams, and M. J. Wutkowski. 2008. *Impact of Savannah Harbor Deep Draft Navigation Project on Tybee Island Shelf and Shoreline*. ERDC/CHL TR-08-5. Vicksburg, MS: US Army Engineer Research and Development Center.

Sorensen, R. 1966. *Ship Waves*. Technical Report HEL-12-2. Berkeley, CA: University of California.

Sorensen, R. M. 1997. *Prediction of Vessel-Generated Waves with Reference to Vessels Common to the Upper Mississippi River System*. ENV Report 4. Rock Island, IL: US Army Corps of Engineers, Rock Island District.

Styles, R., and S. M. Glenn. 2000. "Modeling Stratified Wave and Current Bottom Boundary Layers on the Continental Shelf." *Journal of Geophysical Research: Oceans* 105(C10): 24119–24139. https://doi.org/10.1029/2000JC900115.

Styles, R., S. M. Glenn, and M. E. Brown. 2017. *An Optimized Combined Wave and Current Bottom Boundary Layer Model for Arbitrary Bed Roughness*." ERDC/CHL TR-17-11. Vicksburg, MS: US Army Engineer Research and Development Center.

USACE (US Army Corps of Engineers). 1984. *Shore Protection Manual*. 4th ed. Vicksburg, MS: US Army Corps of Engineers, Coastal Engineering Research Center.

USACE. 2014. *Final Environmental Assessment and Finding of No Significant Impact: Tybee Island, Georgia, Shore Protection Project 2014-2015 Renourishment*. Technical report. Savannah, GA: Savannah District, US Army Corps of Engineers.

USACE. 2020. *Savannah Harbor Deepening Sets Precedent; Four Dredges in Harbor Simultaneously*. Savannah District, US Army Corps of Engineers. https://www.sas.usace.army.mil/Media/News-Releases/Article/2202933/.

USACE-IWR (USACE, Institute for Water Resources). 2021. *Principal Ports of the United States: Waterborne Tonnage for Principal US Ports and all 50 States and US Territories*. US Army Corps of Engineers Institute for Water Resources. https://usace.contentdm.oclc.org/digital/collection/p16021coll2/id/7447.

USACE-SAS (USACE, Savanah District). 2019. *Draft Environmental Assessment and Finding of No Significant Impact: Tybee Island, Georgia Shoreline Protection Project, 2019 Hurricane Harvey, Irma, Maria Emergency Supplemental Renourishment*. Technical report. Savannah, GA: Savannah District, US Army Corps of Engineers.

Work, P. A. 2008. "Nearshore Directional Wave Measurements by Surface-Following Buoy and Acoustic Doppler Current Profiler." *Ocean Engineering* 35:727–737. https://doi.org/10.1016/j.oceaneng. 2008.02.005.

Appendix: Ship Wave Height at Tybee Island

Figures A-1 through A-24 in this appendix show the water depth during vessel passages at Tybee Island. The figures are listed in chronological order according to when the data were measured and the water depth scale varies between graphs. This presentation makes visually identifying the different wave patterns discussed in the main text easier. The 8 Hz time series (blue) is superimposed on a filtered time series to illustrate the primary wave (red) characteristics. Figure 3 includes a schematic defining the amplification of wave height (h_d) that can occur at the trailing edge of the drawdown, which is implicated in generating higher waves at the shore. The value of h_d can sometimes be negative, as on a falling tide if the drawdown is insignificant. The ship type is listed in the title for vessels identified in the AIS record.

Figure A-1. Wake record from *Caroni Plain,* chemical tanker.

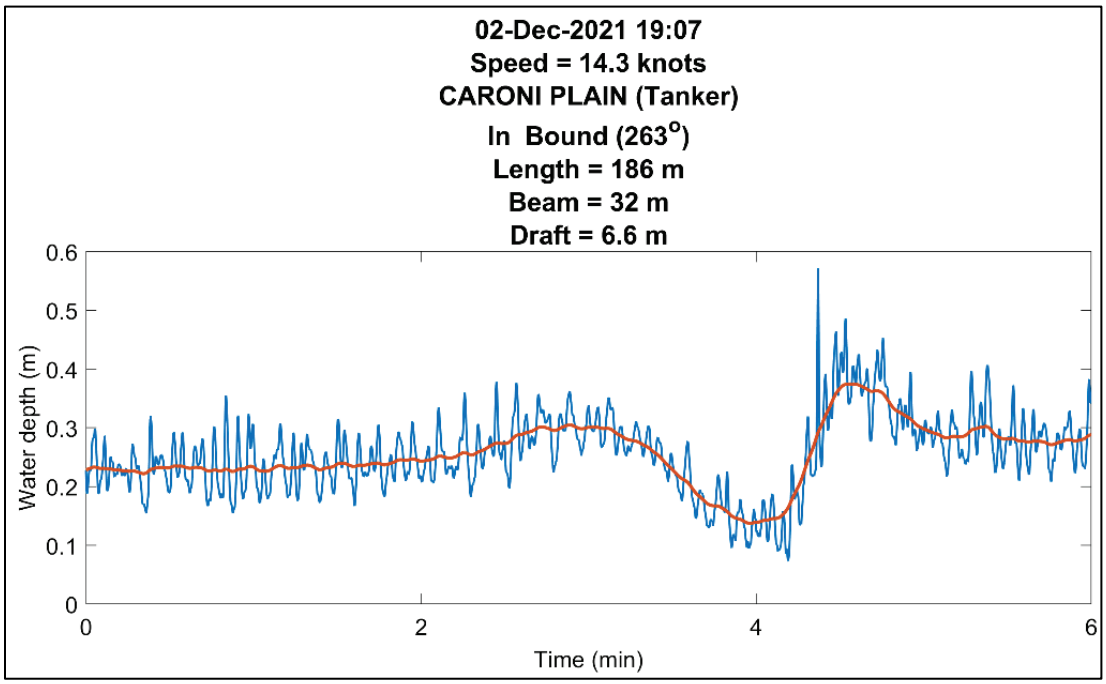

Figure A-2. Wake record from *APL California*, container ship.

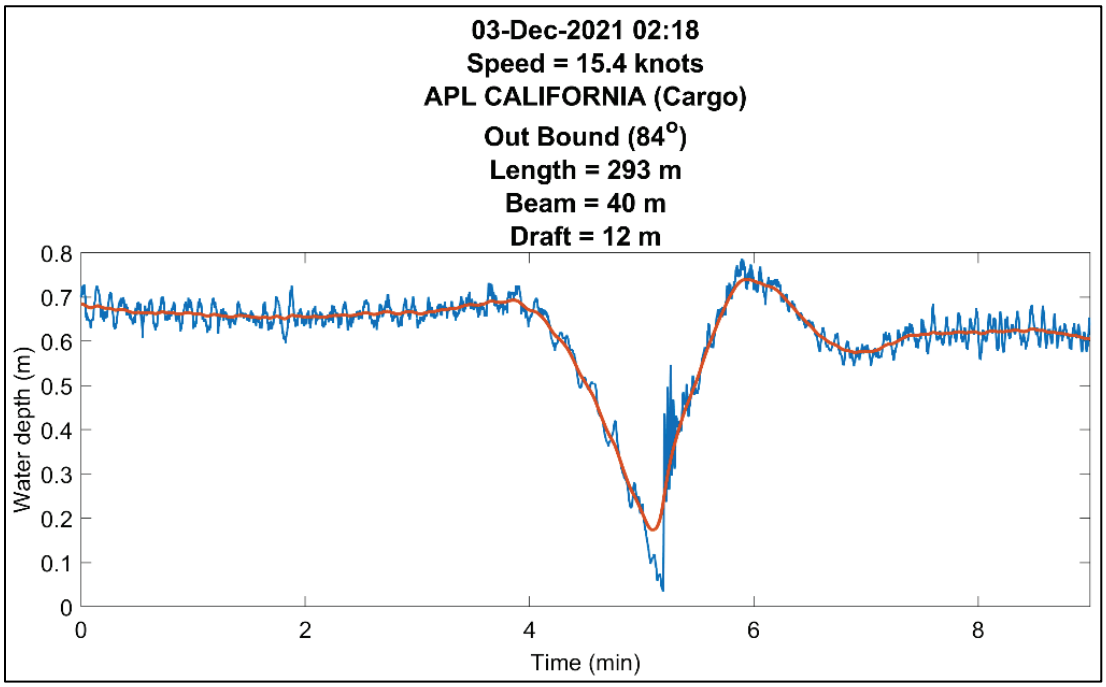

Figure A-3. Wake record from unknown large vessel.

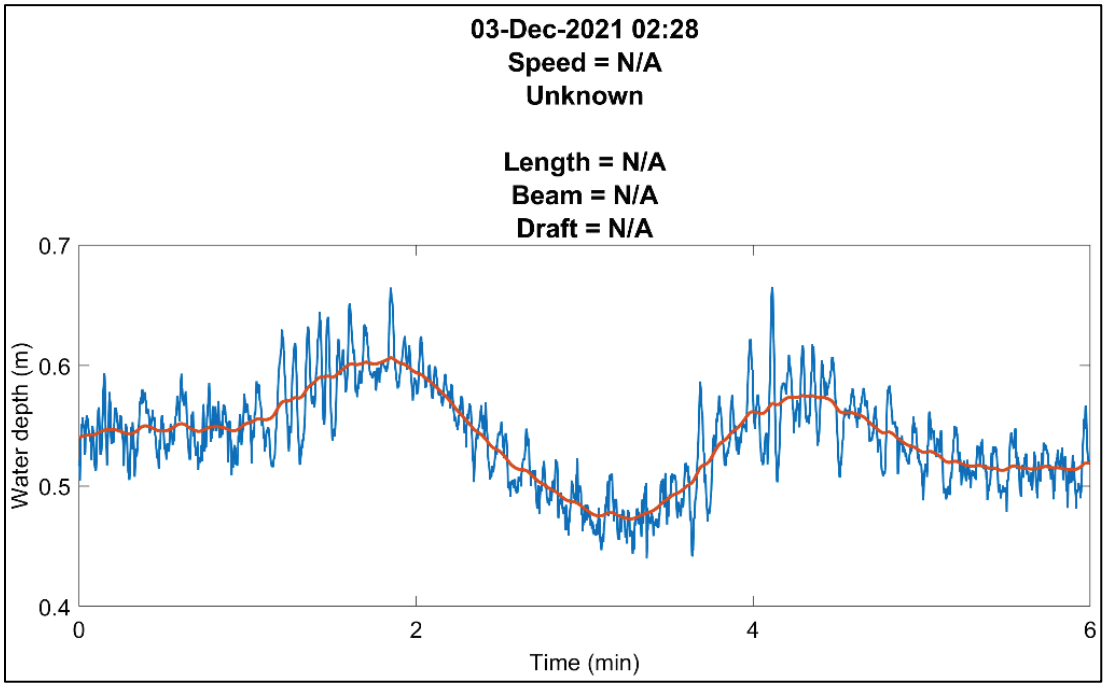

Figure A-4. Wake record from *Nevzat Kalkavan*, general cargo ship.

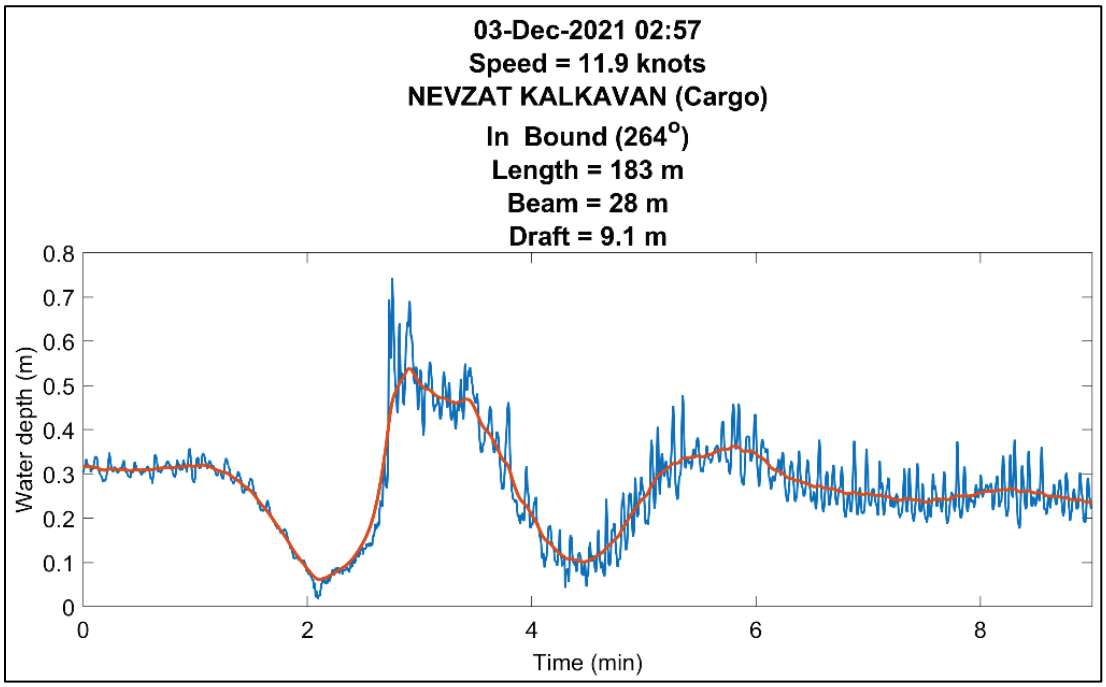

Figure A-5. Wake record from *Vienna Express,* container ship.

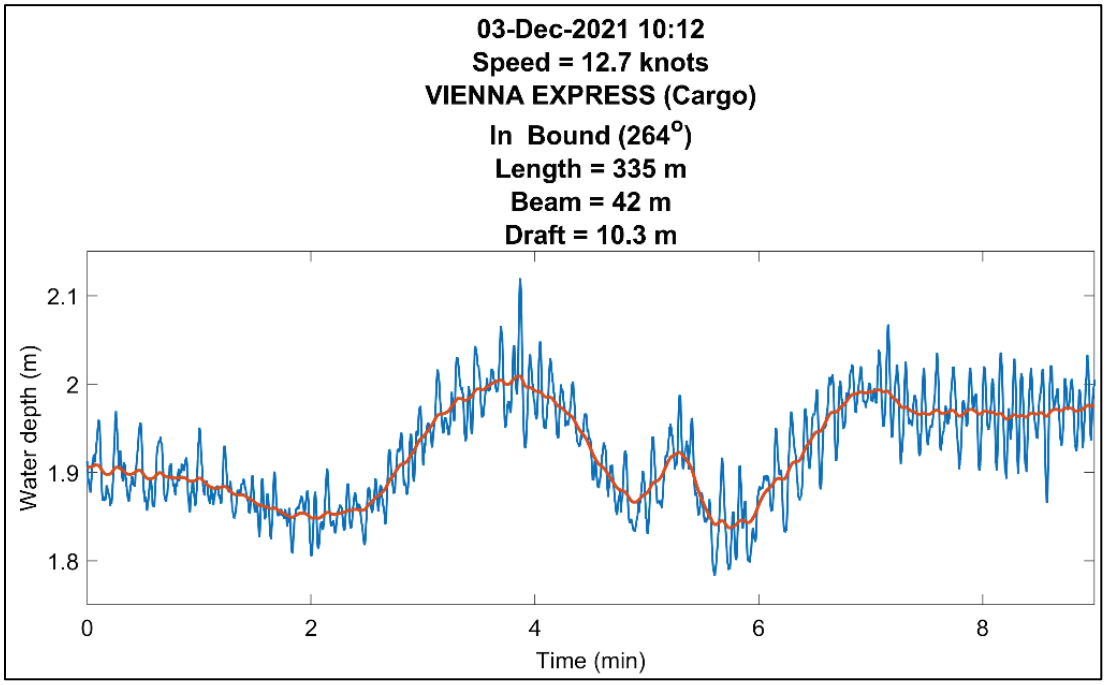

Figure A-6. Wake record from *CMA CGM Argentina*, container ship.

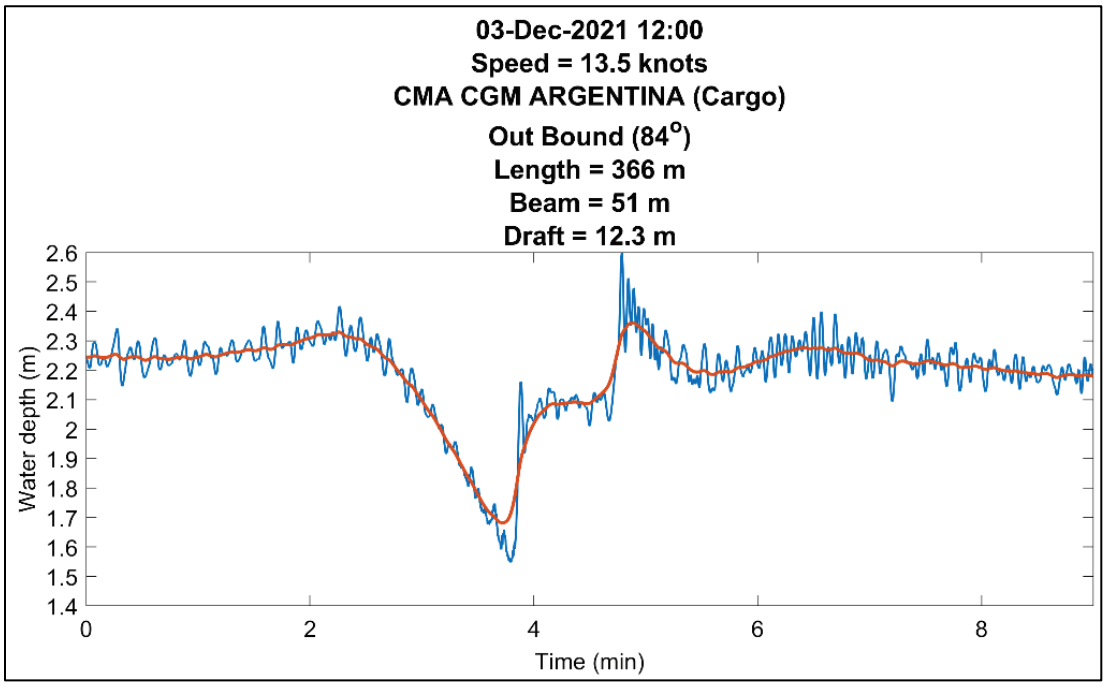

Figure A-7. Wake record from *CS Jenna*, bulk cargo ship.

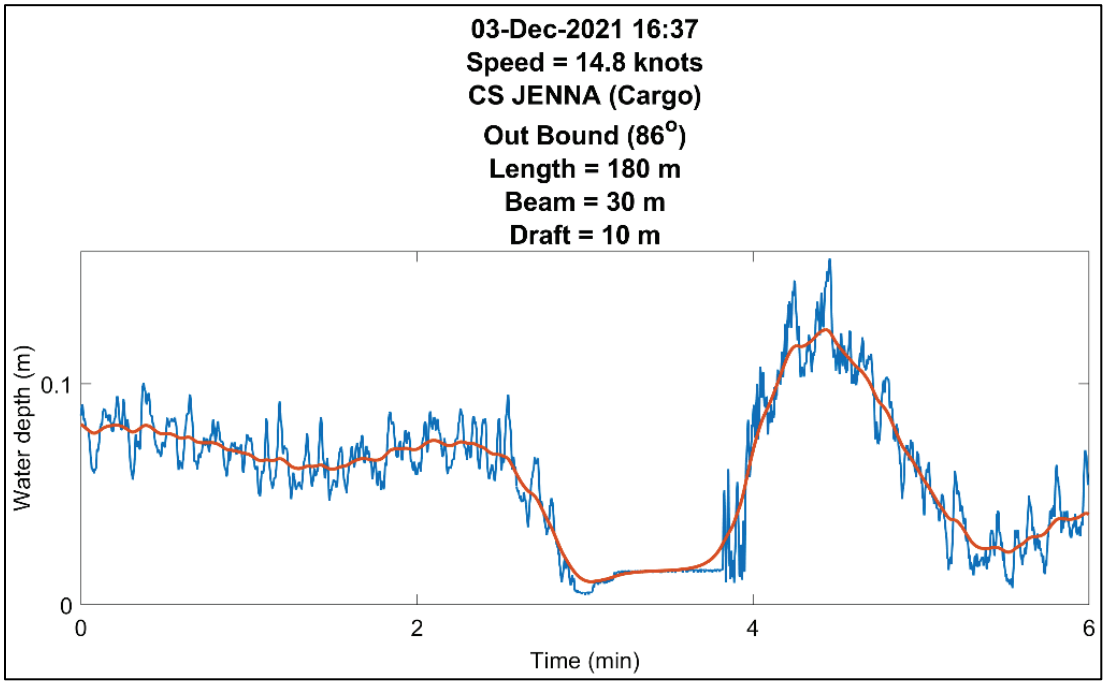

Figure A-8. Wake record from *Isabella,* crude oil tanker.

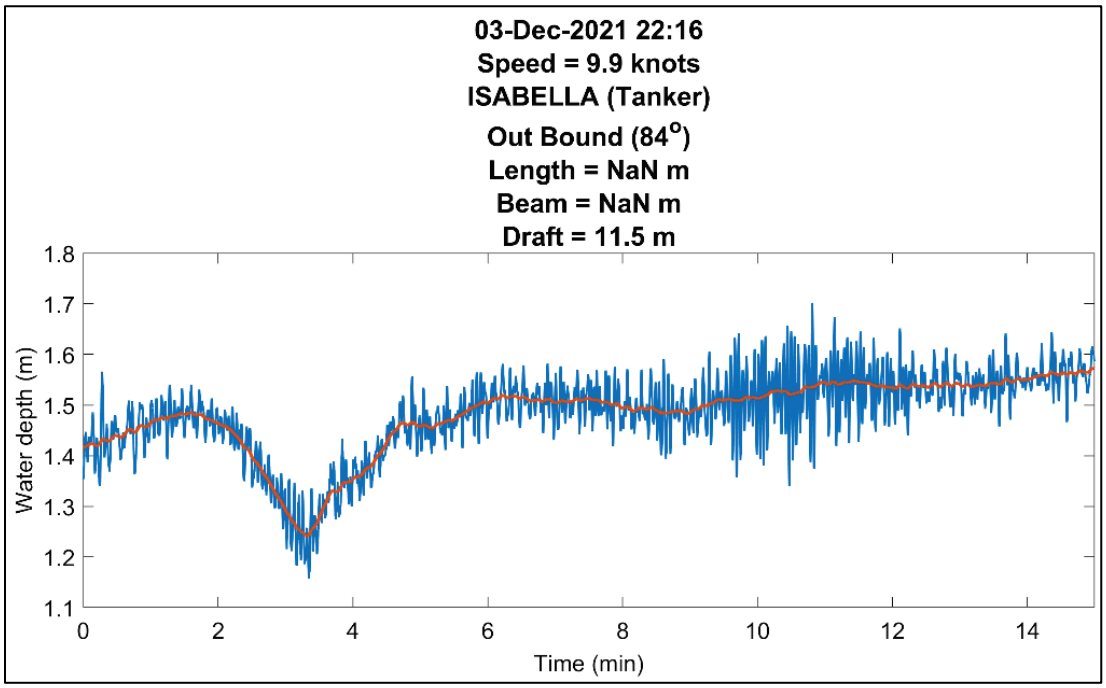

Figure A-9. Wake record from *Grand Uranus*, vehicle carrier.

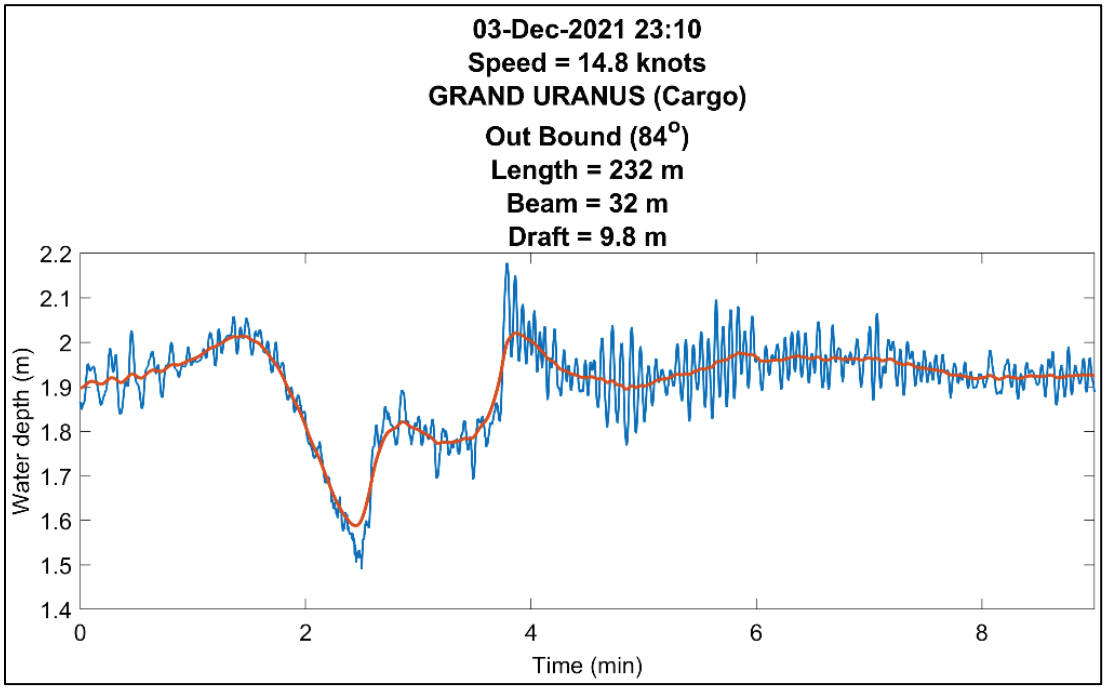

Figure A-10. Wake record from *Tamerlane*, vehicle carrier.

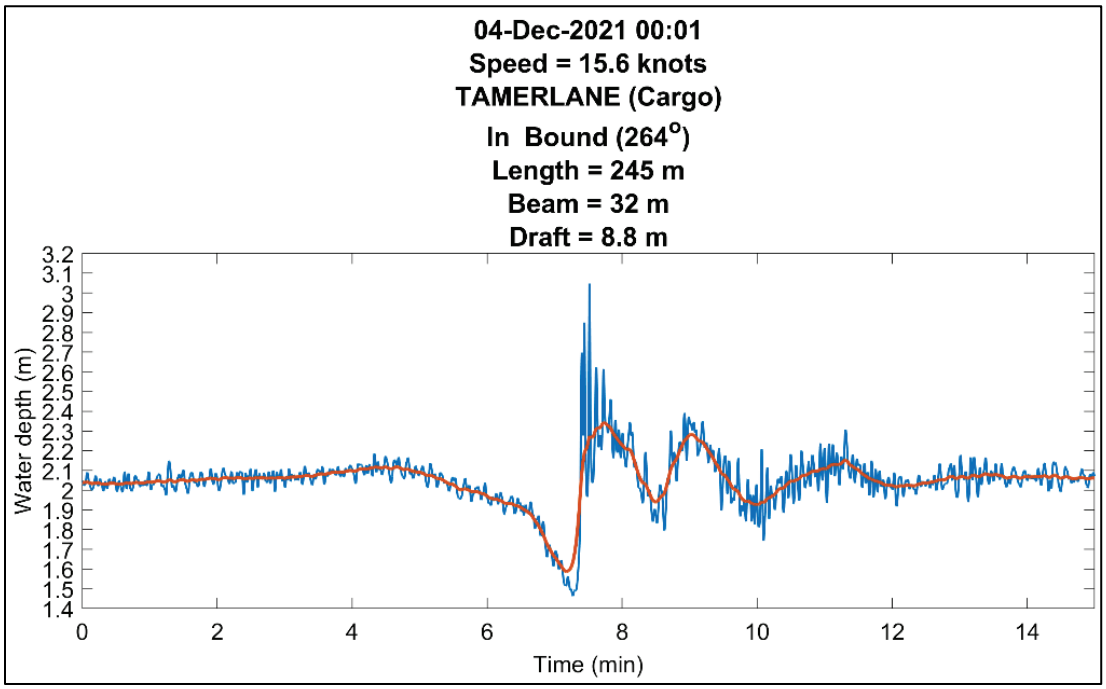

Figure A-11. Wake record from *Industrial Edge*, general cargo ship.

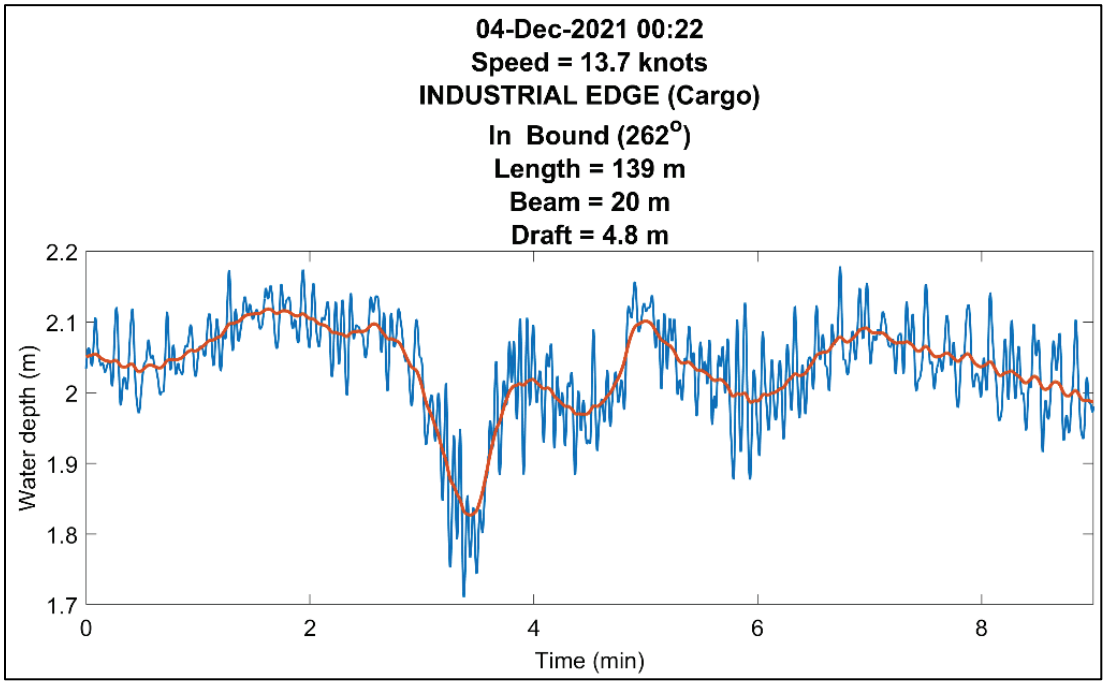

Figure A-12. Wake record from *Zim Luanda*, container ship.

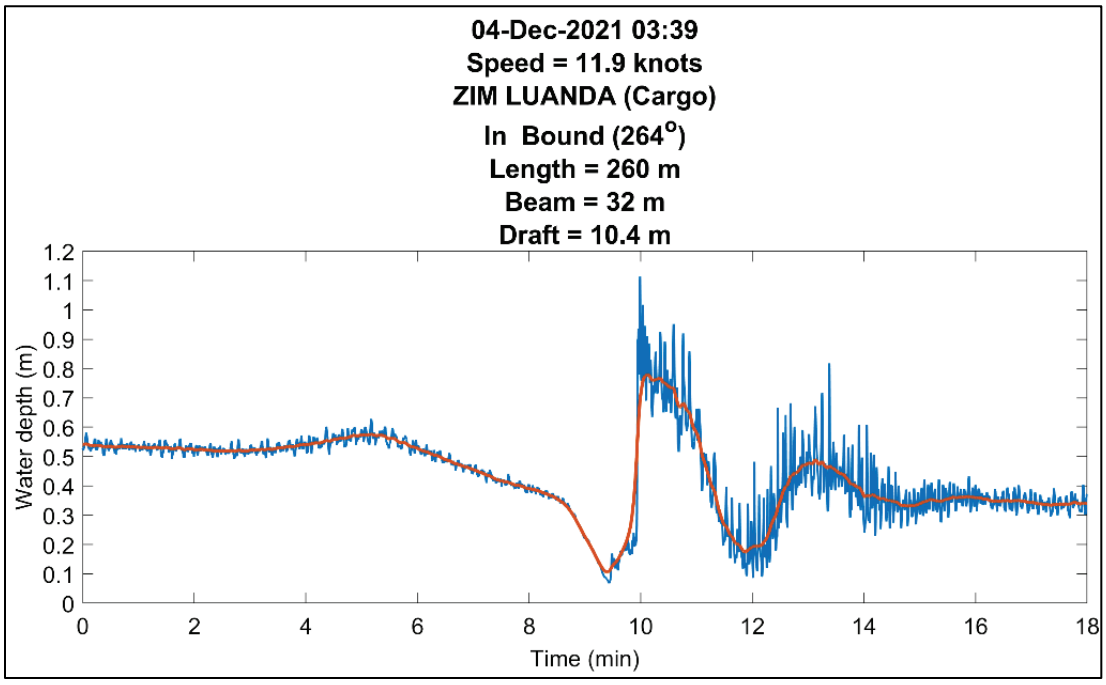

Figure A-13. Wake record from *MSC Tianjin*, container ship.

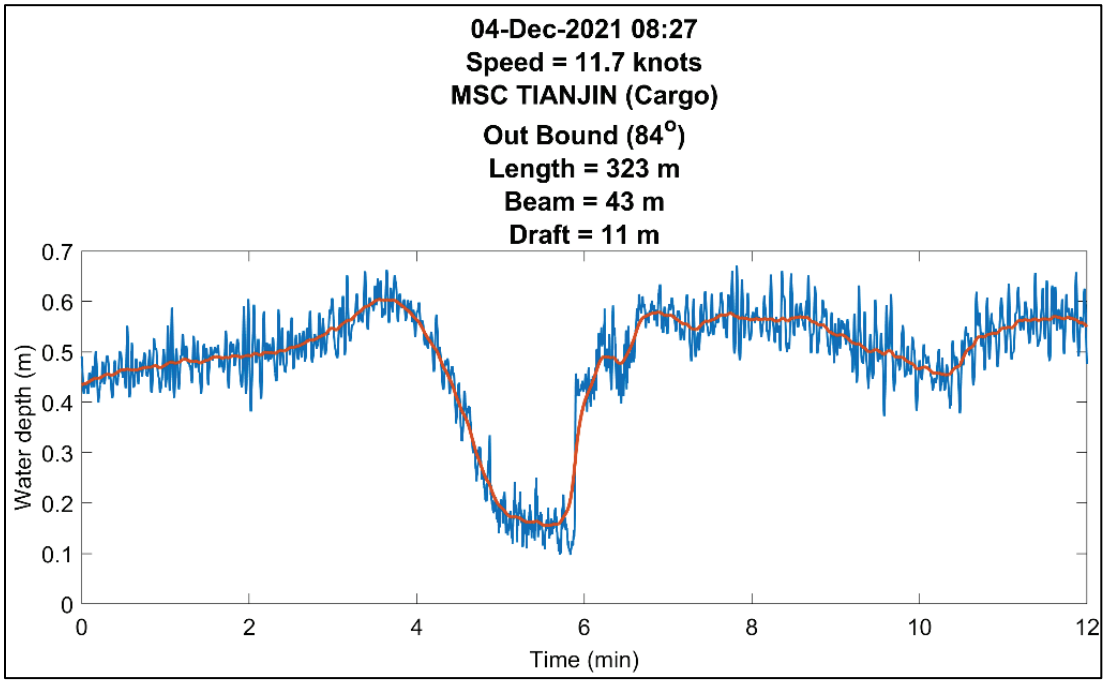

Figure A-14. Wake record from *Cosco Africa*, container ship.

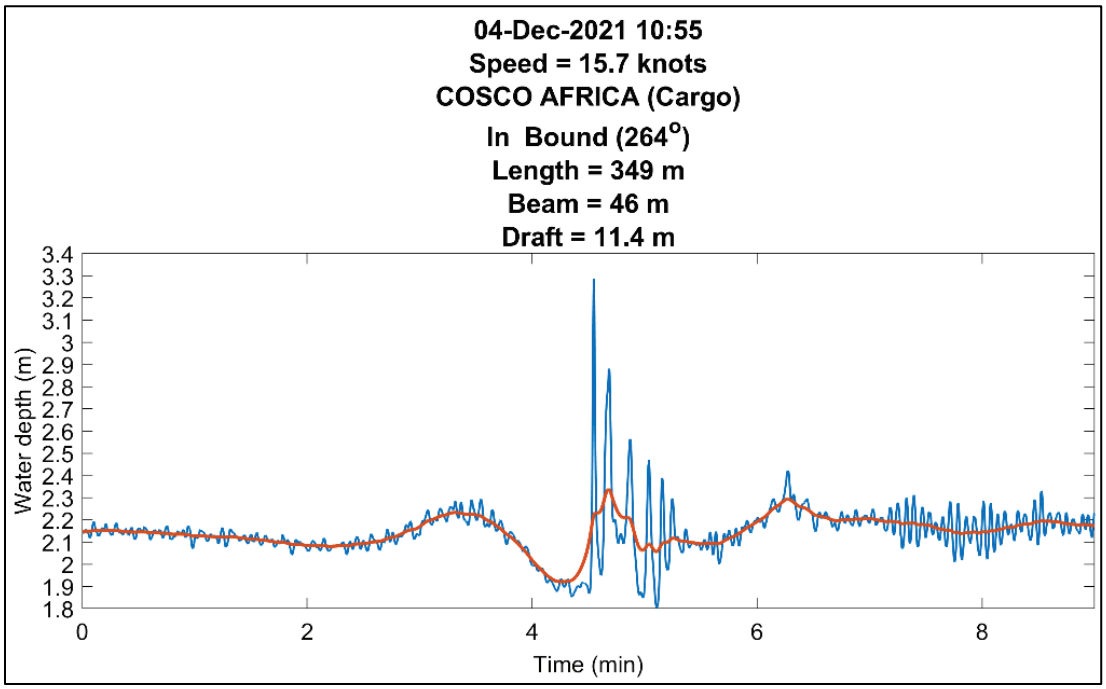

Figure A-15. Wake record from *Drawno,* bulk cargo ship.

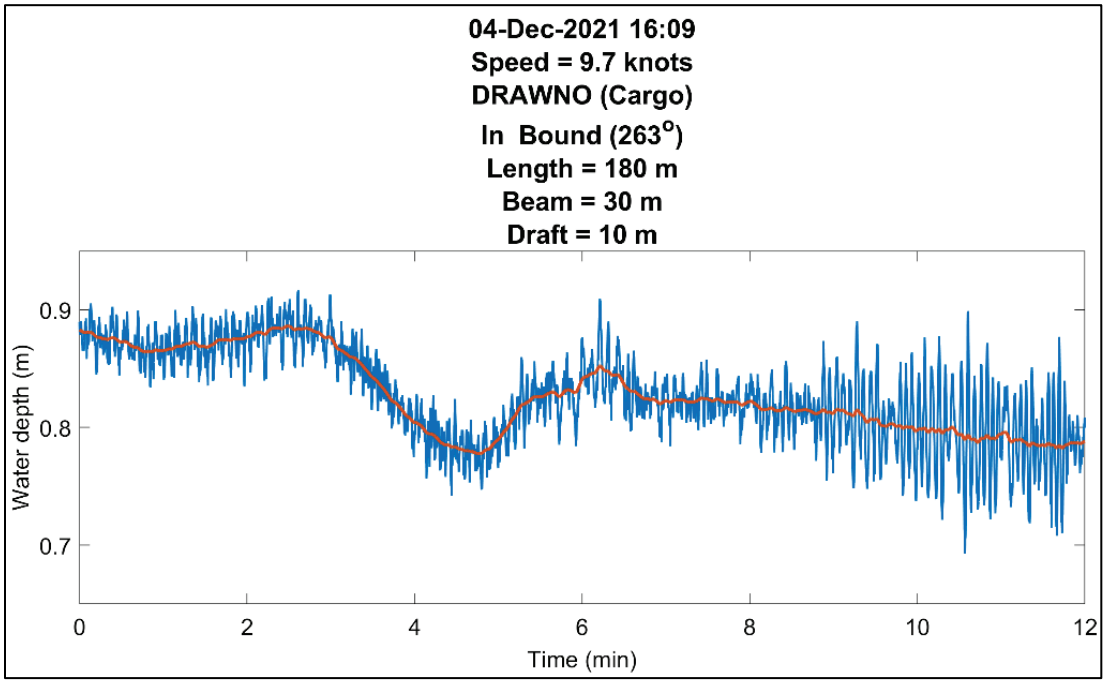

Figure A-16. Wake record from *Grande Senegal*, vehicle carrier.

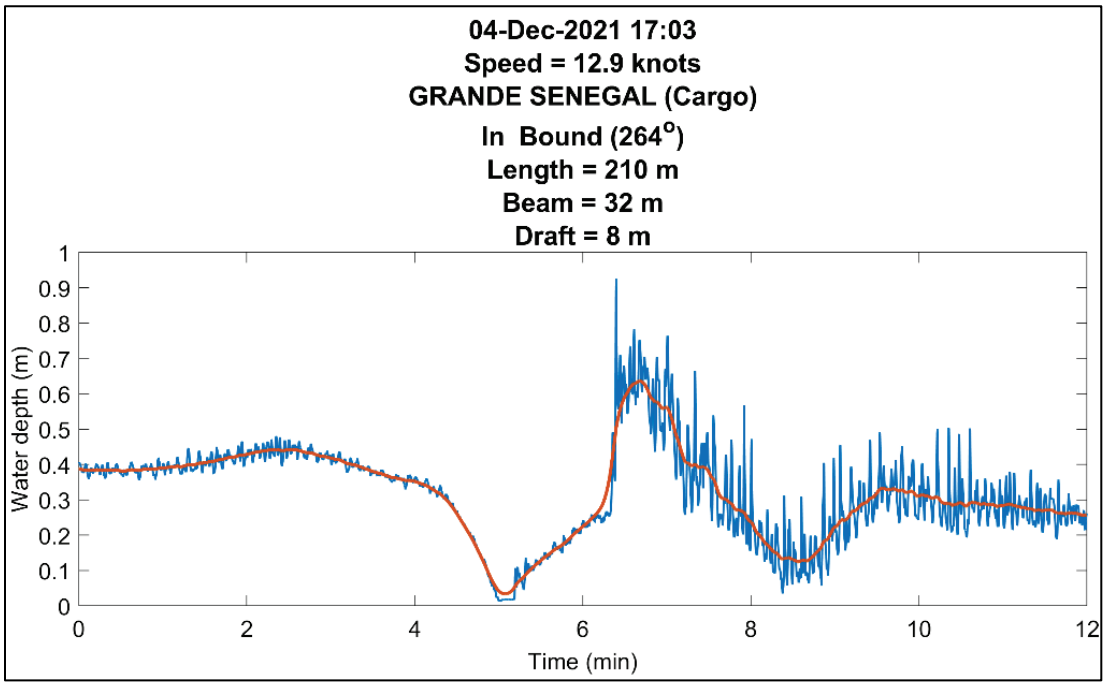

Figure A-17. Wake record from *APL Sentosa,* container ship.

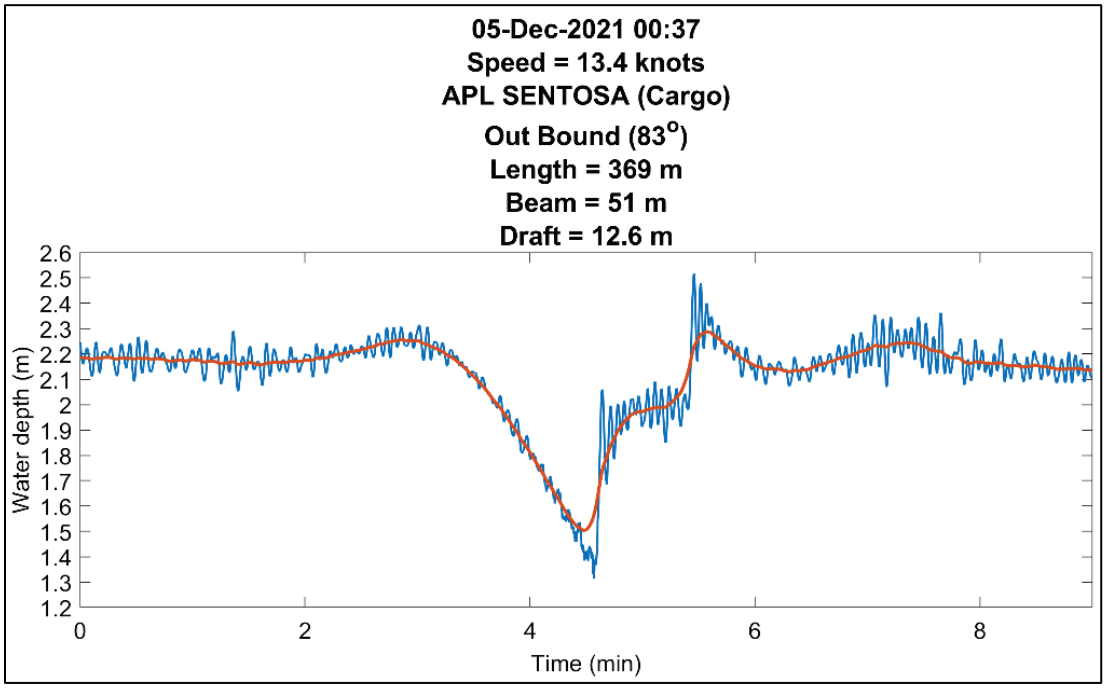

Figure A-18. Wake record from unknown large vessel.

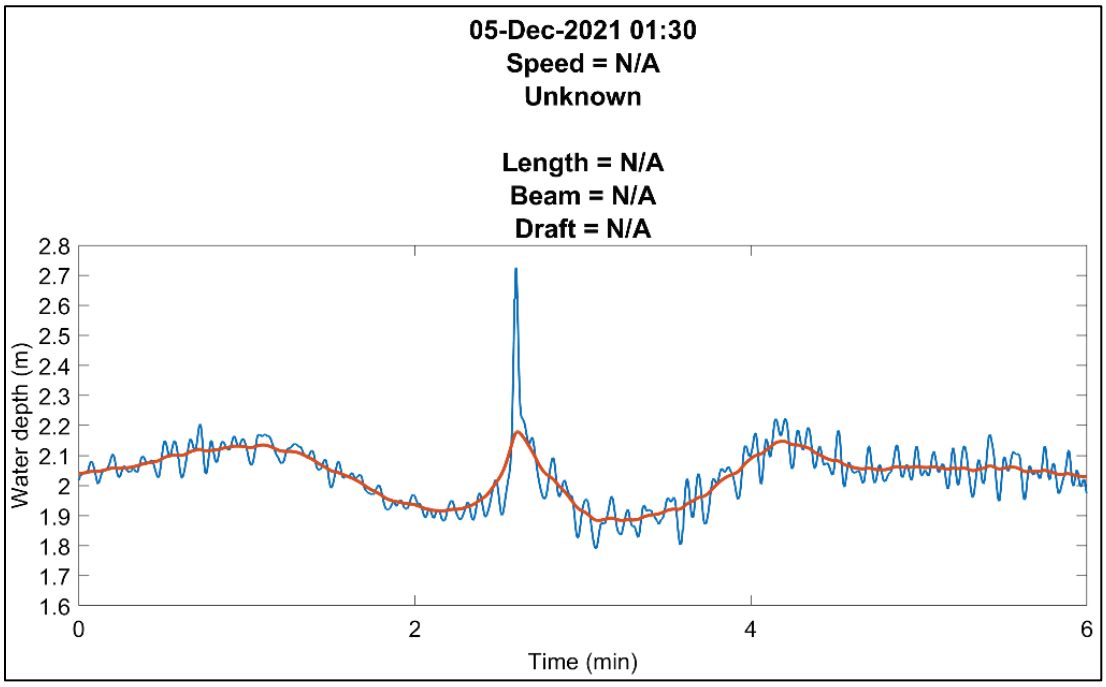

Figure A-19. Wake record from *CPO Bremen*, container ship.

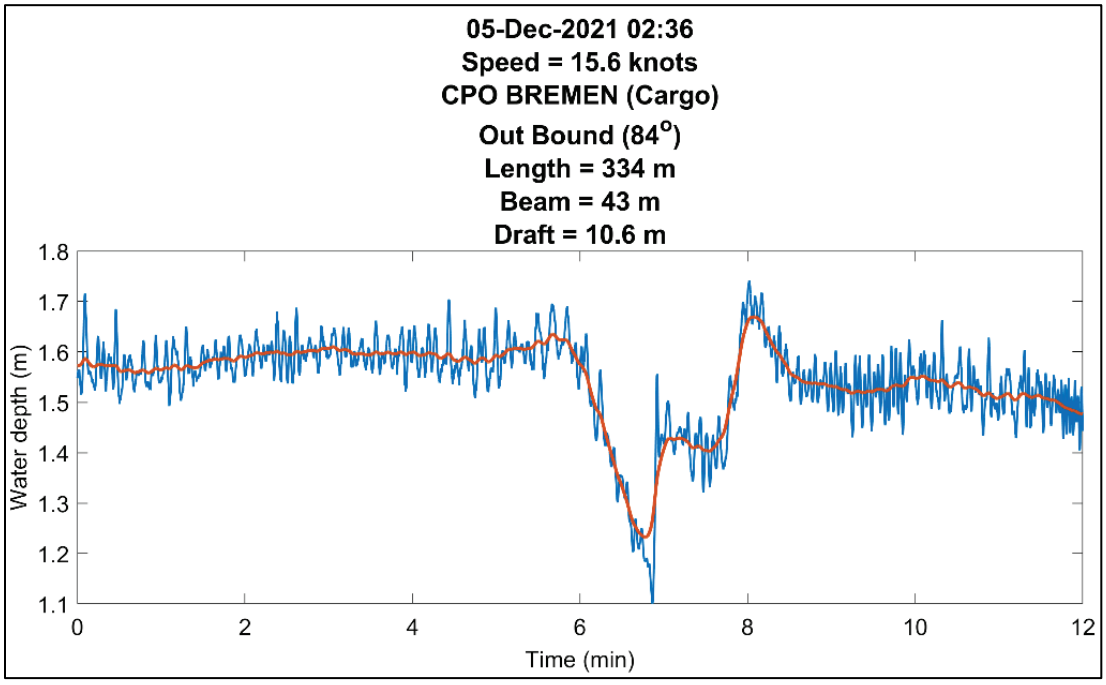

Figure A-20. Wake record from *Vienna Express*, container ship.

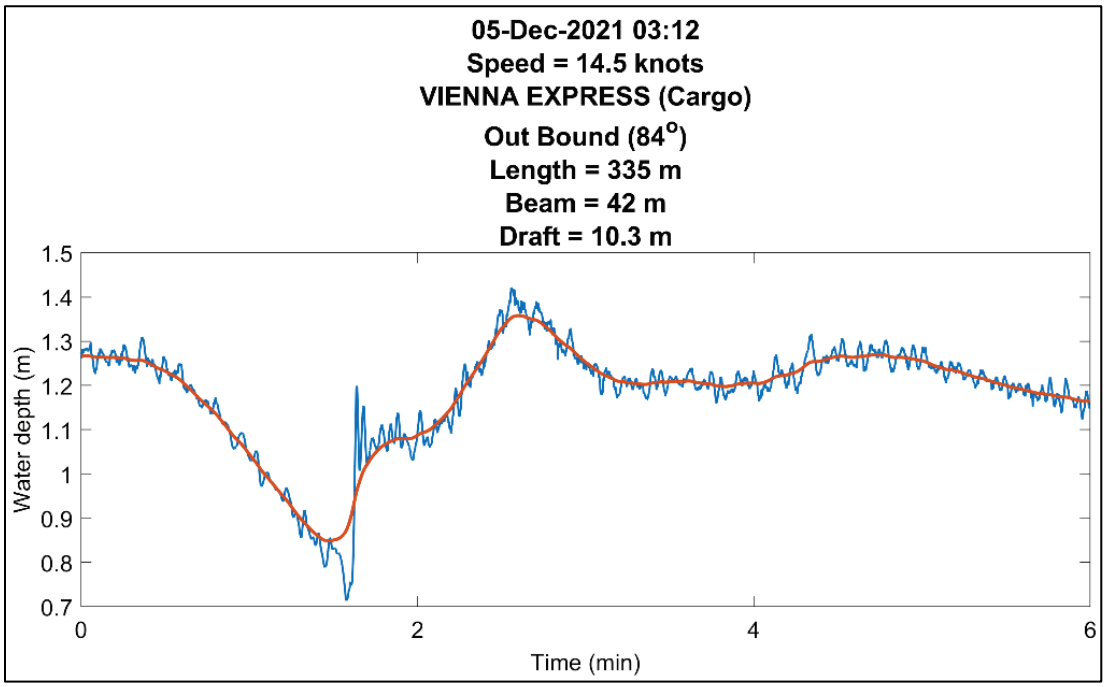

Figure A-21. Wake record from unknown large vessel.

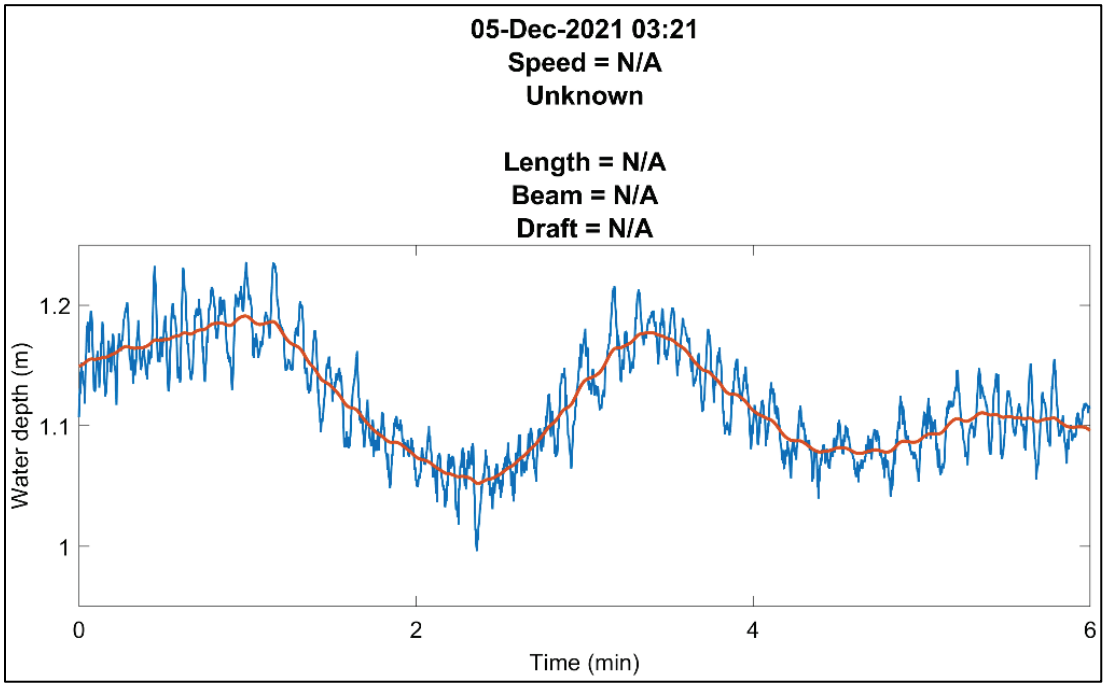

Figure A-22. Wake record from *Maersk Kinloss*, container ship.

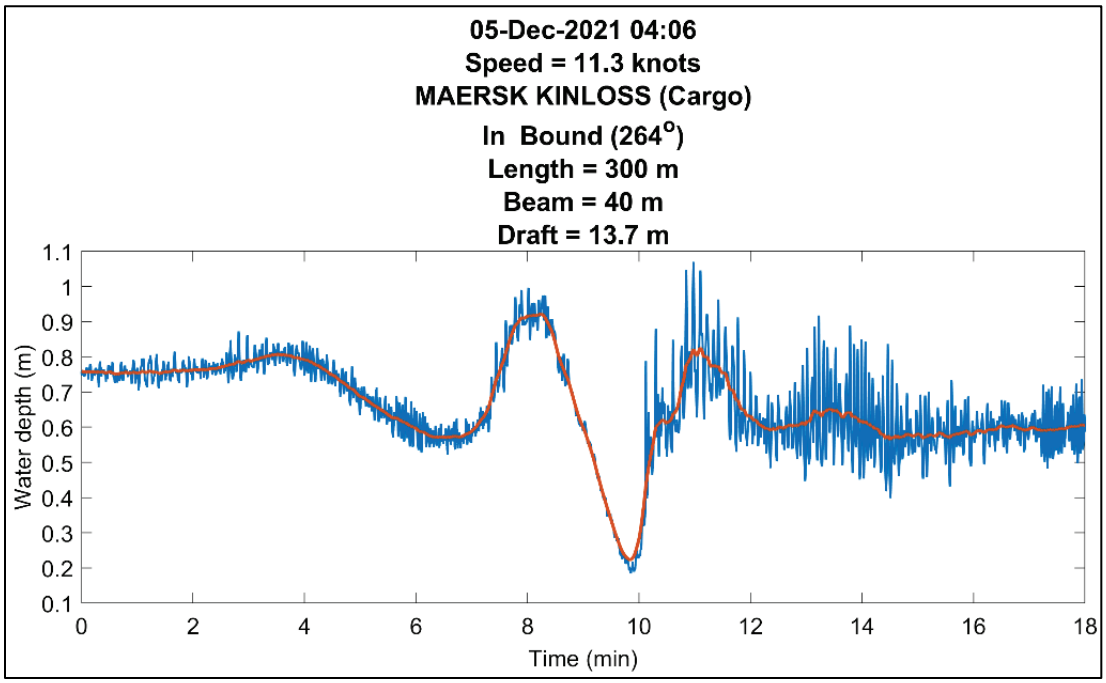

Figure A-23. Wake record from unknown large vessel.

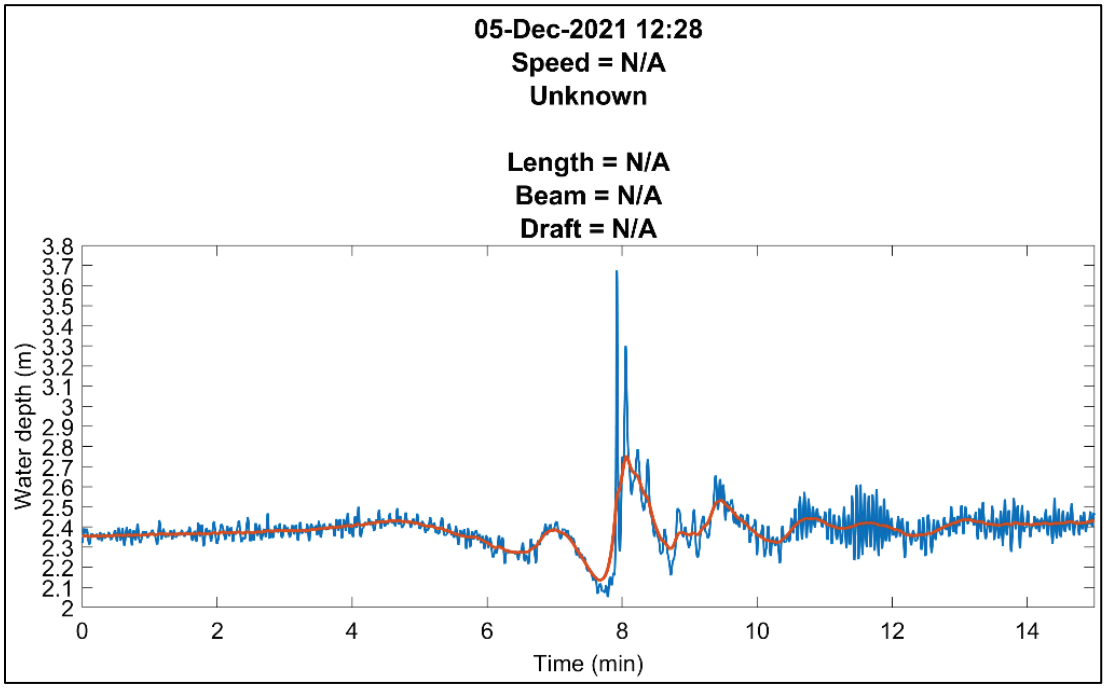

Figure A-24. Wake record from unknown large vessel.

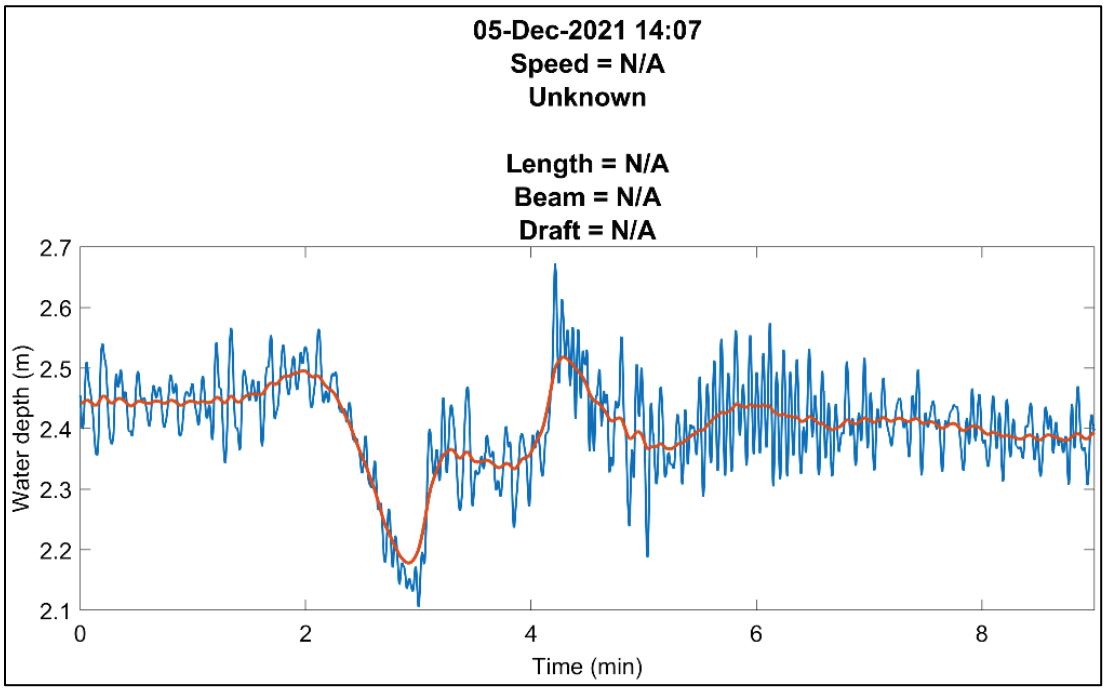

Abbreviations

ADCP	Acoustic Doppler current profiler
AIS	Automated Information System
ERDC	US Army Engineer Research and Development Center
MLLW	Mean lower low water
MLW	Mean low water
MMSI	Maritime Mobile Service Identity
NOAA	National Oceanographic and Atmospheric Administration
SAS	Savannah District
USACE	US Army Corps of Engineers
USGS	US Geological Survey

REPORT DOCUMENTATION PAGE

Form Approved
OMB No. 0704-0188

1. REPORT DATE	2. REPORT TYPE	3. DATES COVERED *(From - To)*
November 2022	Final Report	FY21–FY23

4. TITLE AND SUBTITLE
Ship-Induced Waves at Tybee Island, Georgia

5a. CONTRACT NUMBER

5b. GRANT NUMBER

5c. PROGRAM ELEMENT NUMBER

6. AUTHOR(S)
Rachel Bain, Richard Styles, and Jared M. Lopes

5d. PROJECT NUMBER

5e. TASK NUMBER

5f. WORK UNIT NUMBER

7. PERFORMING ORGANIZATION NAME(S) AND ADDRESS(ES)
Coastal and Hydraulics Laboratory
US Army Engineer Research and Development Center
3909 Halls Ferry Road
Vicksburg, MS 39180-6199

Savannah District
US Army Corps of Engineers
100 W Oglethorpe Ave
Savannah, GA 31401

8. PERFORMING ORGANIZATION REPORT NUMBER
ERDC/CHL TR-22-21

9. SPONSORING/MONITORING AGENCY NAME(S) AND ADDRESS(ES)
US Army Corps of Engineers, Savannah District
Savannah, GA 31401

10. SPONSOR/MONITOR'S ACRONYM(S)
USACE SAS

11. SPONSOR/MONITOR'S REPORT NUMBER(S)

12. DISTRIBUTION/AVAILABILITY STATEMENT
Approved for public release; distribution is unlimited.

13. SUPPLEMENTARY NOTES
Funding Account Code U4384772; AMSCO Code 493017

14. ABSTRACT
Commercial vessels transiting the Savannah entrance channel intermittently generate large wake events at Tybee Island, Georgia, creating a potential hazard for beachgoers. However, not all commercial vessels generate large wakes, and the relationship between vessel dimensions, operating conditions, wake height, and drawdown magnitude is unclear. This study evaluates bathymetric data, high-frequency wave and vessel wake measurements, and broadcast vessel identification over a 4-month period with the goal of providing a quantitative characterization of vessel wake conditions at Tybee Island. Data from 1,386 cargo vessel passages and 202 tanker passages indicate that vessel dimensions (length and beam) are positively correlated with drawdown magnitude and secondary wake height, although large vessels do not consistently generate large wakes. Container ships, which tended to travel faster than tankers, corresponded to the largest wakes in the dataset. A further hypothesis is that tidally modulated energy dissipation may favor smaller vessel wake uprush at low tide and larger uprush at high tide, but this idea cannot be confirmed without additional measurements to quantify nonlinear wave propagation on the beach face. Based on the collected data, the study concludes with four recommendations for reducing risk to beachgoers.

15. SUBJECT TERMS
Savannah Harbor (Ga.), Ships—Wakes (fluid dynamics), Tybee Island (Ga.), Water waves--analysis

16. SECURITY CLASSIFICATION OF:			17. LIMITATION OF ABSTRACT	18. NUMBER OF PAGES	19a. NAME OF RESPONSIBLE PERSON
a. REPORT	b. ABSTRACT	c. THIS PAGE			Richard Styles
Unclassified	Unclassified	Unclassified	SAR	90	19b. TELEPHONE NUMBER *(Include area code)* 601-634-4065